2007

Improving emissions inventories in North America through systematic analysis of model performance during ICARRT and MILAGRO

Marcelo Andrés Mena
University of Iowa

IMPROVING EMISSIONS INVENTORIES IN NORTH AMERICA THROUGH SYSTEMATIC ANALYSIS OF MODEL PERFORMANCE DURING ICARTT AND MILAGRO

by

Marcelo Andrés Mena

An Abstract

Of a thesis submitted in partial fulfillment
of the requirements for the Doctor of
Philosophy degree in Civil and Environmental Engineering
in the Graduate College of
The University of Iowa

July 2007

Thesis Supervisor: Professor Gregory Carmichael

ABSTRACT

During 2004 and 2006 the University of Iowa provided air quality forecast support for flight planning of the ICARTT and MILAGRO field campaigns. A method for improvement of model performance in comparison to observations is showed. The method allows identifying sources of model error from boundary conditions and emissions inventories. Simultaneous analysis of horizontal interpolation of model error and error covariance showed that error in ozone modeling is highly correlated to the error of its precursors, and that there is geographical correlation also. During ICARTT ozone modeling error was improved by updating from the National Emissions Inventory from 1999 and 2001, and furthermore by updating large point source emissions from continuous monitoring data. Further improvements were achieved by reducing area emissions of NOx y 60% for states in the Southeast United States. Ozone error was highly correlated to NOy error during this campaign. Also ozone production in the United States was most sensitive to NOx emissions. During MILAGRO model performance in terms of correlation coefficients was higher, but model error in ozone modeling was high due overestimation of NOx and VOC emissions in Mexico City during forecasting. Large model improvements were shown by decreasing NOx emissions in Mexico City by 50% and VOC by 60%. Recurring ozone error is spatially correlated to CO and NOy error. Sensitivity studies show that Mexico City aerosol can reduce regional photolysis rates by 40% and ozone formation by 5-10%. Mexico City emissions can enhance NOy and O3 concentrations over the Gulf of Mexico in up to 10-20%. Mexico City emissions can convert regional ozone production regimes from VOC to NOx limited. A method of interpolation of observations along flight tracks is shown, which can be used to infer on the direction of outflow plumes. The use of ratios such as O3/NOy and NOx/NOy can be used to provide information on chemical characteristics of the plume, such as age, and ozone production regime. Interpolated MTBE observations can be used as a tracer of

urban mobile source emissions. Finally procedures for estimating and gridding emissions inventories in Brazil and Mexico are presented.

Abstract Approved: _____
Thesis Supervisor

_____
Title and Department

_____
Date

IMPROVING EMISSIONS INVENTORIES IN NORTH AMERICA THROUGH SYSTEMATIC ANALYSIS OF MODEL PERFORMANCE DURING ICARTT AND MILAGRO

by

Marcelo Andrés Mena

A thesis submitted in partial fulfillment
of the requirements for the Doctor of
Philosophy degree in Civil and Environmental Engineering
in the Graduate College of
The University of Iowa

July 2007

Thesis Supervisor: Professor Gregory Carmichael

Graduate College
The University of Iowa
Iowa City, Iowa

CERTIFICATE OF APPROVAL

_____

PH.D. THESIS

_____

This is to certify that the Ph.D. thesis of

Marcelo Andrés Mena

has been approved by the Examining Committee
for the thesis requirement for the Doctor of Philosophy
degree in Civil and Environmental Engineering at the July 2007 graduation.

Thesis Committee: _____
Gregory Carmichael, Thesis Supervisor

_____
Hector Jorquera

_____
Jerald Schnoor

_____
Vicki Grassian

_____
Charles Stanier

To my wife Loreto Stambuk, my son Vicente, and my daughter Olivia

You lot who preach restraint and watch your waist as well
Should learn, for once, the way the world is run
However much you twist or whatever lies that you tell
Food is the first thing, morals follow on

So first make sure that those who are now starving
Get proper helpings when we all start carving
What keeps mankind alive?

What keeps mankind alive?
The fact that millions are daily tortured
Stifled, punished, silenced and oppressed
Mankind can keep alive thanks to its brilliance
In keeping its humanity repressed
And for once you must try not to shriek the facts
Mankind is kept alive by bestial acts

Bertold Brecht

ACKNOWLEDGMENTS

This thesis was funded in part by grants from NASA and NSF. I'd like to thank my advisor Gregory Carmichael for his great support and understanding all these years. He proves that you can run a world-class research group in a hospitable and friendly environment. Also I'd like to thank my committee members Vicki Grassian, Keri Hornebuckle, Michelle Scherer, Hector Jorquera, Charles Stanier, and Jerry Schnoor. Their questions and comments definitely fortified this dissertation. I'd like to thank Dr. Youhua Tang and Tianfeng Chai for their help in getting the model running. I'd like to thank Bhupesh and Sarika for their great conversations and insight on the research. And I'd like to finally thank my friends Dr. Elliott Campbell and future doctor Forrest Meggers for challenging me into translating my research interests in my daily lifestyle, by increasing my bicycle use and decreasing my carbon footprint.

ABSTRACT

During 2004 and 2006 the University of Iowa provided air quality forecast support for flight planning of the ICARTT and MILAGRO field campaigns. A method for improvement of model performance in comparison to observations is showed. The method allows identifying sources of model error from boundary conditions and emissions inventories. Simultaneous analysis of horizontal interpolation of model error and error covariance showed that error in ozone modeling is highly correlated to the error of its precursors, and that there is geographical correlation also. During ICARTT ozone modeling error was improved by updating from the National Emissions Inventory from 1999 and 2001, and furthermore by updating large point source emissions from continuous monitoring data. Further improvements were achieved by reducing area emissions of NOx y 60% for states in the Southeast United States. Ozone error was highly correlated to NOy error during this campaign. Also ozone production in the United States was most sensitive to NOx emissions. During MILAGRO model performance in terms of correlation coefficients was higher, but model error in ozone modeling was high due overestimation of NOx and VOC emissions in Mexico City during forecasting. Large model improvements were shown by decreasing NOx emissions in Mexico City by 50% and VOC by 60%. Recurring ozone error is spatially correlated to CO and NOy error. Sensitivity studies show that Mexico City aerosol can reduce regional photolysis rates by 40% and ozone formation by 5-10%. Mexico City emissions can enhance NOy and O3 concentrations over the Gulf of Mexico in up to 10-20%. Mexico City emissions can convert regional ozone production regimes from VOC to NOx limited. A method of interpolation of observations along flight tracks is shown, which can be used to infer on the direction of outflow plumes. The use of ratios such as O3/NOy and NOx/NOy can be used to provide information on chemical characteristics of the plume, such as age, and ozone production regime. Interpolated MTBE observations can be used as a tracer of

urban mobile source emissions. Finally procedures for estimating and gridding emissions inventories in Brazil and Mexico are presented.

TABLE OF CONTENTS

LIST OF TABLES

LIST OF FIGURES

CHAPTER 1 INTRODUCTION

1.1 Background

Tropospheric ozone concentrations have been increasing since pre-industrial ages, largely due to anthropogenic forcing on the atmosphere [*Wang and Jacob*, 1998]. Ozone is a potent oxidizing compound that has been linked to increase in morbidity and mortality in numerous cities [*Bell et al.*, 2006; *Zmirou, et al.*, 1998; *West et al.*, 2006]. Regional effects are associated to damage to crops, wild plants, and forests [*Aunan and Bernsten*, 2000; *Davidson et al*, 1998; *Diem*, 2003; *Fumagali et al*, 2001; *Ashmore.* 2005]. Globally tropospheric ozone is a greenhouse gas with potential to affect climate change [*Shindell et al.* 2006].Since ozone is not a primary pollutant, controlling ozone production and exposure is based on regulating its precursors. However, the control of ozone production is very complex, due to the non-linearity of the chemistry [*Cardelino et al.*, 1995; *Kleinman et al.*, 2001; *Carnevale et al.*, 2007]. Also there is sometimes a geographical disconnection between ozone precursor reductions and the geographical area that is benefited [*Liang et al.*, 2006]. Finally control policies intended to reduce ozone peak concentrations for a city may increase regional ozone concentrations and increase the extension of non attainment areas [*Rao et al.*, 1996] This scenario can be found in New Hampshire, for example, where elevated ozone episodes have been linked to emissions in upwind metropolitan areas such as New York and Boston [*Mao et al.*, 2004; *NHDES*, 2006]

1.1.1 Ozone production

Regulating agencies formulate precursor reduction policies based on regional ozone production regimes. Historically, ozone production regimes have been categorized as either NO_x (nitrogen oxides) or VOC (volatile organic carbons) limited [*Sillman,* 1995]. Rural areas are considered to be NO_x limited, and urban areas have a mixed regime, tending towards VOC limited conditions [*Sillman*, 1999]. Biogenic VOCs are

important to consider since they shift conditions toward NO_x sensitivity [*Pun et al.,* 2002] making VOC specific control policies less effective. VOC limited conditions have the counter-intuitive characteristic that reducing NO_x emissions may cause an increase of ozone production.

Policies for control of ozone were formulated as the result of the Clean Air Act, based on the state of knowledge of ozone chemistry for that period. However much insight has been gained since the implementation of the Clean Air Act because more chemical reactions have been studied [*Carter*, 1994] and incorporated into models (which have also increased their resolution and complexity). VOC control policies, for example, are believed to lack the specificity to be effective, and reactivity based policies have been proposed [*Avery*, 2006]. Equally, NO_x controls, for power plants should incorporate both location and intensity, as a small power plant can generate more ozone than a large power plant [*Ryerson, et al*., 2001].

1.1.2 Ozone chemistry

Ozone formation occurs through a series of reactions involving sunlight, NO_x, CO, and VOCs. The following formation pathways are summarized from Sillman [1999].

1.1.2.1 Daytime formation of ozone

The daytime formation of ozone is due to the transfer of an O molecule from the photolysis of NO_2. The formation of NO_2 is due to the reaction of HO_2 (product of oxidation of VOCs, CO, and CH_4) with NO, and the reaction of NO with RO_2 (also an oxidation product of VOC).

$$VOC + OH \xrightarrow{O_2} RO_2 + H_2O \quad (1)$$

$$CO + OH \xrightarrow{O_2} HO_2 + CO_2 \quad (2)$$

$$RO_2 + NO \xrightarrow{O_2} \text{secondary VOC} + HO_2 + NO_2 \quad (3)$$

$$HO_2 + NO \rightarrow NO_2 + OH \quad (4)$$

$$NO_2 + h\nu \rightarrow NO + O \quad (5)$$

$$O + O_2 + M \rightarrow O_3 + M \quad (6)$$

1.1.2.2 Nighttime titration of ozone

In conditions of limited sunlight (nighttime mostly) the dominant reaction one in which NO_x emissions destroy ozone in a titration reaction, which is enhanced by low nighttime mixing height. Titration is also important near large point sources of NO_x, in which a net decrease of ozone is measured along their plumes.

$$O_3 + NO \rightarrow NO_2 + O_2 \quad (7)$$

1.1.2.3 Sources of radicals

Ozone formation reactions will carry on as long as there is a source of radicals OH and HO_2. OH is formed from the photolysis of ozone in the presence of water vapor, while HO_2 is the product of oxidation of VOC and CO.

$$O_3 + h\nu \xrightarrow{H_2O} 2OH + O_2 \quad (8)$$

Formaldehyde, which is a ubiquitous VOC, forms HO_2 and CO. The latter can be oxidized to form HO_2, yielding a net 2 HO_2 per photolyzed formaldehyde.

$$CH_2O + h\nu \rightarrow HO_2 + CO \quad (9)$$

$$CO + OH \xrightarrow{O_2} HO_2 + CO_2 \quad (10)$$

1.1.2.4 Sinks of radicals

The ozone formation reaction is slowed down by loss of radicals, primarily by the autocatalytic destruction of HO_2 to form peroxide (H_2O_2, which is removed by wet deposition), and also by the loss of OH by reaction with NO_2 to form nitric acid.

$$2\,HO_2 \rightarrow H_2O_2 + O_2 \quad (11)$$

$$NO_2 + OH \rightarrow HNO_3 \quad (12)$$

These sources and sinks of radicals allow ozone production to be categorized as either NO_x or VOC limited.

1.1.3 Types of ozone production regimes

1.1.3.1 NO_x limited regime

In a NO_x limited regime peroxides are the main sink of radicals, as there is an excess of HO_2 originated from VOC and CO oxidation (VOC saturated). The rate of formation of ozone is determined by the reaction of HO_2 and RO_2 with NO, which increases as NO_x emissions increase. If VOC emissions increase so will ozone production, but less effectively than increases in NO_x emissions.

1.1.3.2 VOC limited regime

A VOC limited regime occurs when nitric acid is the main sink of radicals, because of an excess of NO_2 reacting with OH. Ozone formation will be limited to OH oxidation of CO and VOC (which generate HO_2).

1.1.4 Observation based ozone production indicators

The use of indicator ratios began when Sillman [1995] related observed ozone concentrations to NO_y and NO_z (defined as NO_y-NO_x), along with similar parameters and subtracted background values (NO_y-NO_{yb}, NO_z-NO_{zb}, O_3-O_{3b}). The data showed some strong trends, suggesting that lower O_3 to reactive nitrogen ratios were representative of VOC sensitive conditions, while higher values were more representative of NO_x sensitive conditions (Table 1). It is thought that ratio of peroxide to nitric acid, or NO_y shows an even stronger relationship, as these species relate to central aspects of ozone production regimes [*Sillman*, 1999]. For ratios of peroxide to nitric acid, the higher ratios suggest NO_x limited conditions, and the lower values suggest VOC limited conditions. These relationships are best established using high quality measurements of species that are not typically measured in surface sites, such as NO_z, HNO_3, NO_y, or H_2O_2. These indicators have a caveat: during rain events the loss of nitric acid through wet deposition affects these ratios, making them invalid. Ozone production efficiencies, as defined by Kleinman

(2002) are the sum of odd oxygen species divided by the NO_x consumed. In that study odd oxygen is defined as the sum of NO_2 and O_3, and NO_z as NO_y (total reactive nitrogen=NO_x+HNO_3+PAN).

1.1.5 Ozone control strategies

In the US, the EPA's Air Quality Planning Unit verifies that State Implementation Plans (SIPs) are in place to reduce ozone exposure in non attainment areas., as part of the Clean Air Act. Non attainment areas are defined as those which do not meet the EPA's 8 h average ozone standard of 80ppbv implemented in 2004. These SIPs consider modeling studies using the EPA MODELS3 framework, in which the outcome of different control strategies is evaluated. VOC limited conditions require reductions in VOC (reductions of NO_x can lead to increases in ozone) while NO_x limited conditions require reductions of both NO_x and VOC. The results of these reductions will not necessarily decrease ozone near the source regions. Table 2 shows some ozone control strategies to reduce emissions of NO_x and VOC. These strategies aim at general reductions, but little is said about the geographical relationship between emissions reductions and ozone concentrations, and ultimately ozone exposure.

1.1.6 Kriging

Kriging is used during this research as a tool to interpolate data points along flight paths to generate surfaces. Kriging is a statistical method developed by Georges Matheron, named in honor of D.G. Krige, the conceptual inventor, who used the method to track mining deposits [*Krige,* 1951].. Kriging is based on relating the covariance of the concentrations at two different points to the distance between them, through a relationship that is usually plotted in a semi-variogram. Unknown values are predicted based on the values of neighboring points, weighed by the distance to the unknown point (more weight to closer points, etc). As an example Figure 1 shows how semi variance is related to distance. It is expected to be higher between points 1 and 4 in comparison to

points 2 and 3. Kriging has been previously used for interpolating surface measurements of ozone, particulate matter and estimation of exposure to these compounds [*Liao et al.*, 2006]. It is also used to generate maps of air pollution based on discrete measurements, such as the AIRNOW network [*EPA*, 1999].

1.2 Overview and objectives

This research intends to utilize the information gathered during intensive aircraft measurement campaigns to improve the understanding sources of model error during forecasting, specifically by reducing bias in ozone predictions. The approach that is used combines conventional statistical analysis of model performance with three dimensional data (vertical profiles, and horizontal interpolation of model error), and error covariance analysis (seeing how errors are related between ozone and its precursors). This simultaneous analysis provides guidance to refine emissions inventories and boundary conditions to improve model performance. Chapter 2 focuses on improving ozone modeling during the ICARTT campaign (International Consortium for Atmospheric Research on Transport and Transformation) in the summer of 2004 using high quality emissions inventories. Chapter 3 focuses on improving ozone modeling during the MILAGRO (Megacity Initiative: Local and Global Research Operations), in March 2006, using a lower quality and less refined emissions inventory. Chapter 4 focuses on showing the methodology that was used to develop and grid the emissions inventory the country of Mexico, and a regional emissions inventory for the region of Bahia, in Brazil. Chapter 5 focuses on the use of geospatial interpolation techniques to evaluate the regional impact of Mexico City, and the characterization of air masses and ozone production regimes. Chapters 2 and 3 use a combination of observed and modeled values for analysis, while Chapter 5 uses observed values exclusively.

1.2.1 Improving ozone modeling in North America during ICARTT

During the operational phase of the ICARTT field experiment in 2004, the regional air quality model STEM showed a strong positive surface bias and a negative upper troposphere bias (compared to observed DC-8 and WP-3 observations) with respect to ozone. After updating emissions from NEI 1999 to NEI 2001 (with a 2004 large point sources inventory update), and modifying boundary conditions, low-level model bias decreases from 11.21 to 1.45 ppbv for the NASA DC-8 observations and from 8.26 to −0.34 for the NOAA WP-3. Improvements in boundary conditions provided by global models decrease the upper troposphere negative ozone bias, while accounting for biomass burning emissions improved model performance for CO. The covariances of ozone bias were highly correlated to NO_z, NO_y, and HNO_3 biases. Interpolation of bias information through kriging showed that decreasing emissions in SE United States would reduce regional ozone model bias and improve model correlation coefficients. The spatial distribution of forecast errors was analyzed using kriging, which identified distinct features, which when compared to errors in post analysis simulations, helped document improvements. Changes in dry deposition to crops were shown to reduce substantially high bias in the forecasts in the Midwest, while updated emissions were shown to account for decreases in bias in the eastern United States. Observed and modeled ozone production efficiencies for the DC-8 were calculated and shown to be very similar (7.8) suggesting that recurring ozone bias is due to overestimation of NO_x emissions. Sensitivity studies showed that ozone formation in the United States is most sensitive to NO_x emissions, followed by VOCs and CO. PAN as a reservoir of NO_x can contribute to a significant amount of surface ozone through thermal decomposition. The main conclusions of this chapter have been confirmed by a paper that compared satellite observations of NO_2 from SCIAMACHY (SCanning Imaging Absorption spectroMeter for Atmospheric ChartograpHY) [*Kim et al.*, 2006] and another paper documented the

decrease in NO_x emissions in the Eastern United States from 1999 to 2003 [*Frost et al.*, 2006].

1.2.2 Improving ozone modeling during MILAGRO

The MILAGRO campaign consisted in experiments designed to measure air pollution from Mexico City with the objective of evaluating the regional impact of the city on air quality and chemistry. Chapter 3 focuses on the analysis of model performance comparing modeled values to those observed along C-130 flight tracks. During the forecast stage of the MILAGRO campaign the STEM model [*Carmichael et al*, 1993; *Tang et al.,* 2003a] values extracted along C-130 flight tracks showed a large positive bias in ozone concentrations associated (26%) to positive bias in NO_y (72%) and VOC (128% for C_3H_8, and 380% for ARO1) predictions, as was confirmed by statistical analysis, vertical profiles, and the interpolation of model error. Reducing emissions of NO_x (50%) and VOC (~60%) resulted in reduction of positive bias of ozone to 10% while reducing positive bias of NOy (19% and VOC (7% for C_3H_8 and 26% for ARO_1). Regional ozone bias was reduced to the -25 to 25% range for large portions of Mexico, while reducing ozone bias in Mexico City from 200-300% to 25 to 100%. Remaining ozone bias is highly correlated to CO bias, which in turn is related to VOC bias. Observation based methods suggest that Mexico City is VOC limited, therefore overprediction of VOC will lead to overprediction of O_3. Studying model resolution showed that higher resolution modeling (12km vs. 60km) shows better correlation for CO, VOC, and NO_y (which are more directly related to primary pollutants), while smaller effect on a secondary pollutant such as ozone. Mean nighttime minimum ozone using a higher resolution model is lower in the city (5ppbv) than a lower resolution one (25ppbv), because lower resolution dilutes the nighttime NOx titration effect. A sensitivity study showed that aerosol from Mexico City can reduce photolysis rates of NO_2 by 40%, but only reducing ozone formation by 5-10%.

1.3 Contributions

The main contributions for this research are:

1. Developed a methodology to improve model performance by systematic analysis of conventional statistics complemented with 3D analysis (vertical profiles and horizontal error maps), and error covariance among ozone and its precursors.
2. Showed that ozone predictions during ICARTT and MILAGRO were associated with overpredictions of ozone precursors (NOx for ICARTT and NO_x and VOC for MILAGRO).
3. Showed NO_x emissions in the Eastern United States have decreased in more than 60% for area NOx sources, and by 50% for large point sources.
4. Showed that the areas sampled during ICARTT are largely NO_x limited, and that ozone production is most sensitive to increases in NO_x emissions, followed by VOC, and then CO.
5. Showed that Mexico City is largely VOC limited.
6. Showed that kriging can be used to interpolate model error to provide regional contextualization to model error.
7. Showed that modeled influence of aerosol on photolysis of NO_2 can be reduced by as much as 40%, but dilution of NO_2 only reduces ozone concentrations by 5%.
8. Showed that kriging can be used to interpolate observations to evaluate the shape and direction of the outflow plume from Mexico City. Also showed that comparing surfaces from multiple species allow inference on plume characterization and ozone production regimes.
9. Developed and gridded an emissions inventory for Mexico for 1999 and provided basis for improving it.

Table 1 Values of indicator ratios for NO_x, transitional, and VOC sensitive conditions.

Indicator	VOC sensitive	Transition	NOx sensitive
O_3/NO_y	5	6-8	11
O_3/NO_z	6	8-10	14
O_3/HNO_3	9	12-15	20
H_2O_2/HNO_3	0.15	0.25-0.35	0.6
H_2O_2/NO_y	0.12	0.2-0.25	0.4
H_2O_2/NO_z	0.08	0.12-0.17	0.35

Table 2 Examples of some ozone control strategies

Source type	Strategy
Area and industrial sources [EPA, 2007; TCEQ, 2006]	• Installation of VOC control equipment, and VOC content in coatings. • Control of NO_x through process changes, or by installing catalytic and non catalytic reductions of NO_x. • NOx control standards for small residential and industrial sources
Industrial point sources	• Reductions from industrial and utility boilers in industry, and cement kilns • Emission limits to boilers and turbines
Mobile sources	• On site measurement of older vehicles emissions through open treadmills. • Replace heavy duty diesel engines • Reduce speed limits from 65 to 60 and from 70 to 65 mph. • Reduce aromatic and sulfur content of diesel • Car pooling, telecommuting, flexible work hours, cycling, alternative fuels, Tier II engines. • Controlling evaporative leaks from gas stations by vacuum system that recycles fumes into gas tank. • Reformulated gasoline in areas that are non-attainment. Addition of oxygenates, such as MTBE and ethanol, that decrease VOC and NO_x emissions.

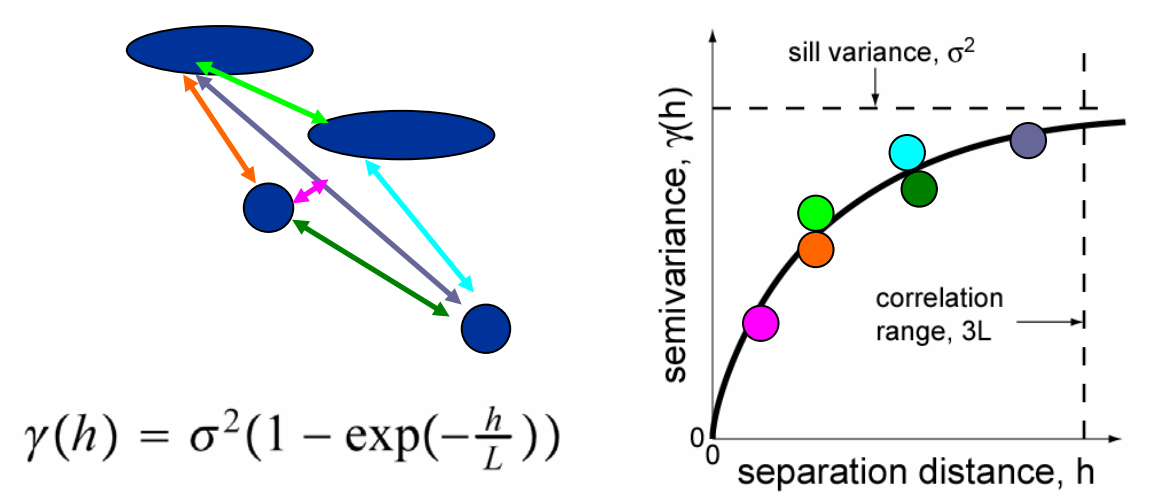

Figure 1 Illustration of a semi-variogram used in kriging (from Michalak, 2006)

CHAPTER 2 IMPROVING OZONE MODELING IN THE UNITED STATES DURING ICARTT

Air pollution models have been used to predict air quality during numerous field campaigns [*Bates et al.*, 1998; *Jacob et al.*, 2002; *Menut et al.*, 2000; *Ramana et al.*, 2004; *Voutard et al.*, 2003], with the objective to both place air pollution in a geographical context for experimental design and, as the data is collected, evaluate our current understanding of atmospheric processes [*Kiley et al.*, 2003] and anthropogenic and biogenic emissions [*Carmichael et al.*, 2003]. During the summer of 2004, the ICARTT field experiment was performed (http://www.al.noaa.gov/ICARTT), which included a NASA experiment called INTEX-A (Intercontinental Chemical Transport Experiment-A), and a NOAA experiment called NEAQS/ITCT-2k4 (New England Air Quality Study - Intercontinental Transport and Chemical Transformation, 2004). During this period NASA DC-8 and NOAA WP-3 aircraft each performed 18 research flights over the continental US, with a special focus on the Northeastern United States. Figure 2 shows the flight tracks of the DC-8 and WP-3 during the mission, and the altitude at which the aircraft flew. The WP-3 aircraft flew at lower altitudes, mostly over the NE United states. More details about the aircraft measurements and main findings are available in Singh et al. [2006]. During the field experiment operations forecasts using the University of Iowa STEM model [*Carmichael and Peters*, 1991; *Tang et al.*, 2003b] were used (along with other models) in support for flight planning. Analysis of the forecasts has shown a persistent positive bias (modeled-observed) for ozone [*Mc Keen et al.*, 2005] in comparison to surface sites in the AIRMAP network in New Hampshire (http://airmap.unh.edu/), and in comparison to the aircraft platform observations. The

objective of this paper is to show that model performance in relation to ozone and its precursors was improved through systematic analysis of model prediction with the observed data to evaluate where model error persists, and how ozone model error is related to model error of other species. The paper also demonstrates how geospatial interpolation through Kriging can be used to provide geographical contextualization to model error, which in turn can be used to improve model performance.

2.1 Methodology

Figure 3 shows the layout of this study, in which systematic data analysis is used to improve model performance by modifying boundary conditions and emissions inventories through an iterative process which included geospatial interpolation of model bias through kriging to provide qualitative support for regional modification of emissions. After selecting the best model run sensitivity studies are carried out to evaluate the contribution of different ozone precursors to ozone formation.

In this study we used the STEM-2K3 model [*Carmichael et al.* 1991]. The model features the lumped species SAPRC99 chemical mechanism [*Carter,* 2000] with an on-line photolysis solver, and the SCAPE II aerosol solver (Simulating Composition of Atmospheric Particles in Equilibrium) [*Kim et al.*, 1993a, 1993b; *Kim and Seinfeld,* 1995]. Meteorological inputs to the model came from MM5 [*Grell et al.*,1995], using the AVN data [*Huang et al*., 1997] during forecasting and NCEP FNL (Final Global Data Assimilation System) analyzed data during post-analysis. For this study the model domain was the continental United States, using a 60km resolution, 62 cells in longitude, and 97 cells in latitude. The model had 21 vertical layers, extending from the surface to

100hPa. The Grell cumulus parameterization [*Grell et al.*, 1995] and the MRF planetary boundary layer parameterization [*Hong et al.*, 1996] were used for the MM5 runs.

During the operational portion of the experiment, anthropogenic emissions were taken from the U.S EPA National Emissions Inventory for the base year of 1999 (NEI 1999) [*EPA*, 2006] while the 2001 update of the same (NEI 2001) was used for the post analysis stage. It should be noted that NEI 2001 has lower emissions of CO, NO_x, and SO_2 than NEI 1999 (Table 3). Modifications were still needed since the simulations with NEI 2001 systematically underestimated light alkanes, and overpredicted aromatic species. The large point source emissions (LPS) used were from the updated inventory by Gregory Frost at NOAA Earth Systems Research Laboratory [*Frost et al.*, 2006], which represents emissions for 2004, the year of the campaign. Upper troposphere lightning NO_x emissions were added to the model in post-analysis based on the National Lightning Detection Network (NLDN), relating emissions to signal strength and multiplicity of flashes. Further information about the lightning emissions used can be found in Tang et al [2007]. Biogenic emissions were estimated using BEIS 2 (Biogenic Emissions Inventory System), [*Geron et al.*, 1994] which generates time-variable isoprene and monoterpene emissions driven by meteorological variables from MM5 simulations. Forest fires that occurred during the ICARTT period were largely outside our regional model domain (in Alaska and Northwestern Canada). Their episodic influence on lateral boundary conditions was incorporated during post-analysis using MOZART NCAR boundary conditions [*Pfister et al.*, 2005] with data assimilated CO concentrations from MOPITT (Measurements of Pollution in the Troposphere instrument on board the TERRA satellite) to constrain the fire emissions influence for the study period, while during the forecast

MOZART GFDL [*Horowitz et al.*, 2003] boundary conditions were used, which did not include episodic fire emissions, but climatological emissions.

The post analysis work focused on improving model performance by carefully comparing predictions with observations, and the use of the error information to identify aspects of the model in need of improvement. Model sensitivity studies were done for factors with significant uncertainty including boundary conditions, anthropogenic emissions inventories, sea salt emissions, lightning NO_x emissions, and dry deposition rates. From these various runs three were selected for detailed analysis in this paper. These are: 1) operational forecasting conditions (Forecast, NEI 1999); 2) the most updated emissions inventory (NEI2001-Frost LPS); and 3) a modification of that emissions inventory (NEI2001-Frost LPS*) that intended to improve model performance by further decreasing the regional NO_x bias. Table 4 shows a summary of the model parameters for the different scenarios compared in this study. Table 3 shows that the total column anthropogenic CO emissions for the domain were reduced by ~40% from NEI 1999 to NEI 2001, and that the NEI2001-Frost LPS estimate increases CO with respect to NEI 2001. The surface NO_x emissions were reduced significantly from NEI 1999 to NEI 2001 (~30%). Figure 4 shows the domain column emissions of NO_x for NEI 1999 (left panel), NEI2001-Frost LPS (center panel), and the decrease of emission from NEI 1999 to NEI 2001-Frost LPS (right panel).

The results from runs with these different conditions for the period July 1 to August 18, 2004, which includes a model spin up period and which spans the times of the DC-8 and WP-3 flights 3-20 for ICARTT, are discussed in this paper. Merged data for both measurement platforms were re-sampled from a 1 second to a 3 minute resolution,

and compared to interpolated data from the 3 h, 60km, and 21-level variable vertical resolution model output.

Kriging is a geospatial interpolation technique [*Oliver and Webster*, 1990] that assumes that bias at a point without observations can be related to points with observations, by an expression which considers three components: an average term, a spatially correlated term, and a random error term. The spatially correlated component is calculated using a semi variogram, constructed by the semi-variance among observations as a function of distance. Kriging has been previously used for interpolating surface measurements of ozone, and particulate matter for health studies, and estimation of exposure [*Liao et al.*, 2006], to generate maps of air pollution based on discrete measurements, such as the AIRNOW network [*EPA*, 1999], and to provide a geographical perspective to ozone analyses [*Blond et al.*, 2003]. Kriging produces a surface of predicted values and uncertainty using a semi-variogram (in this case exponential), which relates percent bias (bias/mean observed*100) to distance among points. The analysis is limited to altitudes less than 4000m. This assumes that the vertical variability in this range is smaller than the horizontal variability. The continuous surface output of Kriging provides geospatial context to bias, and allows the comparison of related bias of different precursors to ozone.

2.2 Data analysis

The surface ozone forecasted during ICARTT has been compared with surface observations and showed a significant high bias for daytime values (~15 ppbv) [*McKeen et al*., 2006]. We anticipated such bias would occur due to the fact that the experiment was conducted in 2004, and that the actual emissions would differ from the 1999 values

used in the forecast. The summer of 2004 presented significant fires in Alaska and Canada which were misrepresented by climatological fires used in the forecast. Additionally, it was found in post analysis that the dry deposition velocities for agricultural crops were incorrectly set to low growing season conditions. These factors all contributed to forecast errors.

Below we compare the forecasted values with aircraft observations. We also compare the results from model runs where the dry deposition velocity has been corrected, and where the emissions and boundary conditions have been updated.

2.2.1 Statistical performance for all flights

The predictions of O_3, CO and NO_y for the various simulation cases are compared with the DC-8 observations in Figure 5 and Table 5. For these comparisons all data from Flights 3-20 are combined together and analyzed by altitude. The predicted values are interpolated to the same spatial location of the observations using tri-linear interpolation. In general the forecast values show a significant positive bias in predicted ozone at altitudes below ~4 km, and a high negative bias above this altitude. The mean bias below 1 km is ~ 11 ppbv, similar to, but slightly lower than the values found from the analysis of the surface AirMap observations. Comparable patterns are found in the forecast for CO and NO_y, with high values at low altitudes and low values at high altitudes. The post analysis runs show significant improvements in the predictions at altitudes below 4 km (see for example the correlation coefficients for the 1-4km range). In the case of ozone the NEI2001-Frost LPS case shows that the low altitude bias is reduced to less than 3 ppbv. The bias in the mid troposphere (4-12 km) is also reduced (by ~ 25%). Similar improvements are found for CO, where the bias above 4km is reduced by updated global

boundary conditions (MOZART-NCAR) that improve the correlation coefficient for CO because of their better representation of the biomass burning emissions from Alaska and northern Canada. Tang et al. [2007] evaluated the impact of boundary conditions on model performance using results from three different global models and found that they dominate the performance of the regional model at these altitudes. The remaining bias reflects the performance skills of the global models used. For NO_y, the bias in the near surface regions is reduced, albeit at a smaller rate, while the negative bias at higher altitudes decreases significantly. The improvements at the higher altitudes reflect the importance of including lightning NO_x emissions. The comparison of the ratio of the standard deviation to the mean value of the predictions and those for the observations shows that the model exhibits a variability that is similar to that of the observations.

Similar results are found for the WP-3 comparisons (Table 6). As shown by comparing the flight operations of the WP-3 and DC-8 were different, with the WP-3 focused largely on the northeast US (Figure 2). This along with the flight altitude differences lead to differences in the statistics in the observed distributions of the DC-8 and WP-3 data. For example, the WP-3 low altitude concentrations on average are higher. In the case of ozone and CO the mean observed values from all flights were 56 and 158 ppbv for the WP-3 and 49 and 138 ppbv, respectively, for the DC-8. The mean bias in the forecast for ozone for the WP-3 was ~8 ppbv, compared to 11 ppbv for the DC-8 comparison. Correlation coefficients for both aircraft were very similar for the 0-1km range (0.71 for DC-8, and 0.63 for WP-3). For the post analysis simulation NEI2001-Frost LPS the bias in predicted ozone at low altitudes was reduced to 1.34 ppbv and the correlation was increased to 0.66. The mean biases for the lower altitude predicted for

CO and NO_y were also reduced significantly (by ~90 and 70%, respectively). For the 1-4km range the ozone correlation improved (R increased from 0.57 to 0.65) and the mean bias decreased from 4.91 to -0.58. CO predictions also improved with R increasing from 0.52 to 0.66, and bias decreasing from 28.37 to 8.79. Note that the CO bias remains significant for the WP-3 flights, from which we can infer that there is still a systematic over prediction of CO for the area that was sampled by WP-3, i.e., the NE United States. For the 4-6km range emissions and boundary condition improvements significantly enhanced ozone modeling performance, with R increasing from 0.15 to 0.46, and bias decreases from -16.19 to -7.83. Similarly CO performance increased due to boundary conditions incorporating biomass burning (R increases from 0.11to 0.36, and the negative bias is improved from -14.57 to -5.28). It is important to note that while the predicted biases in NO_y were reduced significantly in the post-analysis runs, they remain quite high (~1ppbv overprediction when averaged over all altitudes for the DC-8 and WP-3 observations). The NO_y distributions and their comparison with various models used during ICARTT are discussed in detail in Singh et al. [2006]. In Figure 6 we plot the observed and predicted contribution of individual species to NO_y for the DC-8 observations and for the NEI2001-Frost LPS simulations. This plot shows that the predicted contributions are similar to those observed. Nitric acid is shown to compose the largest NO_y fraction below ~4km, above which PAN contributes from 30 to 45% up to about 8 km; the relative contribution of NO in comparison to NO_2 increases with altitude in the upper troposphere (up to 45% of total nitrogen) Within the boundary layer PAN and NO_2 each contribute ~20% to NO_y. The predicted distributions differ in comparison with the observations in that the relative contributions of HNO_3 are lower than those

observed, possibly being linked to overprediction of rainout or washout processes upwind of the sampling. In addition the predicted contribution of NO increases with altitude at a slower rate than observed. This fact is probably related to the treatment of the lightning NO_x emissions. Lightning NO_x emissions at higher altitudes (4-6km) improved the modeling of reactive nitrogen species, decreasing the negative bias of NO_y in the upper troposphere.

Recurring positive bias of NO_y and its components suggest that NO_x emissions in the model are still higher than the actual emission in the summer of 2004. While the emissions used in this simulation have the large point source sector updated to 2004, emissions from the other sectors are based on 2001 values. The transportation sector is the major emission sector for NO_x and transport emissions have shown a downward trend [*USDOT*, 2006]. Continuously monitored emissions of NO_x from large point sources have also decreased [*Frost et al.*, 2006]. So it is most likely that NO_x emissions in 2004 are actually lower than those in 2001 [*Kim et al.*, 2006]. To reflect this case we performed an additional simulation (NEI2001–Frost LPS* case) where the NO_x emissions were reduced by an additional 12% with respect to total NO_x on a national level(but by 60% for area NO_x emissions for selected states, as is discussed in Table 3). The results of this case are also presented in Tables 5 and 6, and Figure 5. The effect of this reduction in NO_x emissions is to further reduce by ~20% the bias in NO_y. Since ozone production in the ICARTT region is largely NO_x limited, this reduction in NO_x emissions also reduced the mean ozone levels by ~ 1ppbv, and further reduced the bias in the lowest layers by 50% (to 1.45 ppbv for the case of the DC-8), compared to the NEI2001-Frost LPS case.

The modeling of volatile organic compounds (VOCs) has always been a challenge due to the uncertainty of volatile organic compound emissions (VOC) emissions inventories in the US [*Parrish et al.,* 2006]. At altitudes above 2km, all model scenarios showed a negative bias for the prediction for ethane, ethene, and propane, largely due to the global model boundary conditions with contributions from errors from imprecise treatment of convective events. In general R values decrease with altitude reflecting the fact that model performance is highly dependent on boundary conditions at higher altitudes.

Error! Reference source not found. shows a quantile-quantile plot of observed and modeled O_3 for the DC-8 for measurements under 4000m altitude range. The forecast values show a systematic overprediction across the whole range, while the NEI2001-Frost LPS* case shows great improvement for values over 55 ppbv, which represented the majority of the points sampled. Figure 8 shows that the frequency for which ozone bias (modeled-observed bias divided by average observed value*100) is between -20 to 20% has increased from 51 to 73% of the time with respect to the forecast, and model error between -5 and 5% has increased from 14 to 23% with respect to forecast. Post-analysis work therefore resulted in a nearly unbiased distribution of ozone errors with a significant reduction in the standard deviation of ozone errors.

2.2.2 Case studies

The results above provide a mission wide perspective. NEI2001-Frost LPS* ozone bias is shown on a flight by flight basis in Figure 9. Generally the bias in the lowest layers is less than 5ppbv, while the bias in the 8-12 km range is large, and particularly high in flights 3, 11, 15, 16, and 17. This is a reflection of the boundary

conditions from the global models. Tang et al. [2007] shows that boundary conditions varied greatly among global models, and depending on the global models used the ozone bias in the upper troposphere varied from large negative to large positive values, reflecting differences in the global models in placing stratospheric intrusion of ozone. To show how the model predictions changed from the forecast to post-analysis details for specific flights were also analyzed. Figure 10 shows how model performance improved during DC-8 flights 12 and 14 (July 25 and 31, 2004). The plots show that at low altitudes (0-1km) the model bias is reduced from 8 to 2 ppb for flight 14, and from 22 to 12 ppbv for flight 12, when using improved emissions. For the upper troposphere the model showed a large biases,(positive for flight 14, and negative for flight 12), which were decreased significantly by using updated boundary conditions from NCAR MOZART. This improvement is reflected in an increase in the correlation coefficients from 0.65 to 0.84 for flight 14, and from 0.01 to 0.78 for flight 12.

2.3 Analysis of model error

The relationship between model errors is a key step in understanding model behavior and identifying model deficiencies. This information is also becoming increasingly important as estimates of error covariance are an important aspect of chemical data assimilation [*Chai et al.*, 2007]. The ICARTT experiment produced observations for a large spectrum of species that are involved in the photochemical oxidant cycle. Thus it is possible to use these data to explore the relationships between the calculated and observed species concentrations with respect to ozone. In this section we analyze two relationships: the correlation of observed ozone concentrations with respect to other measured parameters, and the correlation of ozone bias (or error), with

respect to other species. Simultaneous analysis of these relationships provides valuable insight on ozone chemistry, and sources of model error.

2.3.1 Correlation between model biases.

Comprehensive field experiments such as ICARTT provide an opportunity to examine the complex relationships between the processes that govern ozone distributions in the troposphere. Towards these ends we examined the correlations between the observed ozone, and ozone bias to various species using the DC-8 data and the results are presented in Table 7. Shown are results for the post analysis simulation NEI2001-Frost LPS.

We first examine the relationships between ozone and other parameters using all the DC-8 flight data binned by altitude. Table 7 shows that the observed ozone concentrations at low altitudes (0-1km) are most strongly correlated to HNO_3 (R=0.86), ethyne (R=0.75), CO(R=0.70), acetone (R=0.68), MEK (R=0.65), NO_z (R=0.77), PAN (R=0.64) and NO_y (R=0.63). These species represent the general features important in photochemical production; i.e., precursor emissions of CO, NO_x and non methane hydrocarbons. The correlations are small for short lived species such as NO, propene and isoprene (-0.03, -0.06 and -0.03, respectively), reflecting that the DC8 observations when averaged over 3 minutes map out large spatial scales (i.e., 60 km) and thus represent air masses that have been photochemically aged for many hours. These relationships change with altitude, and the correlations decrease in value. For the 4-8km range, where only the nitrogenous species concentrations show the highest correlation to ozone, with NO_2 (R=0.48), NO_y (R=0.48), NO_z (R=0.47), and PAN (R=0.39). At higher

altitudes (8-12km) correlations HNO_3 (R=0.67), NO_z (R=0.42), NO_y(R=0.27) and with RH (R=-0.35) and CO (R=-0.24) are the highest.)

The decrease in correlations with altitude in the aggregate data reflects many factors, including the fact that the ozone relationships are driven by many processes with distinct correlations. For example stratospheric exchange and convection events result in very different and strong correlations, which show up when the data is first sorted by process, but are lost when all data representing all processes are analyzed together. The high correlations near the surface represent the dominance of the sources and photochemical production processes.

The correlations of the ozone bias with respect to the biases in other species are also shown in Table 7. In general the model biases show similar relationships between species as discussed above for the ozone observations. For altitudes < 1km PAN, CO, MEK, and HNO_3 are among the most highly correlated biases with respect to the ozone bias (0.6, 0.51, 0.48, and 0.47, respectively). The correlation relationships for the biases tend to extend up to ~ 4 km, above which the values tend to decrease. In the upper troposphere the correlation structure is very different than that at the surface, reflecting the different processes and the strong contribution of the boundary conditions to the biases. The simple correlation analysis discussed above shows the complex relationships between ozone and the ozone biases, with those relationships in the lower troposphere reflecting the emissions and the photochemical production processes. To better understand these relations, factor analysis was performed on the observational data, on the model predicted values, and on the biases. Factor Analysis (FA) is essentially a variable reduction of data sets consisting of large number of inter-correlated variables

into a small number of factors, which account for most of the variance in the original variables [*Kulkarni,* 2004]. This technique is frequently used in air quality studies to unravel the hidden source information from a rich ambient data set. It is particularly very useful for source apportionment studies when there is no prior information available about the nature of the major aerosol sources affecting a particular receptor station [*Seinfeld. et al.,* 1998]. Factor Analysis is extremely useful in identifying the relationships among variables that are driven by common processes such as sources, transport, and chemistry. In addition, the Factor Analysis approach is unaffected by errors in modeled emissions, chemistry, or transport [*Millet et al.,* 2006]. In this section, the results obtained by the application of the Factor Analysis to the observed values, the corresponding model predictions and the model errors for the DC-8 at altitudes below 1km are presented. The main objective of this analysis is to identify the underlying relationships between ozone and its other precursor species. All the analyses presented in this section were performed using SAS 9.0 software [*SAS Institute*, 2004]. All rows with missing values were deleted prior to performing the analysis, so all analysis uses identical sampling. The factors were extracted using Eigen value one criterion and the extracted factors were subject to the varimax rotation.

Figure 11 depicts the output obtained from FA analysis. We only show the factor that accounts for the highest variance among the retained factors in each analysis here. The top of Figure 11 in gray shows the factor for the observed species. This factor contains a spectrum of species related to ozone and its precursors, and clustering together those photochemical factors identified in Table 7. The center of Figure 11 in red shows the output from the same analysis conducted using the predicted values (NEI2001-Frost

LPS*). In general the factors identified by the model predictions show many similarities to those based on observations suggesting that the modeled processes are capturing many of the ozone relationships in the real atmosphere. The bottom of Figure 11 shows the output of the factor analysis performed for the model errors. The clustering of errors shows a structure similar to that for the species dependencies. Highest factor loadings appear for primary species such as CO, ethyne and ARO1, as well as for secondary species (the largest factor loading is for PAN). These underlying error structures provide guidance into further model improvements, such as continued improvements in emissions, and improvements in the chemical and physical processes controlling key species such as PAN and HCHO. Furthermore this error structure may also be useful in better definition in the error covariance estimates needed by modern data assimilation techniques as discussed in Chai et al. [2007].

2.3.2 Bias in a regional context

Geographical context is given to the point bias estimations (modeled-observed) by interpolating them through Kriging, generating a continuous surface. Data was restricted to the 0-4km range, for all DC-8flights. The previous section suggested which variables need to be improved to lower ozone bias. The interpolated bias surface gives guidance towards where model bias needs to be improved, and qualitatively how changes in modeled inputs affect the bias. The surface of ozone bias is shown in Figure 12 . For the forecast (left panel) we observe that during the forecast there was a positive bias in the Central and Eastern United States with bias in the range of 10-50%. The biases in CO, NO_y, NO_x, HNO_3, and PAN, which showed strong correlation with ozone bias as discussed previously, were also analyzed. Wherever ozone presented a positive bias in

the forecast CO (Figure 12, left panel), NO_x, NO_y, and HNO_3 (Figure 13, left panels) also presented positive biases. This is particularly clear for NO_y (Figure 13, center left panel) where the bias in some regions of Ohio, North Carolina and Virginia are as large as 300-400%. When the emission inventories were modified, updating to NEI 2001 and the large point sources (Frost LPS), the ozone bias decreased to ~ 5-10% across the domain (Figure 12, top center panel). The bias in CO was reduced through the continental U.S., along with the bias of NO_y. However a positive systematic bias persisted for ozone and NO_y, and its components, in portions of the domain.

The effect of changes in the dry deposition velocities is also apparent for the bias plots for ozone and HNO_3. In the regions dominated by agricultural crops (i.e., the central US) the biases of ozone and HNO_3 are significantly reduced. For those species with low dry deposition rates the effect on bias reductions are small (CO and NO_x). For example, North and South Dakota, regions with negligible changes in NO_x emissions between NEI 1999 and 2001 where ozone bias decreased from 20-50% to -5 to 5%.

As a sensitivity study aimed to further reduce the bias, an additional simulation was conducted with a 60% decrease of NO_x area emissions (12% reduction of total NO_x emissions) for Alabama, Mississippi, Georgia, North Carolina, South Carolina, Tennessee, West Virginia, Indiana, and Ohio, chosen since these states presented the highest bias in NO_y, NO_x, and HNO_3 according to the Kriging results. The results of this run showed enhancement of correlation factors for nitrogen species (Tables 5 and 6), particularly for HNO_3, and NO_y, while decreasing their positive bias. As shown in Figure 12, top right panel, the ozone bias decreased to a range of -10 to 10% for most of the continent, with large portions showing bias in the -5 to 5% range. The offshore ozone

positive bias persists, but to lesser geographical extent, and lower magnitude than the NEI 2001 scenario, and the forecast scenario. NO_y for this same scenario decreases its regional bias to less than 100% over large portions of the domain (Figure 13, center panel). Figure 13 (bottom right panel) shows that HNO_3 bias also decreases significantly with the updated and modified emissions, with some areas presenting a negative bias. Figure 13 (top right panel) shows that NO_x bias decreased in South Carolina, North Carolina, and Virginia from 200-400% to -30 to 50%, in accordance to locations where the ozone bias was decreased.

Special notice must be taken Figure 13 (bottom panels), which shows that forecast CO, using NEI1999 presented positive biases of 30-50% for the Western portion of the United States, which decreased to 20-30% using the NEI 2001. Negative CO bias over Michigan decreased from -30 to -20% to -20 to -10% as a result of improved boundary conditions. The offshore Atlantic positive CO bias decreased from 30-50% to the 10-30% range and from 10-20% to -10 to 10% for the Southeastern US. These changes are due largely to changes in emissions as this region is largely under outflow conditions for the period of study.

2.4 Discussion

2.4.1 Sensitivity analysis

As illustrated in Figure 3 a variety of sensitivity studies were performed to investigate the sensitivity of the model to other important parameters. The most significant parameters studied in terms of reduction of model bias, dry deposition, emissions, and boundary conditions, have been discussed previously. In terms of near surface ozone the largest impacts are due to dry deposition velocities and emissions, with

each contributing equally to the bias reduction. In the mid to upper troposphere, the boundary conditions dominated the improvements.

Simulations were also performed for the Eastern US using a 12km horizontal resolution. The biggest impact was found near the surface for the 12km resolution. For the 0-1km range the mean for the WP-3 increased by 3ppb with a slight increase in correlation to (R=0.71). For CO the 12 km resolution increased the mean value by 5ppb and also increased the correlation coefficient. Biogenic emissions represent an additional source of uncertainty. We repeated a simulation using the BIES3 biogenic emissions algorithm, which led to higher biogenic emissions. Under these conditions the near surface ozone increased by 1 ppbv throughout the Eastern US and CO by 10 ppbv.

2.4.2 Ozone production efficiency

Up to now we have shown that the ozone bias was strongly correlated to NO_z and NO_y bias. We have also discussed that there is geographical concordance of ozone bias with NO_z bias. Previous work has related ozone and NO_z [*Kleinman*, 2005; *Trainer et al.*, 1993], in a relationship for ozone production efficiency (OPE), which for the purposes of this analysis is the slope of the plot of odd oxygen (NO_2+O_3) to NO_z. In Figure 14 the ozone production efficiency for the observed and predicted values for data points less than 4000 m is plotted. For the DC-8 data the observed OPE is 7.8, while the forecast, NEI2001-Frost LPS, and NEI2001-Frost LPS* cases have OPE's of 6.7, and 7.8, respectively. The observed ozone production efficiency for the DC-8 data suggests efficient formation of ozone, typical of NO_x limited conditions. The ozone production efficiency in the area sampled by WP-3 is lower than the DC-8 (Observed OPE=3.49,

Modeled OPE=5.28), which reflects the fact that the area sampled was closer to emission source regions in the North East.

2.4.3 Model sensitivity to emissions

The fact that the modeled and observed production efficiencies are similar suggests that the underlying ozone relationships of the model are reasonably well represented, and therefore that the results of sensitivity studies may be meaningful. Further insights into ozone production can be seen by comparing the change in ozone to changes in emissions. The mean predicted near surface ozone (0-1km) values for the NEI 2001 Frost LPS* is shown in Figure 15 , in which higher values are found in California, Arizona, and the Atlantic states. The sensitivity of O_3 to emissions of precursors is also shown in Figure 16 . These simulations were done for the period of July 21 to August 18, 2004, in the absence of anthropogenic VOCs, CO, and reduced NO_x. The contribution of each precursor is calculated as the difference between the average daytime surface ozone concentration in the presence of a precursors minus the concentration in the absence of the precursor, normalized by the total yearly emissions of the precursor (ppb ozone formed/(Tg precursor/year)). Ozone formation is most sensitive to changes in NO_x (as is also shown in Figure 15), especially in the Midwest, where ozone per Tg of NO_x/year increases by 10-20ppbv (Note that NO_x sensitivity was calculated based on 30% reduction of total NO_x). For reference, 1 Tg of NO_x/year is roughly equivalent to the emissions of 28 coal fired power plants of 2500MW (36,000 tonnes NO_x/year each) [*Miller and Van Atten,* 2004]. In the Northeast US ozone is equally sensitive to NO_x and anthropogenic VOCs, while in large parts of the western US, ozone is more sensitive to VOCs. CO effects are similar to VOCs, but smaller on a per Tg/year basis. Since CO

emissions are larger than VOCs, total CO effects on ozone can be in the same order of magnitude. Figure 16 shows that VOCs and CO contribute to a large portion of ozone formation in portions of the Northeast United States.

As pointed out above, NO_x plays an important role in ozone production. Furthermore an appreciable fraction of NO_y is composed of PAN (representing ~ 20% near the surface and ~50% at 6-8 km altitudes, Figure 6), and ozone levels and errors were shown to be significantly correlated with those for PAN. PAN plays important roles as both a key photochemical product and as a reservoir for NO_x. To assess the role of PAN on ozone production we conducted a simulation where PAN levels within the regional domain (but not in the boundary conditions) were continuously set to zero. In this way the formation of PAN was allowed, but the thermal decomposition source of NO_x was blocked, by setting PAN concentrations consistently to zero. The impact of PAN on predicted mean surface ozone for the month of July is shown in Figure 17, right panel. This indirect ozone production pathway of PAN via production of NO_x is estimated be over 20% throughout the continental US with large regions with values between 30-50%. This impact extends to all altitudes with values exceeding 8% throughout the domain at an altitude of 5.6 km. Differences become small above this height as the PAN levels are dominated by the boundary conditions values, which were not changed, and the low rates of PAN thermal decomposition due to cool temperatures. The results point out the importance of accurately predicting PAN levels, which requires the close coupling between the regional and global models, as PAN sources and sinks reflect process occurring throughout the vertical extent of the atmosphere and over large geographic scales. Figure 17, left panel, shows results for a sensitivity analysis where the

formation of PAN itself is blocked. As PAN is a reservoir for NO_x under these conditions, with its formation pathway is blocked, a greater fraction of NO_x is oxidized into nitric acid, with the net effect of more ozone being formed. Mean surface ozone concentration increases up to ~7ppb.

2.5 Conclusion

The comprehensive ICARTT aircraft observations were used to evaluate and improve ozone prediction for the STEM model by simultaneously analyzing model performance with conventional statistics, mean vertical profiles, and geospatial interpolation to provide a comprehensive three dimensional context on model performance, laying the groundwork for subsequent model improvement.

The STEM model forecasts of ozone were found to have a significant positive high (overprediction) bias near the surface and a large negative bias in the upper troposphere. These biases were due in part to model errors, which included the use of outdated emissions in the forecasts (i.e., the use of NEI 1999 emissions) out of season dry deposition velocities for agricultural crops, and the use of global model boundary conditions (BCs) that were based on climatological biomass burning emissions. Post analysis simulations were conducted using corrected dry deposition velocities, NEI 2001 inventory with point source emissions updated to 2004, and BCs from global models using biomass burning emissions reflective of 2004 fire activity. These changes resulted in a decrease in low altitude (0-1km) mean ozone bias from 11.21 to 1.45 ppbv in comparison to DC-8 observations and from 8.26 to -0.34 ppbv for the WP-3 data. The upper troposphere ozone negative bias persisted, but was reduced in magnitude. In

addition the post analysis simulations resulted in a nearly unbiased distribution of ozone errors with a significant reduction in the standard deviation of ozone errors.

A series of analyses were performed to study the structure of the ozone errors. These included the correlation of ozone errors with errors in other species. In general the model ozone errors show high correlation for altitudes < 1km with the errors in PAN, CO, MEK, and HNO_3. These correlation relationships for the biases tended to extend up to ~ 4 km, above which the values decreased. To better understand the relationships among these errors, factor analysis was applied. The clustering of errors shows a structure similar to that for the species dependencies, and included contributions from meteorological features of temperature and RH, precursor species such as CO, ethyne and aromatics, as well as photochemical products such as HNO_3, PAN, H_2O_2 and HCHO.

The spatial distribution of the model errors were examined using Kriging. The geospatial distribution of forecast errors identified distinct features, which when compared to the errors in the post analysis simulations, helped document model improvements. For example, changes in the dry deposition to crops was shown to reduce substantially the high bias in the forecasts in the Midwest, while the updated emissions accounted for the decrease in bias in the eastern US. In addition, improvements in boundary conditions from global models, which accounted for biomass burning emissions, improved model performance for CO in the upper troposphere, in comparison to the forecast stage.

Nitrogen species, namely NO_y, NO_z, and HNO_3 showed positive bias during forecast stage, which decreased during post-analysis. Reductions in these biases due largely to emission changes resulted in reduction of ozone bias, especially in the 0-4km

range. However a persistent high NO_y bias suggests that the NEI 2001 NO_x emissions are still overestimated. Kriging was shown to provide a geospatial analysis of these biases, and to provide information that can help guide further regional modification of emissions.

Predicted ozone production efficiency (OPE) was studied and shown to be similar to the observed OPE (calculated values of OPE of 7.83 in comparison to observed OPE of 7.79 for the DC-8). The OPE for the WP-3 (observed 3.49, modeled 5.28) was lower than for the DC-8, suggesting that the area sampled by the WP-3 was closer to the source regions of NO_x.

Simulations with perturbed emissions found ozone formation to be most sensitive to changes in NO_x, especially in the Midwest, where ozone per Tg of NO_x/year increases by 10-20ppbv. However in the Northeast US ozone was found to be equally sensitive to NO_x and anthropogenic VOCs, while in large parts of the western US, ozone was more sensitive to VOCs. CO effects were found to be similar to those for VOCs, but smaller on a per Tg/year basis. Since CO emissions are larger than VOCs, total CO effects on ozone can be in the same order of magnitude.

The results presented here help demonstrate how more detailed analysis of errors can improve model performance. These results also point out that the underlying error structure is complicated, but that the underlying error structure can provide guidance into further model improvements, such as continued improvements in emissions, and improvements in the chemical and physical processes controlling key species such as PAN and HCHO. Furthermore this error structure may also be useful in better definition in the error covariance estimates needed by modern data assimilation techniques.

Table 3 Total column emissions in model domain, in Tg/year, including point source, area, and aviation emissions (CO emissions reported as Tg C/year, and NO_x emissions as Tg N/year)

	Emissions (Tg/year)		
	CO (as CO)	NOx (as N)	VOCs (as C)
NEI 1999	40.7	7.1	15.7
NEI 2001	25.0	5.2	13.5
NEI 2001-Frost LPS	26.8	4.8	13.8
NEI 2001-Frost LPS*	26.8	4.2	13.8

Table 4 Summary of model parameters for scenarios studied during forecast and post-analysis

Scenario	Parameters					
	National Emissions Inventory	Biogenic Emissions	Boundary Conditions	Lightning NO_x	Dry Deposition	Meteorology
Forecast	1999	BEIS 2	MOZART-GFDL, climatological fires	no	dormant agricultural lands	MM5 and forecasted AVN global model
NEI2001-Frost LPS[a]	2001, Frost Large Point Sources. VOCs adjusted by increasing alkanes and alkenes, and decreasing aromatics.	BEIS 2	MOZART NCAR, burned area biomass burning emissions [*Pfister et al.*, 2005]	yes	nondormant agricultural lands	MM5 and NCEP FNL reanalyses

[a]Parameters for NEI2001-Frost LPS* are the same but reducing area NO_x emissions by 60% for Alabama, Mississippi, Georgia, North Carolina, South Carolina, Tennessee, West Virginia, Indiana, and Ohio.

Table 5 Model performance statistics for selected species: Modeled vs. Observed data, DC-8 Platform

	O_3				CO				NO_y			
	0-1km											
	Forecast	Frost LPS	Frost LPS*	Obs	Forecast	Frost LPS	Frost LPS*	Obs	Forecast	Frost LPS	Frost LPS*	Obs
Mean modeled (ppbv)	60.12	51.82	50.36	48.92	148	136	136	138	4.16	3.24	2.95	1.85
mean bias (ppbv)	11.21	2.90	1.45	-	9.75	-2.48	-1.84	-	2.70	1.40	1.11	-
S.D./Mean modeled	0.39	0.34	0.33	0.33	0.36	0.29	0.27	0.28	0.77	0.66	0.67	0.92
R	0.71	0.70	0.72	-	0.61	0.68	0.68	-	0.59	0.59	0.56	-
	1-4km											
Mean modeled (ppbv)	58.97	54.68	53.32	57.34	131	127	125	119	2.76	2.26	2.09	0.93
mean bias (ppbv)	1.63	-2.66	-4.02	-	11.37	5.20	5.82	-	1.83	1.36	1.19	-
S.D./Mean modeled	0.31	0.26	0.25	0.20	0.14	0.11	0.11	0.26	0.87	0.74	0.72	0.88
R	0.40	0.48	0.50	-	0.49	0.65	0.65	-	0.49	0.52	0.51	-
	4-12km											
Mean modeled (ppbv)	63.71	67.97	67.89	80.20	79	85	85	98	0.46	1.43	1.43	1.05
mean bias (ppbv)	-16.49	-12.23	-12.31	-	-19.37	-12.64	-12.60	-	-0.59	0.43	0.42	-
S.D./Mean modeled	0.01	0.00	0.00	0.01	0.00	0.00	0.00	0.20	1.25	1.37	1.37	0.60
R	0.56	0.47	0.47	-	0.06	0.33	0.33	-	-0.13	0.10	0.10	-

*Modified area NO_x emissions, SD: Standard deviation

Table 6 Model performance statistics for selected species: Modeled vs. Observed data, WP-3 Platform

	O_3				CO				NO_y			
	0-1km											
	Forecast	Frost LPS	Frost LPS*	Obs	Forecast	Frost LPS	Frost LPS*	Obs	Forecast	Frost LPS	Frost LPS*	Obs
Mean modeled (ppbv)	64.52	57.60	55.93	56.27	202.81	163.56	164.49	158.60	7.77	5.03	4.79	3.91
mean bias (ppbv)	8.26	1.34	-0.34	-	44.24	4.96	5.89	-	3.87	1.12	0.88	-
S.D./Mean modeled	0.38	0.31	0.30	0.35	0.31	0.24	0.24	0.24	0.65	0.63	0.65	0.72
R	0.63	0.66	0.69	-	0.43	0.42	0.42	-	0.28	0.29	0.29	-
	1-4km											
Mean modeled (ppbv)	65.07	62.05	59.59	60.16	164.04	143.34	144.46	135.66	5.00	3.58	3.34	2.38
mean bias (ppbv)	4.91	1.89	-0.58	-	28.37	7.67	8.79	-	2.62	1.20	0.96	-
S.D./Mean modeled	0.34	0.27	0.26	0.23	0.38	0.28	0.28	0.34	0.86	0.71	0.73	0.88
R	0.57	0.63	0.65	-	0.52	0.66	0.66	-	0.64	0.64	0.65	-
	4-6km											
Mean modeled (ppbv)	50.61	59.74	58.97	66.80	92.08	101.37	101.77	106.66	0.82	1.34	1.29	1.13
mean bias (ppbv)	-16.19	-7.06	-7.83	-	-14.57	-5.28	-4.88	-	-0.31	0.21	0.16	-
S.D./Mean modeled	0.14	0.20	0.19	0.16	0.13	0.24	0.24	0.33	0.67	0.62	0.64	0.35
R	0.15	0.44	0.46	-	0.11	0.36	0.36	-	0.24	0.40	0.39	-

SD. Standard Deviation.

Table 7 Correlation coefficients of observed parameters versus observed ozone, and bias (modeled-observed) of parameters to ozone bias, at different altitude ranges, for DC-8 platform (Bias calculated with respect to NEI2001-FrostLPS)

Compound	Observation Correlation Coefficients				Bias Correlation Coefficients.			
	0-1km	1-4km	4-8km	8-12km	0-1km	1-4km	4-8km	8-12km
Acetone	0.68	0.21	0.11	-0.12	0.42	0.15	0.10	-0.14
ARO2	-0.02	0.11	0.31	-	0.04	0.04	0.89 (n=6)	-0.95
ARO1	0.47	0.40	0.01	0.07	0.09	0.07	0.13	0.02
Acetaldehyde	0.38	-0.07	0.04	0.10	0.24	0.20	-0.07	0.12
CO	0.70	0.44	0.08	-0.24	0.51	0.44	0.19	-0.32
Ethene	0.24	0.06	-0.04	-0.07	0.04	-0.05	0.02	-0.05
Ethyne	0.75	0.48	0.14	0.00	0.18	0.25	0.26	-0.07
H_2O_2	0.51	0.24	-0.29	-0.28	0.28	-0.01	-0.27	-0.29
Formaldehyde	0.53	0.07	-0.09	-0.12	0.20	0.11	0.18	-0.04
HNO_3	0.86	0.50	0.19	0.67	0.47	0.45	0.44	0.36
HO_2	0.48	0.23	-0.14	-0.28	0.15	0.09	0.14	-0.10
Isoprene	-0.03	-0.03	-0.19	-	-0.48	-0.38	-0.34	-
MEK	0.65	0.17	0.08	-0.14	0.48	0.44	0.11	-0.03
NO	-0.03	-0.06	0.19	-0.04	-0.17	0.07	0.10	0.04
NO_2	0.15	0.07	0.48	0.14	-0.07	0.20	0.20	0.10
NO_y	0.63	0.30	0.48	0.27	0.34	0.55	0.39	0.10
NO_z	0.77	0.37	0.47	0.42	0.45	0.57	0.50	0.28
OH	0.55	0.24	0.23	0.12	0.24	0.23	-0.09	-0.01
PAN	0.64	0.46	0.39	0.03	0.60	0.64	0.43	-0.05
Propane	0.40	0.16	0.06	-0.10	0.14	0.14	0.01	-0.10
Propene	-0.06	0.05	0.06	-	-0.25	-0.12	0.13	-
RH	-0.21	-0.38	-0.28	-0.35	-0.14	-0.05	-0.03	-0.08
SO_2	0.28	0.12	0.09	0.04	0.07	0.35	0.17	-0.01

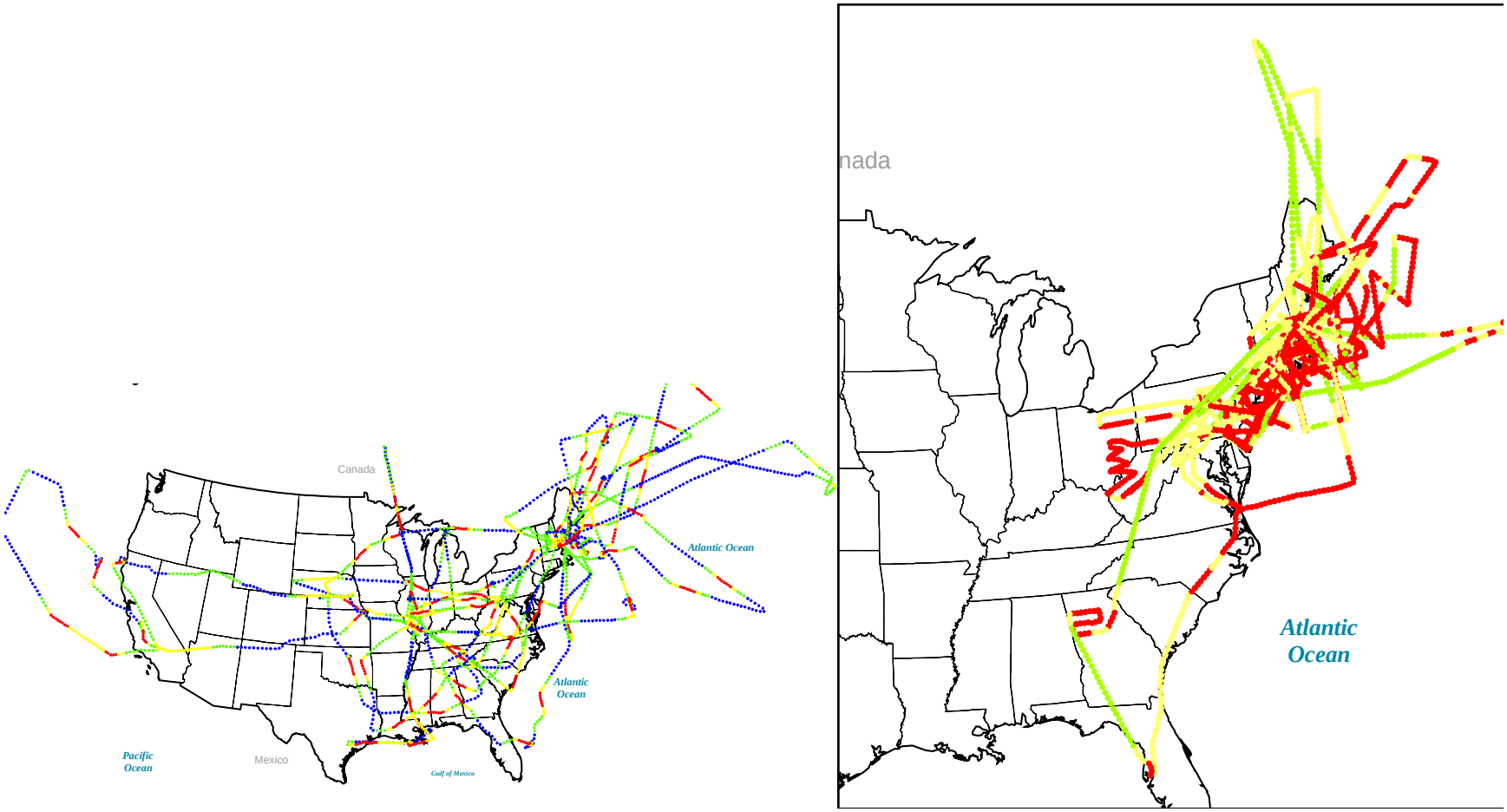

Figure 2 Flight tracks and altitude range for ICARTT: Red 0-1km, Yellow: 1-4km, Green: 4-8km, Blue: 8-12km (Left: DC-8, Right: WP-3)

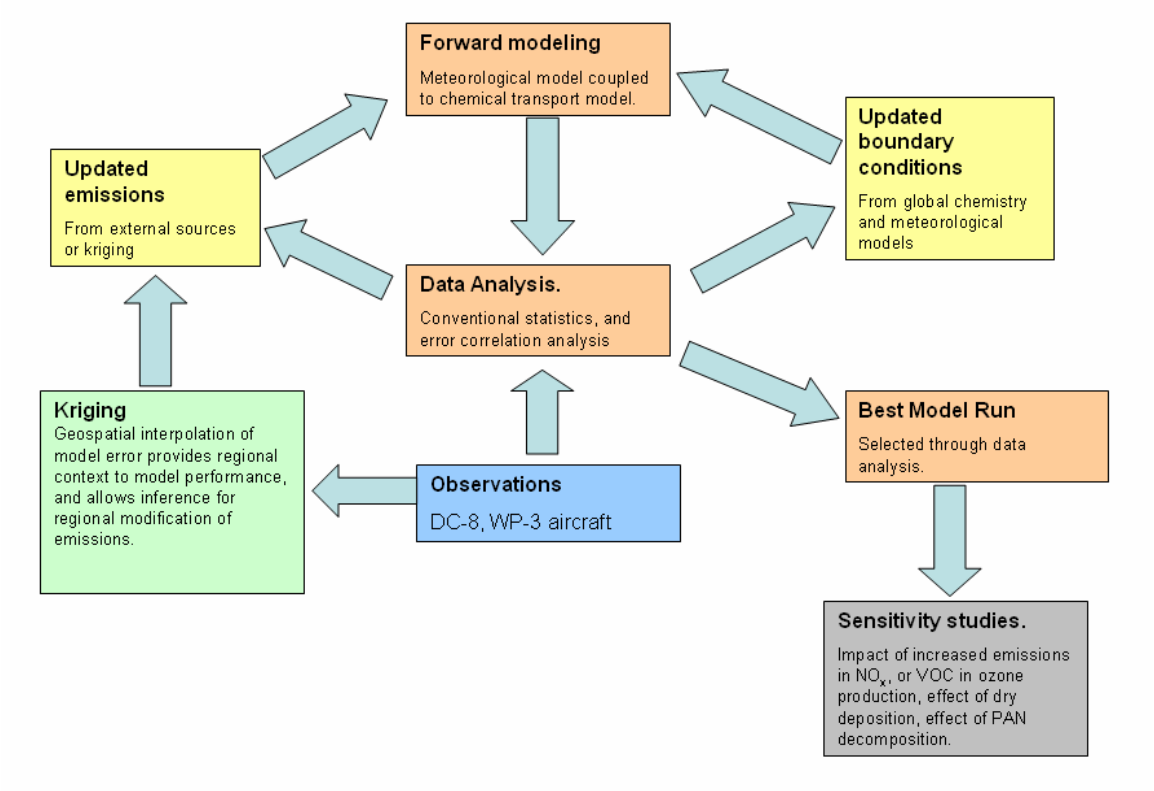

Figure 3 Study framework for data analysis and sensitivity studies

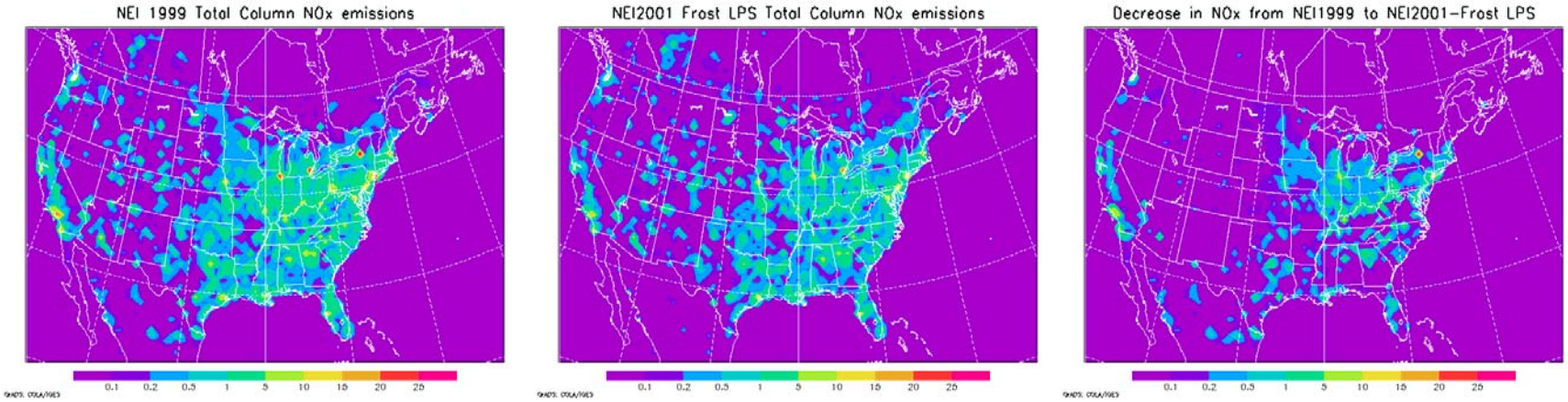

Figure 4 Total Column NO_x emissions Left: NEI 1999, Center: NEI 2001-Frost LPS emissions, Right: Decrease in NO_x emissions from NEI 1999 to NEI 2001- Frost LPS (Scale in tonnes/km^2/year)

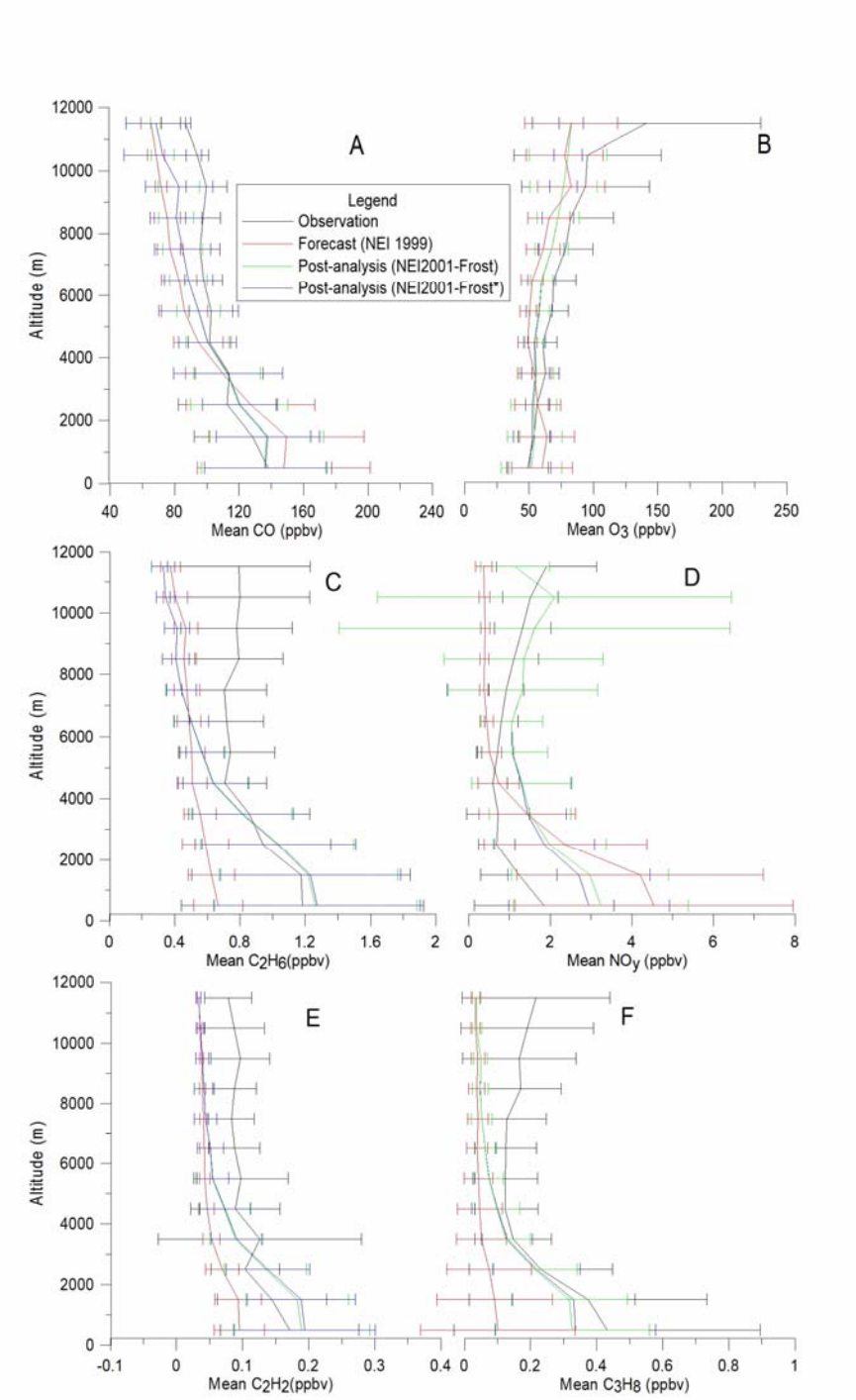

Figure 5 Observed and 60km-simulated O_3, CO, and NO_y vertical profiles and standard deviations for all DC-8 flights. A.) CO. B.) O_3 C.) Ethane D.) NO_y E.) Ethyne F.) Propane. Blue: NEI 2001-Frost LPS*. Red: Forecast, NEI 1999. Black: Observed

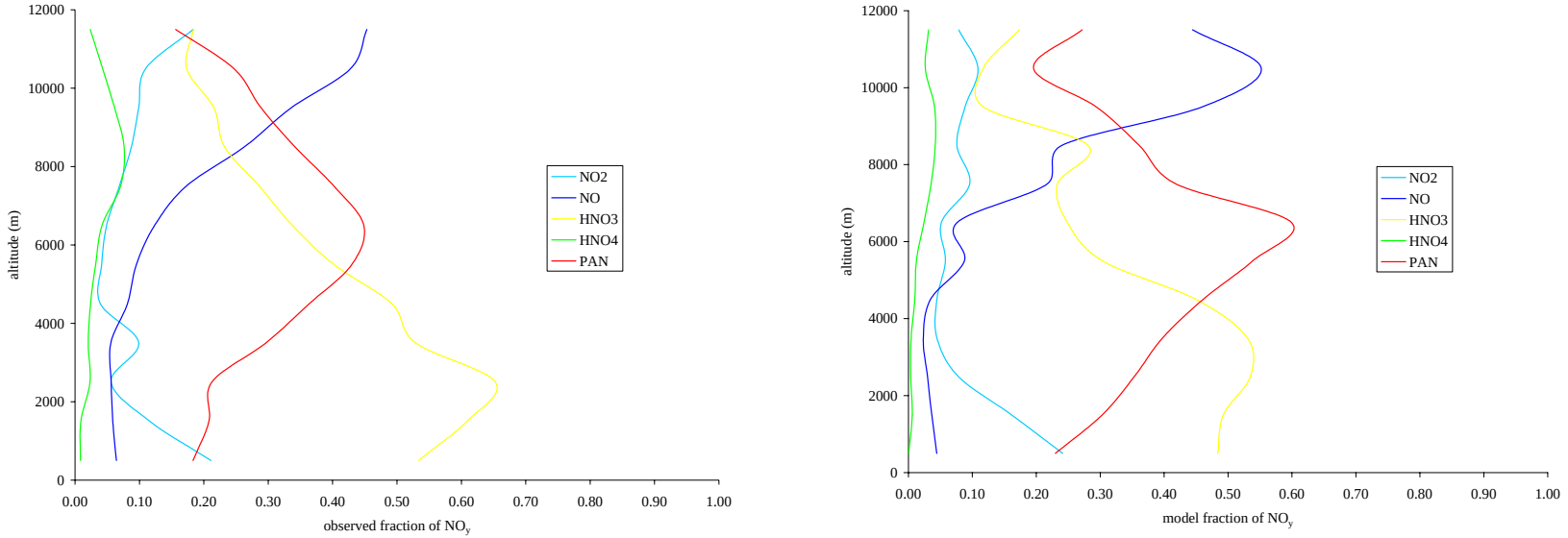

Figure 6 Comparison of mean contributions to NO_y along the DC-8 flight tracks as a function of altitude. Left: observed values; Right: predicted for the NEI2001-Frost-LPS case. Values are plotted as fraction of total NO_y, defined as the sum of NO_2, NO, HNO_3, HNO_4, and PAN

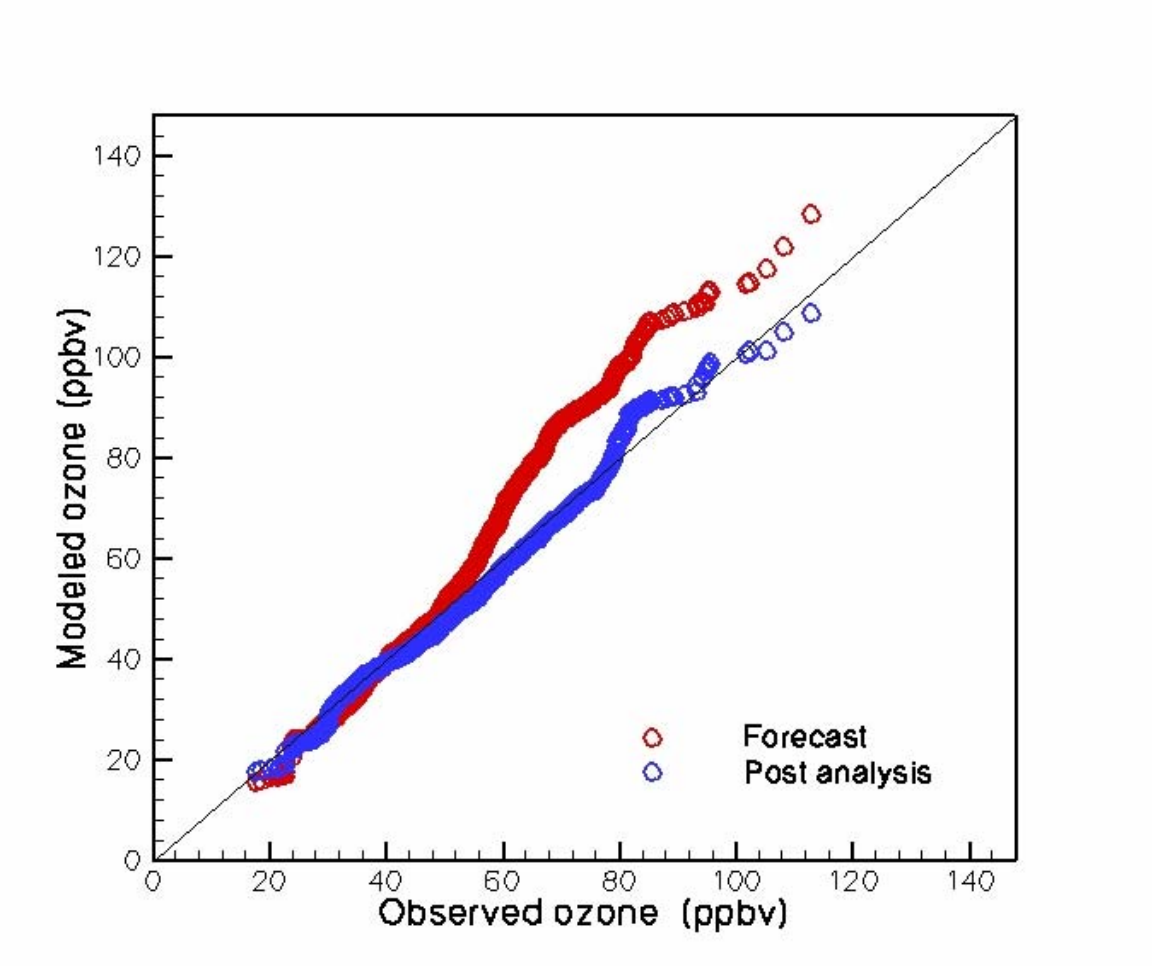

Figure 7 Quantile-quantile plot of modeled ozone with observed ozone for DC-8 platform, data points collected at altitude less than 4000m, STEM-2K3, Forecast: NEI 1999, Post Analysis: NEI2001-Frost LPS*. MOZART-NCAR boundary conditions

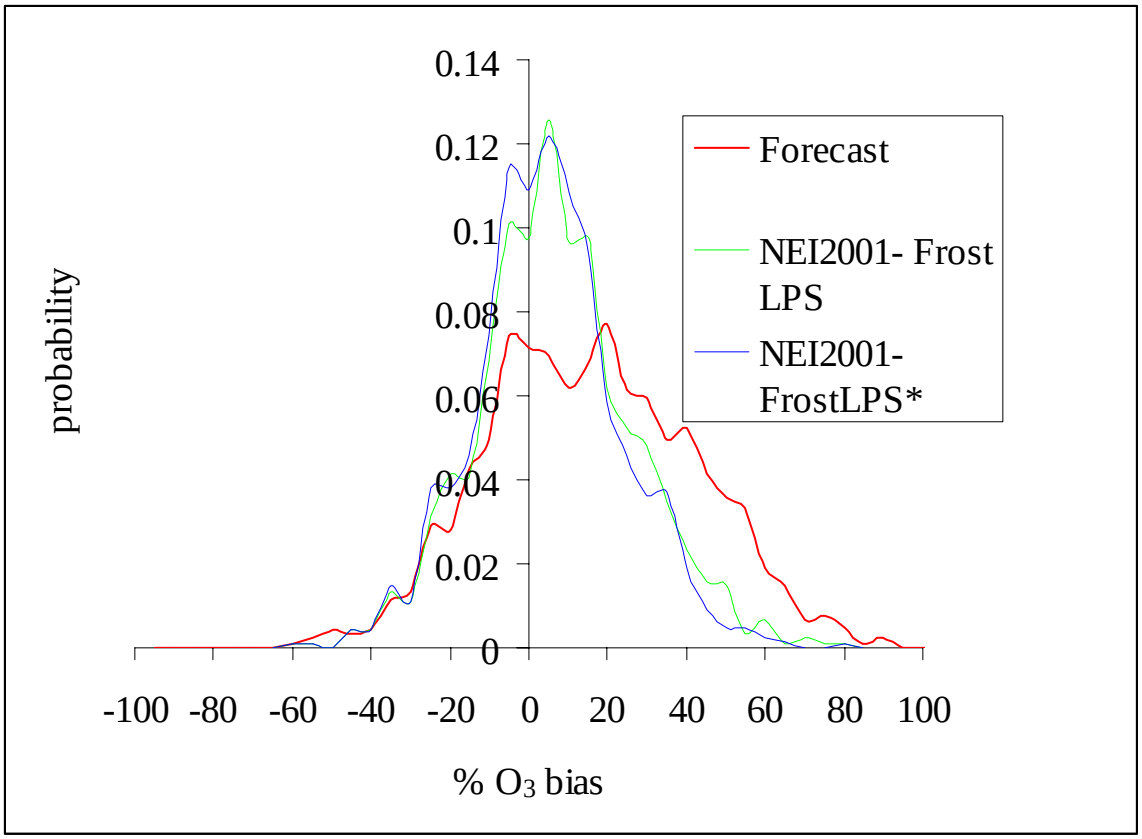

Figure 8 Probability distribution of % ozone bias for Forecast (NEI 1999) and post analysis runs (NEI2001-FrostLPS and NEI2001-FrostLPS*) for DC-8 measurements under 4000m

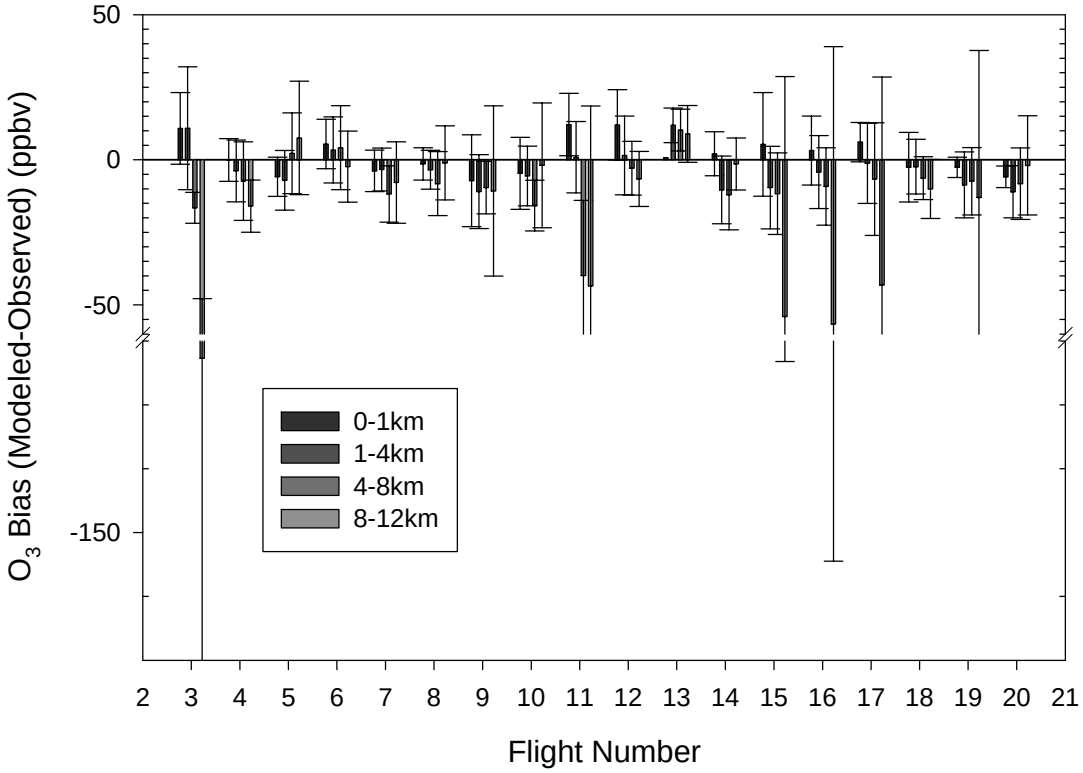

Figure 9 Mean ozone bias for DC-8 flights 3-20, separated by altitude range. NEI2001-FrostLPS* case. Error bars represent standard deviation

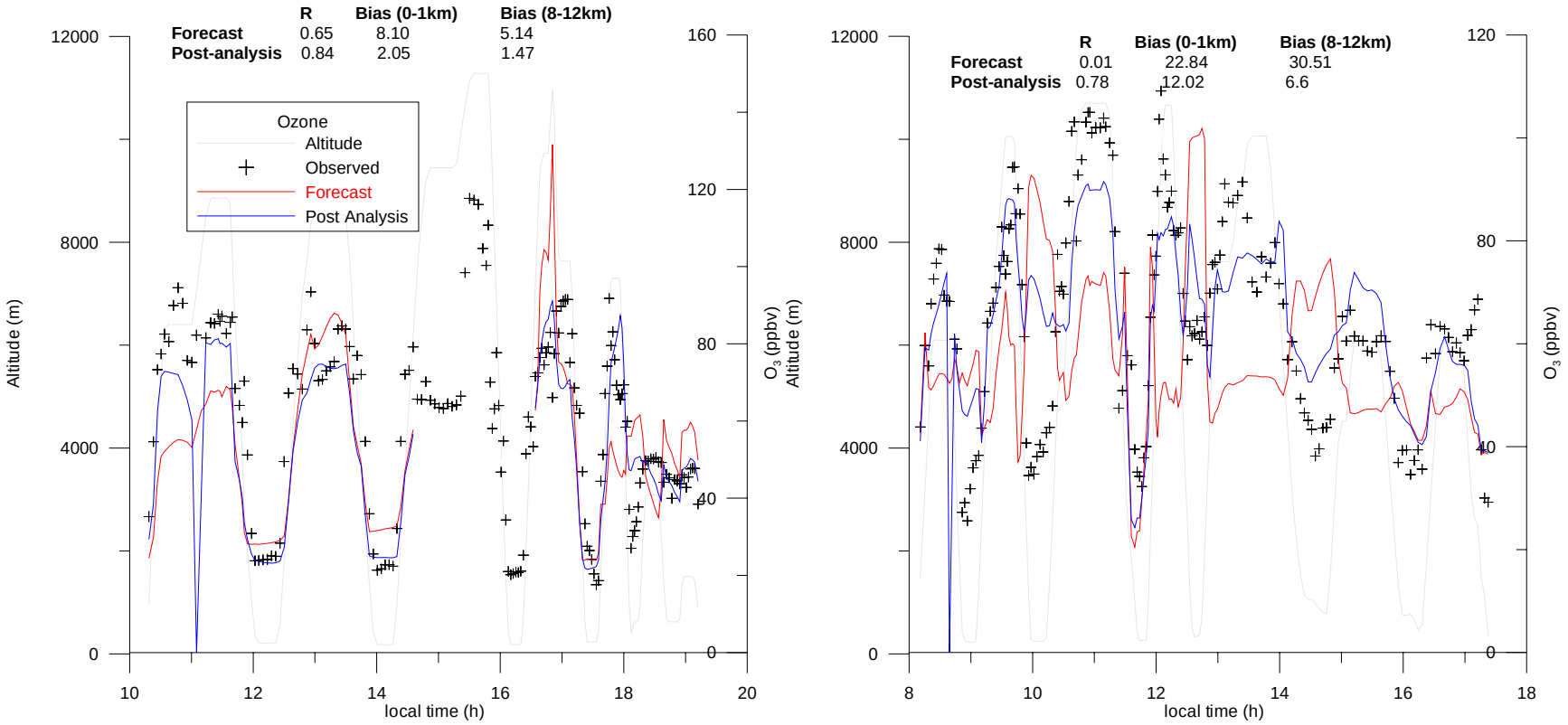

Figure 10 Time series of observed and modeled ozone along Left: DC-8 Flight 14 flight track (July 31, 2004). Right: DC-8 Flight 12 track (July 25, 2004). Absence of modeled data denotes that flight went beyond model boundaries. Forecast run: NEI 1999, MOZART boundary conditions. Post analysis: NEI 2001-Frost LPS*, RAQMS boundary conditions

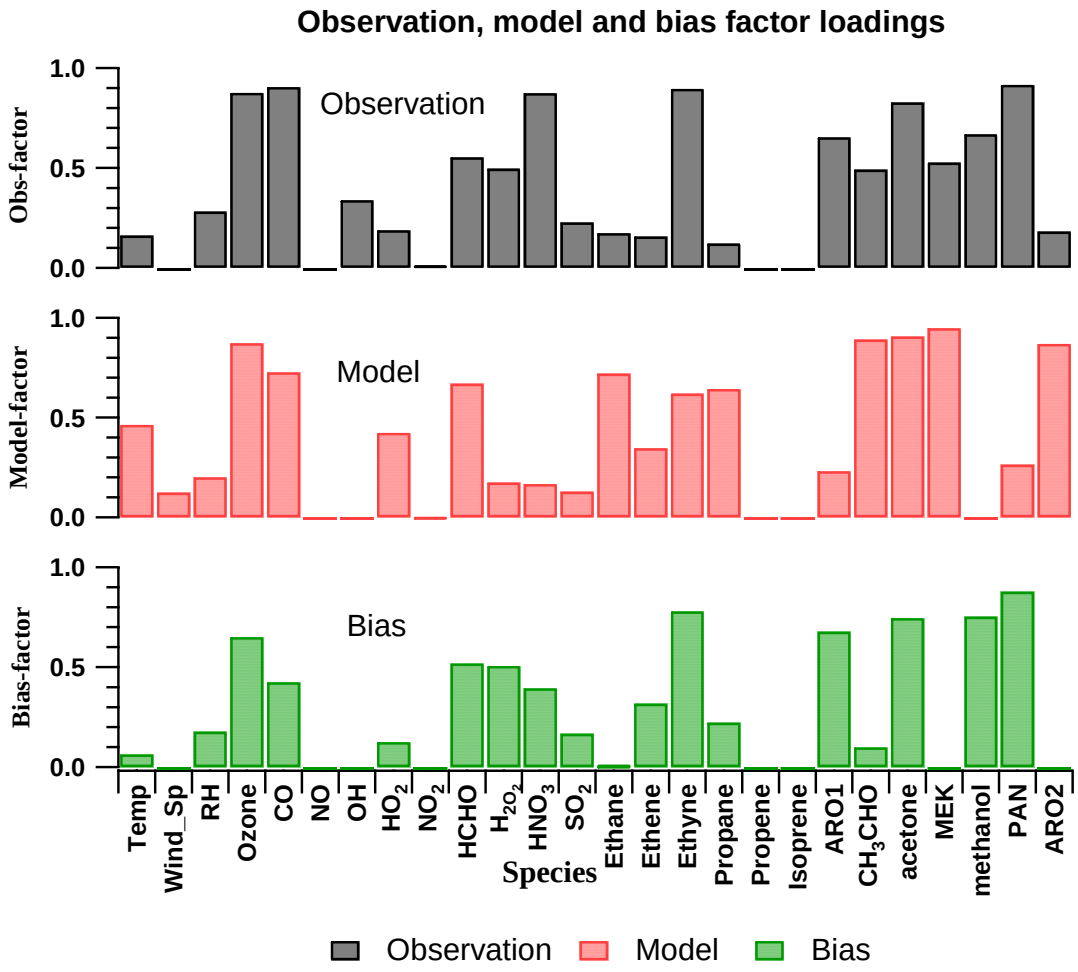

Figure 11 Factor analyses for DC-8, points in 0-1km range. Top: Observations. Center: Model. Bottom: Bias of model with respect to observations. Factor criteria – Eigen value one, varimax rotation

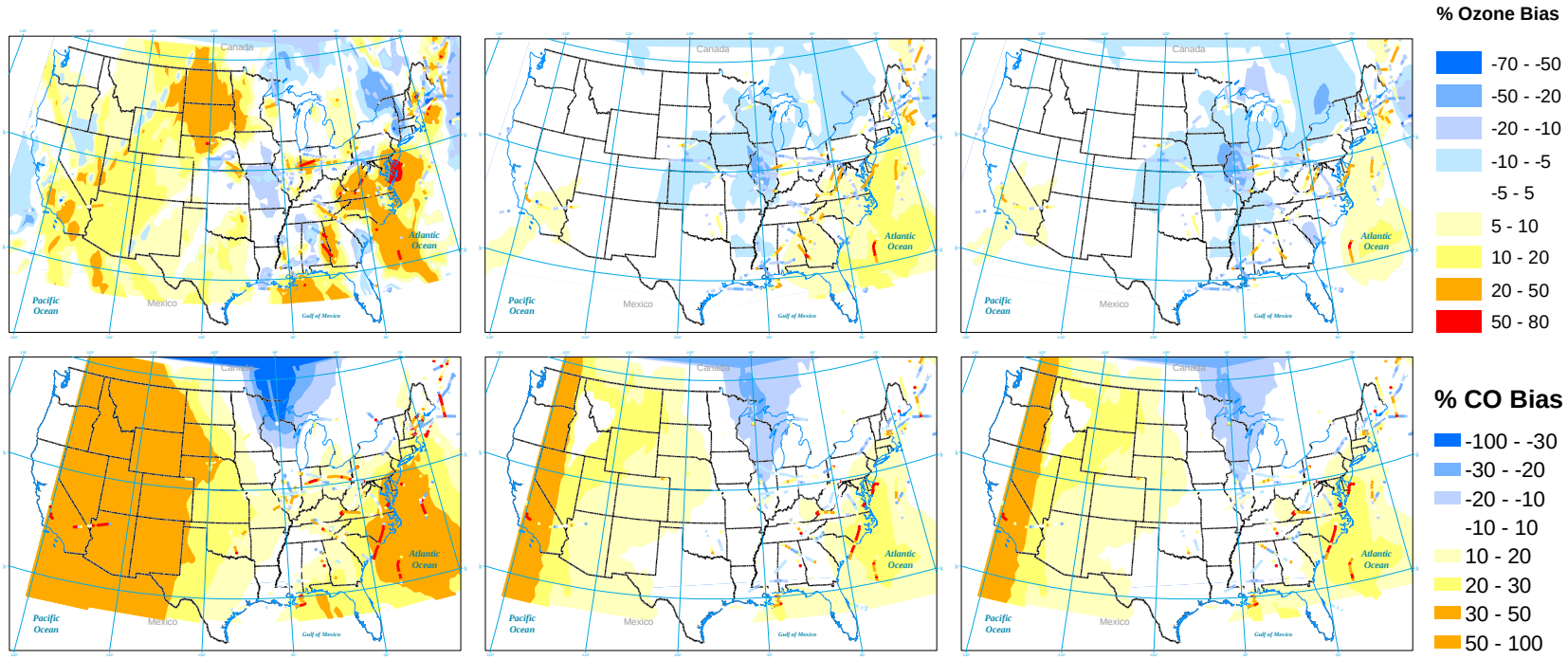

Figure 12 Kriged ozone (n=1208) and CO (n=1001) percent bias (modeled-observed) for alt<4000m, DC-8 platform, Top: Ozone. Bottom: CO. Left Panels: Forecast, NEI 1999 Center Panels: NEI 2001-Frost LPS. Right panels: NEI 2001-Frost LPS*

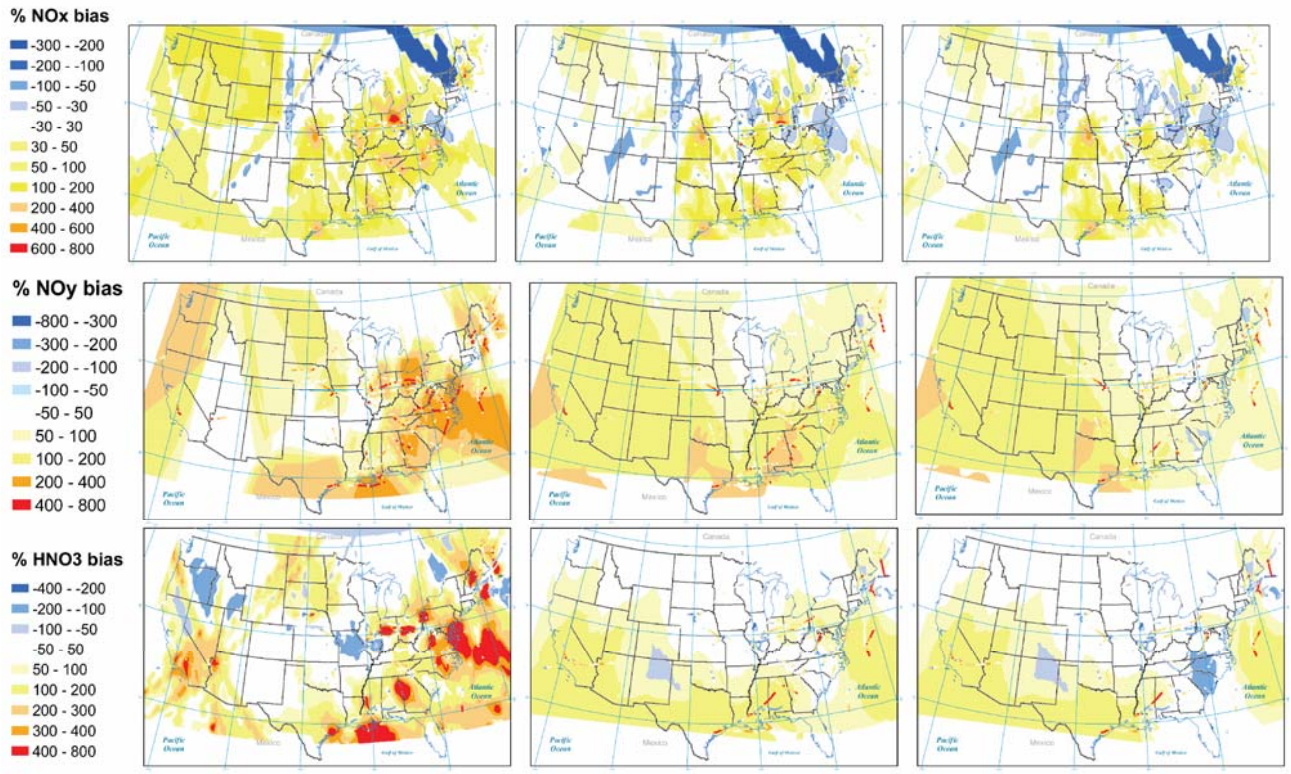

Figure 13 Kriged NO_x (n=1028) and NO_y (n=902) and HNO_3 (n=1157) percent bias (modeled-observed) for alt<4000m, DC-8 platform, Top: NO_x. Center: NO_y . Bottom: HNO_3. Left Panels: Forecast, NEI 1999 Center Panels: NEI 2001-Frost LPS. Right Panels: NEI 2001-Frost LPS*

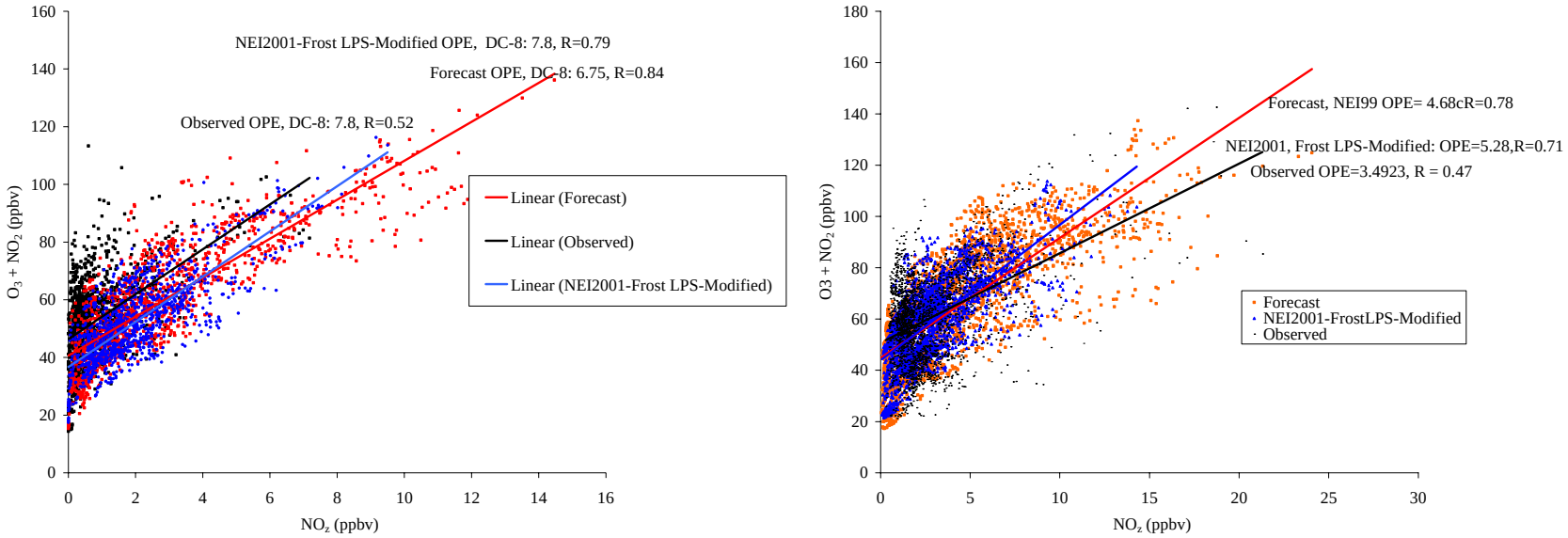

Figure 14 Observed and Modeled Ozone Production Efficiency (OPE). Left: DC-8. Right: WP-3 for data points with altitude<4000m, all flights. Red: Forecast, NEI 1999. Blue: NEI 2001-Frost LPS*

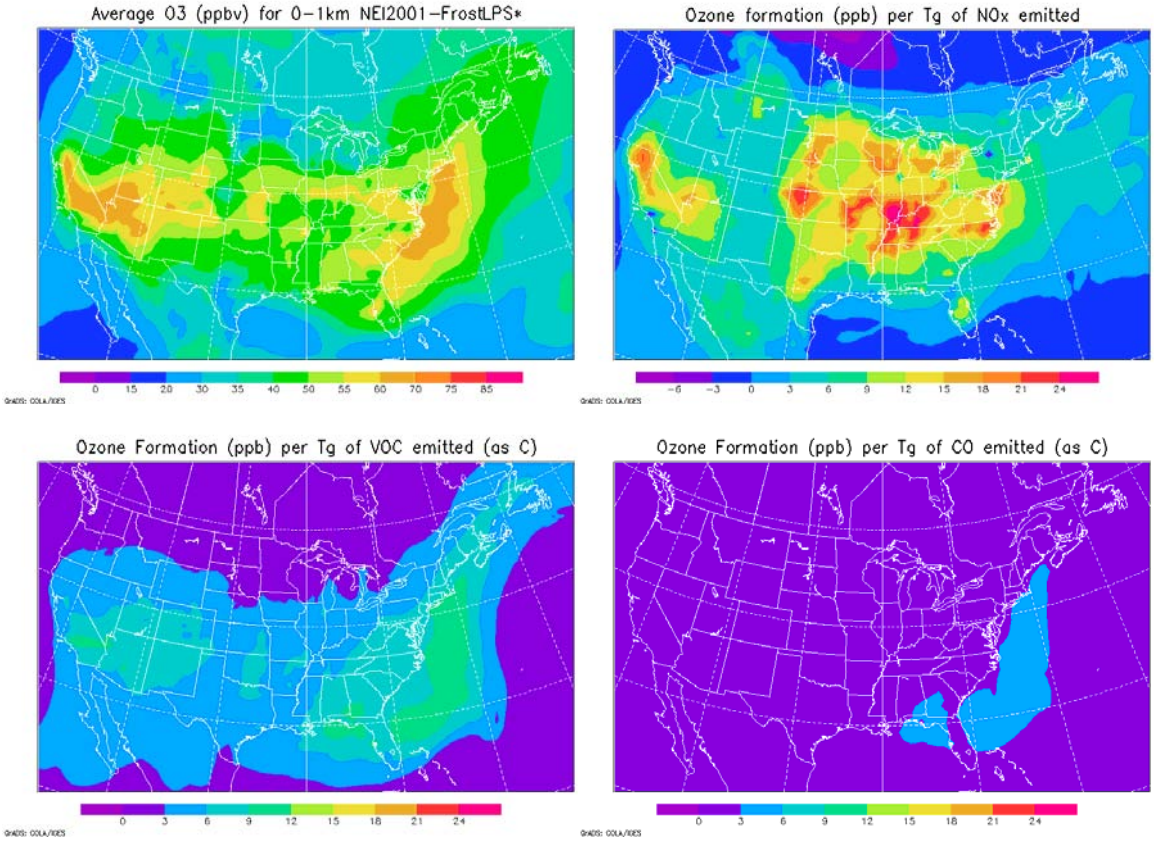

Figure 15 Sensitivity analyses for ozone formation in North America. Top Left: Modeled near surface ozone (0-1km average) for NEI-2001-FrostLPS* case. Modeled Net ozone formation (ppbv/(Tg of precursor/year)): Top Right: NO_x, Bottom Left: Anthropogenic VOC emissions. Bottom Right: Anthropogenic CO. July 21 to August 18, 2004

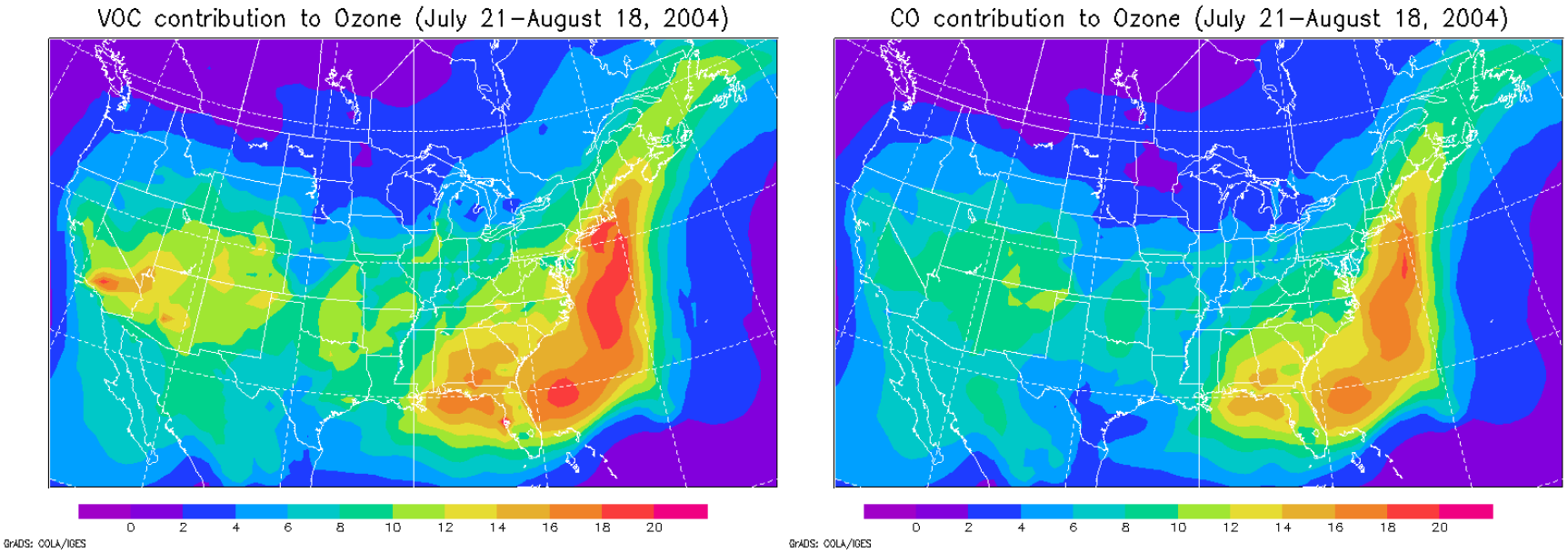

Figure 16 Average surface ozone contribution (ppbv) due to anthropogenic VOC (left) and anthropogenic CO (right), calculated as the difference between average 0-1km ozone for NEI 2001-FrostLPS*, and the same in scenario in the absence of VOC and CO, respectively. Study period: July 21 to August 18, 2004

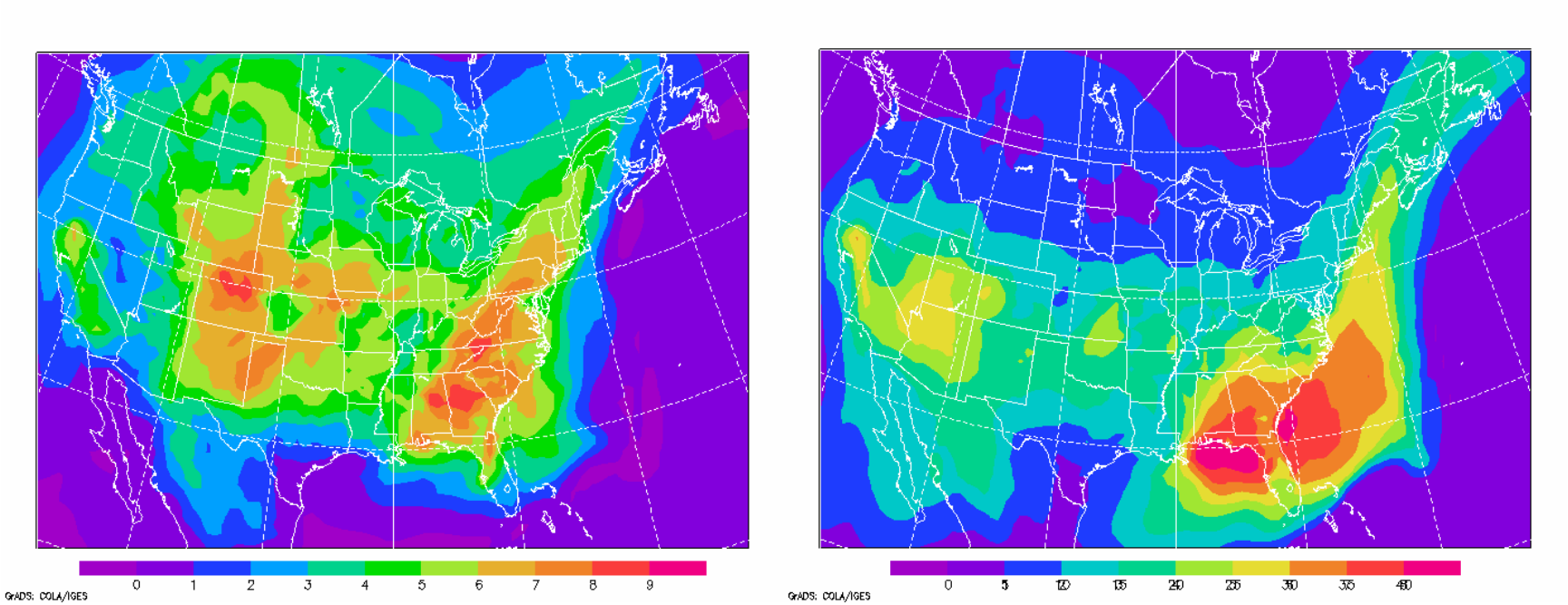

Figure 17 Calculated impact of the thermal decomposition of PAN on ozone. Left: Average difference between surface ozone with the formation of PAN and with the formation of PAN blocked. Right: Average difference between surface ozone concentration with unconstrained PAN and with PAN concentrations set to zero. Study period: July 21 to July 28, 2004

CHAPTER 3 IMPROVING OZONE MODELING IN MEXICO CITY

3.1 Introduction

Megacities are defined as metropolitan areas with more than 10 million people [*Mage et al.*, 1996]. Megacities generally have air quality problems, especially those in the developing world [*Mayer*, 1999]. Megacities also have noticeable impact on regional air quality and photochemistry [*Gurjar et al.*, 2005; *Guttikunda et al*, 2005]. In the case of Mexico City,(population ~20 million), poor ventilation (associated with constraining topography), and low efficiency combustion (largely due to lower oxygen content at ~2200m above sea level) make it one of the most polluted cities in the world [*Molina et al.*, 2004]. Recently an intensive atmospheric chemistry measurement campaign MILAGRO MEX [*NCAR*, 2006] was carried out with the intention of evaluating the regional impact of Mexico City on the surrounding area's atmospheric chemistry and meteorology. This campaign included multiple aircraft measurement platforms (DC-8, B-200, and J-31 operated by NASA, a C-130 operated by NCAR, a G-1 operated by DOE, and a Twin Otter operated by the University of Montana). The range and maneuverability of that these aircraft was different, as were their sampling strategies. The C-130 sampled near the city, performing zig zags and spirals at multiple altitudes with an altitude range from 0-6.5km. The DC-8 performed direct flights to and from Houston, with limited spirals, and a higher altitude range (0-12km). The measurements however provide great context regarding the regional impact of a megacity such as Mexico City on surrounding areas.

The effect of growth of megacities, even when holding emissions constant, is of increased ozone production, largely due to effects on meteorology contingent on land use changes that cause increased temperatures [*Civerolo et al.*, 2007]. Megacities are also the source of considerable amounts of aerosol, which affect photochemical reactions involved in ozone production and destruction. A study in Mexico City showed that

observed photolysis rates of NO_2 at an urban site were 10-30% lower than at a nearby rural site [*Castro et al.*, 2001].

Mexico City average 1h ozone and NO_2 concentrations have decreased from 1990 to 1998 largely attributed to the use of non attainment area fuel (oxygenated with MTBE and with low sulfur), and increased fuel emission standards for vehicles [*Schifter et al.*, 2007]. Further reducing emissions of NO_x will not necessarily reduce ozone exposure, as Mexico City is under a VOC limited ozone production regime [*Tie et al.*, 2007]. In fact reducing NO_x emissions in model studies causes an increase of ozone concentrations in the city [*Lei et al.*, 2006]. It is believed that leaked liquid petroleum gas (LPG) is linked to increased ozone concentrations, as was shown in experimental work by Jaimes-Lopes et al. [2005]

Work by West [2005] suggests that CO and VOC emissions inventories have to be scaled by a factor of 2 and 3, respectively. De Foy et al. [2006] carried out a modeling constraint study in which CO and SO_2 emission estimations were deemed appropriate for the city, when comparing to the top down work of Schifter at al. (2005). It is difficult to summarize previous emissions inventories as they do not consider the same geographical extension, differ in methodology, and use emission factors that vary from year to year.

This research consists of analyzing model performance through conventional statistical analysis (correlation coefficients, slopes, normalized bias) in conjunction with error covariance analysis (how ozone and its precursor errors are interrelated), and three dimensional contextualization of model performance (horizontal interpolation of model error along flight tracks, and vertical profiles derived from aircraft data), as a basis to modifying emissions inventories and boundary conditions to improve ozone modeling. Also a significant portion of this chapter will cover aspects regarding the regional impact of Mexico City emissions in photochemistry, air quality, and ozone production regimes. Finally a small section evaluating meteorological performance and the effect of model resolution will be presented.

3.2 Methods

3.2.1 Stem model

In this study we used the STEM-2K3 model [*Carmichael et al.* 1991] to carry out air quality simulations. The model features full chemistry using a lumped species SAPRC99 chemical mechanism [*Carter*, 2000] with an on-line photolysis solver, and the SCAPE II aerosol solver (Simulating Composition of Atmospheric Particles in Equilibrium) [*Kim et al.*, 1993a, 1993b; *Kim and Seinfeld,* 1995]. The chemical transport model is coupled to a meteorological model.

3.2.2 Meteorological model

Meteorological inputs to the model came from WRF V2.1.2 (http://www.wrf-model.org/index.php), using the NCEP Global Forecasting System 1 x 1° analyses for meteorological boundary conditions (http://www.emc.ncep.noaa.gov/modelinfo). For this study the model domain used two nested domains, the first one, using a 60km resolution, 100 cells in longitude, and 64 cells in latitude, while a nested domain was run using a 12km resolution, 110 cells in longitude, and 95 cells in latitude(Figure 18). The model had 21 vertical layers, extending from the surface to 100hPa. The Grell Grell-Devenyi ensemble cumulus parameterization [*Grell et al.*, 1995], the YSU planetary boundary layer parameterization, and then NOAH land surface model were used for the WRF runs.

3.2.3 Emissions inventories

During the forecast stage of this study a gridded national emissions inventory for Mexico did not exist. The model used an emissions inventory for the Mexico City area developed by UNAM for 1999 [*Tie et al*, 2007] which included detailed speciation of VOCs. For surrounding areas in Mexico south of 21N the Emission Database for Global Atmospheric Research (EDGAR 2.0) 1° resolution anthropogenic area emissions

inventory was used [*Olivier et al.*, 2002], while for areas north of 21°N a 36km resolution anthropogenic emissions inventory was used, using data developed during the BRAVO campaign [*Kuhns et al.*, 2005] for the 6 states in Mexico which share a border with the United States (Baja California, Sonora, Chihuahua, Coahuila, Nuevo León, and Tamaulipas). A limited number of point sources from Mexico were also used in the inventory. During post-analysis (I-run) the emissions inventory used in forecast (F-run) was modified as a result of data analysis described in this chapter. Also during post-analysis a new emissions inventory was released in the form of a report which was not readily usable for modeling. For this reason during this research the Mexico National Emissions Inventory was consolidated and gridded as is explained in Chapter 4.

3.2.4 Biomass burning and biogenic emissions

During the forecast biomass burning emissions of CO (and BC and OC by scaling factors) were provided by the RAQMS [*Pierce at al.*, 2007] using an ecosystem based wild fire emissions processor. Biogenic emissions were estimated using BEIS 2 (Biogenic Emissions Inventory System), [*Geron et al.*, 1994] which generates time-variable isoprene and monoterpene emissions driven by meteorological variables from WRF simulations.

3.2.5 Boundary conditions

During the real time forecasting (F-run) boundary conditions for the model were taken from NASA's Real-time Air Quality Modeling System (RAQMS) [*Pierce et al.*, 2003], a global chemical model with a 1.4° resolution. During post-post analysis (G and I runs) the Model for Ozone and Related Chemical Tracers (MOZART)[*Horowitz et al.*, 2003] was used for boundary conditions, which was run by the NCAR ACD group at a 0.7° resolution using MOPITT assimilated CO concentrations [*Pfister et al.*,2005]. Figure 19 shows the average top and lateral mean concentrations for RAQMS and MOZART that were used during forecasting and post-analysis.

Table 8 shows a summary of the model configuration used during this research.

3.3 Results

3.3.1 Statistical analysis

When comparing observed and modeled values along C-130 flight tracks during the forecast stage (Run F) ozone predictions showed great positive bias (~26.4 for ozone, 22% for CO, 128% for propane, 380% for aromatic, 72% for NO_y, as shown in Table 9). The predicted values were compared to one minute averaged observations using the same spatial location and time by tri-linear interpolation. Mean profiles of observed and modeled values (Figure 20) show that during the forecast stage (F run, in red) positive bias on ozone prediction was persistent at all altitudes, especially near the 2.5-4.5km above sea level range, which is the altitude at which the Mexico City plume was sampled. Additionally in those altitude ranges CO, NO_y, C_3H_8, and ARO_1 show large positive biases. Figure 21 shows that model error for ozone is highly correlated to bias in CO (r^2=0.60) and NO_y (r^2=0.75). The bias in NO_y in turn is correlated to errors in CO (r^2=0.66), ARO_1 (r^2=0.73), and C_3H_8 (r^2=0.80). At the same time these errors, show regional correspondence, as is shown in Figure 22 (which shows the geospatial interpolation of point bias estimations for the C-130 flight tracks). Where ozone bias is highest (such as near Mexico City, and portions to the West and North), NO_y is also very high. The forecast model also shows that Mexico City is on average largely VOC limited, albeit the overprediction of modeled NO_y and VOC. These three pieces of information (that the model overpredicted O_3, NO_y, and VOC during the forecast, that the overprediction of O_3 and its precursors were highly correlated, and that this overprediction showed a geographical structure) provided guidance on where and how the emissions inventory used during forecasting need to be modified during post-analysis to reduce model bias and enhance model performance, as is shown in the next section.

From previous experience it was known that positive bias in the 6-7km range (and higher for the DC-8) is largely dependent boundary conditions [*Mena-Carrasco et al.*, 2007;*Tang et al.*, 2007]. Figure 19 shows the mean top and lateral boundary conditions comparing RAQMS (F-run) and MOZART (G-run) mean CO and O_3 concentrations. RAQMS boundary conditions tend to represent higher stratospheric intrusion of ozone. Mean values over Mexico City (15km high) tend to be 50 ppbv higher for RAQMS. MOZART boundary conditions tend to represent higher incoming CO concentrations into the model domain, particularly mean CO coming from biomass burning in Central America, and Southeast United States anthropogenic CO near the surface of the Northeast of the domain. Figure 20 shows that using MOZART boundary conditions (G run) decreased positive bias of ozone at the 6-7km range with little influence on the mean profiles, and marginal change in statistical performance (Table 9).

Once boundary conditions were selected for post analysis, model improvement was contingent on modifying emissions based on results during forecast. For a new post-analysis run (I-run) emissions in Mexico City were reduced by 50% for NO_x, and volatile organic compounds were reduced from 40-70% (60% for C_3H_8, alkanes from 40-70%, aromatics by 70%, and ethene by 60%). The result of this run is shown in Figure 20 and Table 9. Positive bias of NO_y, C_3H_8, and ARO_1 in the 2.5-4.5km is largely reduced. Overall the normalized ozone bias is reduced from 26% to %10 from forecast (F run) to post-analysis (I run) at the same time that NO_y bias is reduced from 72% to 19%. VOC (represented as ARO1 and C_3H_8) positive bias is greatly reduced (ARO1 from 381% to 26%, and propane C_3H_8 from 129% to 7%.

3.3.2 Correlation among concentration species

The previous section focused on conventional data analysis, looking at things such as correlation coefficients and normalized bias. However further data mining gives additional information on sources of model error. As in the previous chapter, three types

of correlations can be used to evaluate model performance as a basis to improve modeling. These are: correlation among mixing ratios of ozone and precursors, correlation between modeled and observed species, and finally the correlation between model error of ozone and its precursors. Simultaneous analysis of these correlations provides guidance on sources of model error that are lost with simple observed-modeled correlations. This analysis will be based on post-analysis run I, which considered decreased emissions of VOC and NO_x, as described the previous section.

Ozone mixing ratios are highly correlated to PAN (R=0.88), CO (0.84), acetylene (0.81), NO_z,(0.80), and C_3H_8 (0.78) with other compounds showing weaker correlations, as is shown in Table 10. Also photochemical reaction rates and radicals show much weaker correlation. Table 11 shows a summary of which compounds show highest correlation for each flight, and in total (excluding compounds that are components of others, such NO being part of NO_x, or PAN being part of NO_y). In this table you can unravel new relationships, such as CO and ethyne mixing ratios being highly correlated (implying collocated emissions from combustion processes). Also you can see that the mixing ratios of primary pollutants, such as NO, NO_2, NO_x (the sum of both) are correlated to compounds linked to combustion processes (C_3H_8, C_2H_2). Reactive nitrogen species such as HNO_3, PAN, NO_y, and NO_z in turn are associated longer lived compounds, such as CO, O_3, and the HCHO (not long lived, but formed from oxidation of CO). That is, NO_y and its components are related to compounds associated to plume aging. Similarly, HCHO concentrations are related to its direct precursor, CO, and aged species such as NO_z and NO_y. ARO1 (benzene + toluene) is related to C_2H_2 (as both are thought to be collocated emissions from mobile sources) as has been previously shown in work by Parrish et al. [1998].

3.3.3 Model correlation coefficients

Comparison modeled and observed values extracted along the C-130 flight tracks shows highest correlation for photolysis rates (R=0.91), HCHO (R=0.77), followed by CO (R=0.76), C_2H_2, (0.76),and C_3H_8 (0.75). Secondary species such as PAN (R=0.64), HNO_3 (R=0.38), and O_3 (R=0.58) showed much smaller correlation coefficients. Finally modeling of SO_2 shows inadequate modeling performance (R=0.17) largely due to the quality of the information available in the emissions inventory used in this study.

3.3.4 Correlation between model biases

Table 13 shows the correlation coefficients between ozone bias and the bias of other species. While there is some flight to flight variability, CO bias is most highly correlated to ozone bias (R=0.76), followed by NO_z, NO_y, PAN (a component of both of the previous), C_2H_2, HCHO, and C_3H_8. Shorter lived species such as radicals, NO, and NO_2 show weaker correlations. SO_2, and some selected photolysis rates show almost no correlation to ozone bias. The same way high observed values of CO, C_2H_2, and PAN are correlated to high observed ozone, when CO and C_2H_2, and PAN are overpredicted, so is ozone. When looking at the highest correlations of model error among the other species, you can see (Table 14) that CO error is most correlated to NO_y error, while C_3H_8 error is most correlated to C_2H_2 error, and vice versa. This information provides valuable insight, as it implies that reducing CO error would reduce O_3 error, but also that of its precursors. This suggests that a data assimilation strategy to recover emissions scaling factors would be very effective if the target compound was CO. This allows the use tracer adjoint runs that are less computationally demanding than a full chemistry run.

It should be noted that PAN and HNO_3 errors are largely uncorrelated to NO_x and its components, and more related to the concentration of VOC and CO. Also the CO error is highly correlated to C_3H_8 and C_2H_2, the latter highly correlated among themselves.

3.3.5 Bias in a regional context

The previous section showed the numerical relationships among ozone bias and the bias of its precursors. This section qualitatively documents model improvements from forecast to post-analysis. Figure 23 shows the interpolated ozone and NO_y bias during the post analysis (I-run). Ozone bias and NO_y bias show great geographical correspondence in addition to numerical correlations between O_3 and NO_y bias (Table 13). Model bias of ozone was reduced across large parts of Mexico to ~25-25%, while bias in Mexico City bias was reduced to 25-100%. NO_y bias was reduced significantly, to 25-100% west of Mexico City, and to ~-25 to 25% for large portions of Mexico City. Some offshore negative bias between the cities of Veracruz and Tampico suggest that some emissions from those areas are misrepresented by the emissions inventory.

Figure 24 shows that the probability distribution of model bias along C-130 flight tracks from the forecast stage to post analysis runs improves greatly. The probability that model bias is within the -25 to 25% range increases from 53% to 62% from forecast (F-run) to post-analysis (I-run), and in the -10 to 10% range from 24% to 30%. More importantly, large overprediction (bias over 100%) decreased from 6.3% to 0.9% when comparing forecasting to post-analysis.

3.3.6 Case studies

In the previous section it was shown that during forecast model bias for ozone was associated with model bias of CO, NO_y, and VOC. Figure 25 shows that for flight 2 (March 8, 2006) post-analysis runs with reduced NO_x and VOC emissions greatly improved ozone modeling by reducing model bias of ozone (from 16.1 to 6ppbv mean bias), at the same time reducing NO_y and C_3H_8 bias (the first from 80% to 20% and the second from 155% to 2%, even though correlation coefficients remain constant from

forecasting to post-analysis). CO concentrations in turn show modeling improvement of R^2 from 0.43 to 0.52 while slightly reducing bias. Since CO emissions were not modified, this can be attributed to improved estimation of secondary CO (formed from VOC oxidation).

3.4 Effect of Mexico City on regional chemistry

From the previous section it has been established that modeling of Mexico air quality during March 2006 has improved, and that ozone is modeled within 25% more at least 63% of the time (Figure 24), establishing a basis to support additional sensitivity studies. Three main issues will be discussed in this next section: the influence of Mexico City emissions on photochemistry, air quality, and ozone production regimes.

3.4.1 Influence of Mexico City on photochemistry

Aerosol concentrations in megacities are known to have great influence in photolysis rates associated with ozone formation [*Tang et al.*, 2003]. In this study a sensitivity run in which the influence of aerosol studies by analyzing the difference between a full chemistry run (I-run) and a run in which the effect of aerosol on photolysis rates is excluded (I-AOD run). For J[NO_2] it was found (Figure 26) that aerosols can reduce rates by 40% in areas downwind of Mexico City, and reduces ozone concentrations by ~5-10% (largely due to dilution of NO_2 downwind). These may be conservative estimations, because while correlation coefficients modeling photolysis rates (Table 12) are high, near the city photolysis rates are overpredicted by as much as 25% (bottom panel). This may be the reason why modeled ozone production efficiency (calculated as the slope between NO_z and odd oxygen, O_3+NO_2) is higher (4.95) than the observed OPE (3.60) (Figure 27). These results suggest that Mexico City aerosol emissions preclude ozone from forming to its maximum potential concentration.

3.4.2 Influence of Mexico City on ozone production regimes.

Figure 28 shows that using ozone production regimes indicator ratios (such as O_3/NO_y as described in section 1.1.4), areas near Mexico City (altitude <2.5km, and closer to 200km, as is shown in the left panel) tend to be VOC sensitive, or in the transition range towards NO_x limited. This suggests that decreasing ozone concentrations in Mexico City would require reducing VOC emissions. However in outflow events the Mexico City plume can extend its influence on ozone production chemistry, as is shown in Figure 29, which shows that for March 11, 2006 (for which *Fast et al.* [2007] suggest that flow is to the NE) surrounding areas as much as 200km North of Mexico City are under VOC limited conditions. During that day the DC-8 flew into the city Figure 29 (bottom left panel) and encountered the transition from NO_x limited conditions (high O_3/NO_y ratios) to VOC limited conditions (very low O_3/NO_y). An adjoint analysis (running the model backwards to suggest origin of air masses) performed with high resolution 4km meteorology shows that transition point originated over Mexico City (Figure 29, bottom right).

The next day (March 12, 2006) the C-130 sampled areas east of Mexico City (Figure 30, bottom left) which were not under the influence of Mexico City emissions (flow from city was to the North. Observed and modeled O_3/NO_y for that day is 10 and 11 respectively (Figure 30, right panel) in the NO_x limited range.

Similar results were found for other flights. Therefore, while Mexico City is VOC limited, outflow conditions can transform surrounding areas from NOx to VOC limited conditions.

3.4.3 Effect of Mexico City on air quality.

A sensitivity run without the emissions from Mexico City was compared to the base run (I-run) to evaluate the footprint of Mexico City on surrounding areas. Figure 31 shows that Mexico City can enhance daytime surface ozone 30% in Mexico City, and 5-

10% in the state of Hidalgo, roughly 100km north of Mexico City. To the west Mexico City can contribute to 10-15% of mean maximum surface ozone near Toluca. The regional contribution of CO due can reach up to 10-20% of Hidalgo's mean CO. The average modeled outflow tends to be southwesterly. The impact of Mexico City on regional NO_y is higher, contributing to 20-30% of mean NO_y to areas E and NE of the city, and from 35-45% of NO_y in Hidalgo. These contributions are important, but only represent mean surface calculations. For specific outflow patterns and at higher altitude ranges the impact of Mexico City emissions can be illustrated to a larger extent. For example for March 19, 2006 (in which the C-130 sampled elevated ozone and NO_y off the coast of Texas) the contribution of Mexico City to regional NO_y in the 1-5.4 km range can be as large as 10-20% of values over the Gulf of Mexico and 40-70% over portions large portions of Hidalgo (Figure 32, left panel). Similarly these emissions can contribute 2-5% of ozone concentrations over the Gulf, with contributions as large as 10-20% some 200km north of the city (over the state of San Luis de Potosí, right panel).

3.5 Meteorology and model resolution

3.5.1 Modeling meteorological parameters

Evaluating model performance with respect to meteorology allows separating sources of model error due to emissions and transport. Plots of modeled and observed temperature, humidity, and wind velocity are shown in Figure 33. Correlation coefficients for meteorological parameters decrease with altitude. Temperature correlation coefficients mostly exceed 0.9. Wind velocities tend to be underpredicted, with observed values exceeding modeled values in ~20-30%.for measurements lower than 4km. Relative humidity correlation coefficients exceed 0.7 for all altitude ranges. The model tends to overpredict relative humidity at the 2-4km range, which could influence photolysis rates.

3.5.2 Effect of model resolution on performance

Model resolution has multiple effects starting from the effect on land use representation, the resolution of topography, and the necessity of meteorological model parameterization of processes that are relevant at smaller resolution [*Glendening,* 2006]. Figure 34 shows that when comparing model runs for 60km vs. 12km resolution run the coarser resolution creates less concentrated, broader plumes, while the 12km resolution model generates more concentrated and thinner plumes. Also flow patterns south of Mexico City in the 12km resolution show more complex flow patterns, and even areas of confluence, which the 60km resolution does not capture. The resolution of emissions have an important effect on ozone chemistry, as nighttime fresh NO_x emissions titrate ozone in urban areas, decreasing nighttime concentrations, which are carried over to the next day. Figure 35 shows that mean nighttime ozone concentrations from March 1 to 30, 2006 were considerably higher for the 60km resolution

Figure 36 shows that when comparing observed to modeled values, the coarser resolution (in Red) presents lower concentrations, and plumes that are sampled longer in time, while the finer resolution shows narrower, and more intense plumes, which show greater agreement to observations. However increasing model resolution beyond 12km would not necessarily increate model performance. Table 15 shows the comparison of modeled and observed mean values and correlation coefficients for selected species. While mean modeled values for the 60km and 12km versions are similar, correlation coefficients are substantially better for the 12km version for all species except O_3, which is a secondary pollutant that has regional presence and lower variability than the other compounds.

3.6 Conclusion

During the forecast stage of MILAGRO the STEM model presented 2-3km bias on ozone prediction associated to a positive bias of NO_y and VOC, while at higher 6km

or higher, a positive bias associated to boundary conditions. Updating boundary conditions and decreasing Mexico City emissions of NO_x and VOC decreased mean model bias from 26 to 10%, at the same time reducing NO_x bias from 72% to 19%, C_3H_8 from 129 to 7%, and ARO_1 bias from 381% to 26%. Geographical interpolation of recurring ozone error shows that model error is associated to CO and NO_y to the west of Mexico City. Probability distributions of model error shifted towards lower bias distributions during post-analysis. C-130 extracted values showed cumulative distribution in the -25 to 25% range increased from 53 to 62% (when comparing forecast to post-analysis) and large bias (over 100%) decreased from 6.3% to 0.9%.

Sensitivity studies show that Mexico City is VOC limited in terms of ozone formation, but that outflow patterns can influence surrounding regions, transforming them from VOC to NO_x limited. Mexico City aerosol can influence photochemistry by decreasing modeled photolysis rates at up to 40% while decreasing ozone formation by 5-10%. Error interpolation of $J[NO_2]$ suggests that this effect is in fact underestimated, showing that aerosol have a masking effect ozone formation to its maximum potential formation. Mexico City impact on modeled maximum daytime ozone concentrations for surrounding areas is not high, however at higher altitudes (1-5.4km range) Mexico City can contribute to 10-20% of ozone concentrations over the Gulf of Mexico, and 20-30% of NO_y concentrations.

Model resolution is important to correctly predict minimum ozone concentrations, as high resolution emissions show a bigger effect of NO_x emissions on nighttime ozone titration. Also lower resolution model runs showed diluted and broader plumes than higher resolution runs and observations. Resolution plays an important role in placing primary pollutants as CO, NO_x, and C_3H_8, as correlation coefficients with respect to observations are much higher for higher resolution runs. O_3, a secondary pollutant, is less dependent on resolution, as expected.

Table 8 Summary of model parameters and configuration

Scenario	Parameters			
	National Emissions Inventory	Biogenic/Biomass Burning	Boundary Conditions	Meteorology
Forecast (F-run)	4km 1999 Metropolitan Mexico City, 1° EDGAR South of 21N, 36km Bravo inventory north of 21N. Point sources for Mexico City and border states.	BEIS 2/RAQMS Real-time Biomass Burning	RAQMS with chemical data assimilation	WRFV2.1.2
Post-analysis (G-run)	Same as before	BEIS 2/RAQMS Real-time Biomass Burning	MOZART NCAR, with MOPITT assimilated CO[*Pfister et al.*, 2005]	WRFV2.1.2
Post-analysis (I-run)	Reduced Mexico City emissions for NO_x (50%),C_3H_8 (60%), ALK3 (40%), ALK4 (70%), ALK5 (70%), ARO1 (70%), ARO2 (70%), ethene (60%), C3H8 (60%), OLE2 (80%), and acetone (30%)	BEIS 2/RAQMS Real-time Biomass Burning	MOZART NCAR, with MOPITT assimilated CO[*Pfister et al.*, 2005]	WRFV2.1.2
NEI99	2.5km Mexico National Emissions Inventory (Description in Chapter 4)	BEIS 2/RAQMS Real-time Biomass Burning	MOZART NCAR, burned area biomass burning emissions [*Pfister et al.*, 2005]	WRFV2.1.2

Note: For detailed definition of ALK3, ALK4, ALK5, ARO2, and OLE2, see Carter [2000]

Table 9 Model performance statistics for selected species during MILAGRO: Modeled vs. Observed data, C-130 Platform

	O3				CO				C_3H_8				ARO1			
	Obs	F	G	I	Obs	F	G	I	Obs	F	G	I	Obs	F	G	I
Mean	58.73	74.23	71.70	66.12	146.86	179.65	188.66	184.72	1.84	4.22	4.22	1.98	0.27	1.29	1.24	0.34
SD/mean	0.33	0.45	0.44	0.29	0.58	0.57	0.48	0.46	1.77	2.28	2.20	1.84	2.00	2.72	2.68	2.68
R		0.54	0.60	0.58		0.60	0.66	0.67		0.70	0.75	0.75		0.58	0.63	0.64
%Bias		26.40	17.47	10.31		22.33	28.47	25.78		128.80	128.67	7.45		380.97	361.60	26.43
	NO_x				NO				NO_2				NO_y			
	Obs	F	G	I	Obs	F	G	I	Obs	F	G	I	Obs	F	G	I
Mean	0.82	0.52	0.52	0.51	0.16	0.12	0.12	0.12	0.65	0.42	0.39	0.38	2.99	5.15	5.06	3.57
SD/mean	4.40	3.32	3.23	2.70	2.87	3.75	3.77	3.75	2.85	3.14	3.09	2.73	1.53	1.78	1.71	1.45
R		0.62	0.63	0.70		0.45	0.45	0.55		0.66	0.65	0.71		0.61	0.66	0.63
Bias		-36	-37	-38		220	219	210		-36	-39	-41		72	69	19

SD: standard deviation. F: RAQMS boundary conditions, base emissions. G: NCAR boundary conditions, base emissions. I: NCAR boundary conditions, reduced emissions inventories

Table 10 Correlation coefficients among mixing ratios of ozone and other gaseous species, C-130 aircraft

Flight Number	1	2	3	4	5	7	8	9	10	11	12	13	Total
PAN	0.93	0.98	0.95	0.63	0.87	0.93	0.97	0.72	-0.20	0.76	0.93	0.66	0.88
CO	0.94	0.86	0.91			0.64	0.88	0.13	-0.62	0.18	0.91		0.84
C_2H_2	0.85	0.93	0.88	0.74	0.93	0.64	0.87	-0.09	-0.43	0.25	0.91	0.58	0.81
NO_z	0.92	0.97	0.93	0.74	0.93	0.86	0.93	0.40	-0.45	0.56	0.60	0.41	0.80
C_3H_8	0.81	0.90	0.84	0.24	0.90	0.66	0.86	0.48	-0.43	0.20	0.90	-0.05	0.78
NO_y	0.84	0.94	0.82	0.74	0.94	0.70	0.82	0.05	-0.42	0.51	0.83	0.23	0.75
HCHO					0.90	0.48	0.82	-0.18	-0.47	0.16	0.88		0.74
ARO_1	0.78		0.82	0.53	0.77	0.45	0.60	-0.12	-0.07	-0.08	0.73		0.65
C_2H_6	0.91	0.91	0.87	0.34	0.88	0.27	0.86	-0.23	-0.35	-0.24	0.78	0.01	0.61
HNO_3	0.72	0.81	0.61	0.64	0.84	0.35	0.44	0.51	-0.34	0.54	0.60	0.43	0.56
NO_2	0.68	0.81	0.57	0.60	0.77	0.11	0.55	-0.19	-0.40	0.16	0.77	0.03	0.53
NO_x	0.68	0.83	0.53	0.59	0.78	0.12	0.53	-0.18	-0.36	0.20	0.74	0.03	0.52
NO	0.68	0.82	0.36	0.42	0.76	0.16	0.40	-0.15	-0.29	0.01	0.56	0.03	0.44
OH					0.47	0.14	0.13	0.46	0.02	-0.22	0.25	-0.01	0.34
HO_2	0.46	0.09	0.40	0.44	0.52		0.56	0.45	0.35	-0.07	0.37		0.29
SO_2		0.42	0.01	0.28	0.78	0.16	0.10	0.04	-0.13	-0.04	-0.01	0.16	0.09
C_2H_6	0.73	0.84	0.35	-0.05	0.28	-0.21	0.28	-0.40	-0.26	-0.04	0.75	0.32	0.08
H_2O_2		-0.29	0.09	0.69	0.60	0.03	0.16	0.11	-0.33	-0.19	-0.54	-0.04	0.04

Table 11 Flight by flight summary of species with maximum correlation to mixing ratios of ozone and its precursors, C-130 observations

	1	2	3	4	5	6	7	8	9	10	11	12	13	Total
O_3	CO	PAN	PAN	C_2H_2	C_2H_2			PAN	PAN	CO	PAN	PAN	PAN	PAN
CO	C_2H_2	C_2H_2	C_2H_2			HCHO	C_2H_2	C_2H_2	NO_y	C_2H_2	C_2H_2	HCHO		C_2H_2
NO	C_3H_8	C_3H_8	C_3H_8	C_2H_2	HCHO	ARO_1	SO_2	CO	CO	C_2H_6	C_2H_4	HCHO	C_3H_8	C_3H_8
NO_2	C_2H_2	C_3H_8	C_2H_4	C_2H_2	HCHO	ARO1	C_2H_4	C_2H_2	CO	C_2H_4	HCHO	CO	C_3H_8	C_2H_2
NO_x	C_2H_2	C_3H_8	C_2H_4	C_2H_2	HCHO	ARO1	C_2H_4	C_2H_6	CO	C_3H_6	HCHO	CO	C_2H_6	C_2H_2
PAN	O_3	O_3	O_3	C_2H_2	O_3	O_3	CO	O_3	O_3	O_3	C_2H_2	O_3	O_3	O_3
HNO_3	C_2H_2	C_3H_8	CO	C_2H_2	HCHO	C_3H_8	CO	C_3H_6	C_3H_8	ARO_1	CO	C_2H_2	C_2H_6	C_2H_2
NO_y	C_2H_2	C_2H_2	C_2H_2	C_2H_2	O_3	CO	C_2H_2	CO	CO	C_3H_6	CO	CO	C_3H_8	CO
NO_z	CO	O_3	O_3	C_2H_2	O_3	CO	C_3H_8	CO	CO	C_2H_6	CO	C_2H_2	C_2H_6	CO
C_3H_8	C_2H_2	C_2H_2	C_2H_2	SO_2	C_2H_2	C_2H_2	C_2H_2	CO	PAN	C_2H_2	C_2H_4	C_2H_4	C_2H_2	C_2H_2
C_2H_2	C_3H_8	C_3H_8	C_3H_8	NO_z	C_3H_8	C3H8	C_3H_8	C_3H_8	NO_z	C_3H_8	C_3H_8	C_3H_8	C2H4	C_3H_8
ARO_1	C_2H_2		C_2H_2	NO_y	C_3H_8	C_2H_2	NO_y	NO_y	C_2H_6	C_2H_6	C_2H_2	NO_2	CO	C_2H_2
HCHO					C_2H_2	CO	CO	NO_y	NO_y	CO	CO	CO		CO

1: 03-04, 2: 03-08, 3: 03-10, 4: 03-12, 5: 03-16, 6: 03-18, 7: 03-19, 8: 03-22, 9: 03-23, 10: 03-28, 11:03-29, 12: 03-30, 13:03-31

Table 12 Correlation coefficients between modeled and observed species along C-130 flight tracks, I run: NCAR-MOZART boundary conditions, RAQMS forecasted biomass burning emissions, Modified emissions inventory, 12km resolution model

	1	2	3	4	5	6	7	8	9	10	11	12	13	Total
$J[O_3 \rightarrow O_2+O]$	0.98	0.97	0.96	0.98	0.88	0.87	0.99	0.61	0.70	0.66	0.98	0.80	0.80	0.91
HCHO					0.79	0.80	0.80	0.76	0.23	0.64	0.35	0.74		0.77
CO	0.81	0.72	0.56			0.75	0.73	0.60	0.22	0.49	0.16	0.70		0.76
C_2H_2	0.89	0.85	0.65	0.64	0.23	0.78	0.71	0.68	0.14	0.54	0.38	0.70	-0.07	0.76
C_3H_8	0.87	0.85	0.62	0.19	0.18	0.79	0.76	0.69	0.21	0.47	0.24	0.70	-0.19	0.75
C_2H_4	0.91	0.85	0.65	0.51	0.17	0.60	0.76	0.68	0.31	0.50	-0.01	0.66	-0.10	0.73
NO_2	0.77	0.86	0.69	0.50	0.28	0.85	0.78	0.77	0.72	0.32	0.55	0.61	0.26	0.71
NO_x	0.80	0.87	0.64	0.51	0.28	0.82	0.75	0.72	0.73	0.28	0.54	0.61	0.15	0.70
PAN	0.84	0.72	0.55	0.60	0.36	0.77	0.71	0.52	0.15	0.62	0.41	0.72	0.64	0.64
ARO_1	0.87		0.70	0.23	0.20	0.74	0.74	0.53	0.06	-0.22	-0.09	0.50		0.63
NO_y	0.83	0.55	0.63	0.66	0.24	0.82	0.77	0.66	-0.19	0.37	0.40	0.64	0.71	0.63
O_3	0.73	0.73	0.56	0.55	0.26		0.72	0.52	0.21	-0.03	0.32	0.68	-0.09	0.58
NO_z	0.80	0.73	0.50	0.62	0.24	0.79	0.75	0.59	-0.02	0.46	0.33	0.52	0.75	0.57
NO	0.86	0.80	0.43	0.65	0.24	0.73	0.42	0.41	0.66		0.57	0.47	-0.06	0.55
C_2H_6	0.81	0.47	0.38	0.73	0.42	0.40	0.71	0.54	0.41	0.57	0.29	0.64	-0.46	0.52
C_3H_6	0.88	0.78	0.70	0.25	0.10	0.51	0.48	0.28	0.40	-0.05	-0.06	0.60		0.52
HNO_3	0.66	0.53	0.15	0.26	0.06	0.76	0.47	0.41	0.04	0.11	-0.05	0.23	0.48	0.38
SO_2		0.32	0.08	0.50	0.15	0.14	0.36	0.37	0.03	0.16	-0.03	0.00	0.83	0.17

1: 03-04, 2: 03-08, 3: 03-10, 4: 03-12, 5: 03-16, 6: 03-18, 7: 03-19, 8: 03-22, 9: 03-23, 10: 03-28, 11:03-29, 12: 03-30, 13:03-31

Table 13 Correlation coefficients of bias (modeled-observed) of selected species to ozone bias, for C-130 flight tracks. I-run: NCAR-MOZART boundary conditions, RAQMS forecasted biomass burning emissions, Modified emissions inventory, 12km resolution model

Flight	1	2	3	4	6	7	8	9	10	11	12	13	Overall
CO	0.75	0.76	0.84			0.62	0.90	0.66	0.72	0.72	0.89		0.76
NO_z	0.62	0.93	0.93	0.62	0.89	0.78	0.91	0.67	0.46	0.82	0.86	0.57	0.74
PAN	0.65	0.90	0.93	0.72	0.85	0.72	0.88	0.76	0.79	0.84	0.91	0.50	0.72
NO_y	0.55	0.90	0.81	0.63	0.90	0.67	0.75	0.53	-0.04	0.80	0.91	0.59	0.70
C_2H_2	0.74	0.68	0.65	0.77	0.84	0.65	0.77	0.93	-0.04	0.64	0.90	0.29	0.70
HCHO					0.48	0.50	0.76	0.77	0.19	-0.01	0.87		0.69
C_3H_8	0.65	0.81	0.67	0.22	0.85	0.56	0.75	0.91	-0.14	0.57	0.79	-0.19	0.66
C_2H_4	0.70	0.55	0.59	0.23	0.49	0.24	0.68	0.70	0.20	0.39	0.91	-0.12	0.61
C_2H_6	0.36	0.67	0.71	0.28	0.74	0.46	0.49	0.80	0.59	0.46	0.69	0.12	0.51
HNO_3	0.46	0.69	0.45	0.36	0.88	0.20	0.81	0.83	0.60	0.12	0.80	0.63	0.49
ARO_1	0.63		0.47	0.44	0.72	0.32	0.43	0.43	-0.13	0.65	0.76		0.48
C_3H_6	0.82	0.21	0.33	0.16	0.17	-0.01	0.09	0.77	-0.31	0.30	0.84	-1.00	0.37
NO_2	0.11	0.60	0.37	0.26	0.75	0.11	0.13	-0.10	-0.30	0.24	0.31	0.56	0.22
NO_x	0.10	0.57	0.30	0.22	0.75	0.13	0.10	-0.09	-0.29	0.24	0.33	0.61	0.21
H_2O_2		0.09	0.09	0.29	0.06	0.13	0.31	0.44	-0.07	-0.27	0.57	-0.82	0.18
OH					0.57	0.30	0.22	0.08	0.50	-0.36	-0.01	0.59	0.16
NO	0.08	0.34	0.10	-0.01	0.66	0.17	-0.05	0.06	-0.27	-0.02	0.31	0.64	0.13
HO_2	-0.22	-0.02	0.57	0.25	0.42		0.51	0.25	0.25	0.31	-0.11		0.08
SO_2	0.75	0.76	0.84			0.62	0.90	0.66	0.72	0.72	0.89		0.08

Table 14 Flight by flight summary of species with maximum correlation to bias of ozone and its precursors. C-130 observations

	1	2	3	4	5	6	7	8	9	10	11	12	13	Total
O_3	CO	NO_z	NO_z	C_2H_2	NO_y		NO_z	NO_z	C_2H_2	PAN	PAN	PAN	NO_y	CO
CO	C_2H_2	NO_z	NO_z			HCHO	HCHO	NO_z	NO_y	NO_z	C_3H_8	HCHO		NO_y
NO	NO_2	NO_2	NO_2	NO_2	NO_2	ARO_1	C_3H_6	SO_2	NO_2	NO_2	C_3H_8	NO_2	NO_2	NO_2
NO_2	NO	NO_y	NO	C_2H_2	NO	NO_y	NO_y	NO_y	HCHO	NO	C_2H_6	NO	NO_y	NO_y
NO_x	C_2H_6	C_2H_6	C_3H_8	C_2H_2	SO_2	CO	HCHO	SO_2	HCHO	C_2H_6	C_2H_6	CO	SO_2	SO_2
PAN	C_2H_2	C_2H_2	CO	C_2H_2	O_3	CO	CO	C_2H_2	C_3H_8	O_3	CO	C_2H_2	C_2H_2	C_2H_2
HNO_3	C_3H_6	O_3	C_3H_6	C_2H_2	O_3	C_2H_6	J[NO_2]	C_2H_2	C_3H_8	CO	C_2H_2	C_3H_6	O_3	C_2H_2
NO_y	C_3H_8	O_3	CO	C_2H_2	O_3	CO	CO	CO	CO	HCHO	CO	C_2H_2	O_3	CO
NO_z	HCHO	C_3H_6	C_3H_6	C_2H_2	C_3H_6	CO	C_3H_6	C_2H_4	O_3	ARO_1	C_2H_4	C_2H_6	C_3H_6	C_2H_4
C_3H_8	C_2H_2	C_2H_2	C_2H_2	HNO_3	C_2H_2	C_2H_2	C_2H_2	C_2H_2	C_2H_2	C_2H_2	C_2H_2	C_2H_2	C_2H_2	C_2H_2
C_2H_2	ARO_1	C_2H_4	C_3H_8	PAN	C_3H_8	C_3H_8	C_3H_8	C_3H_8	C_3H_8	C_3H_8	C_3H_8	C_3H_8	C_3H_8	C_3H_8
ARO_1	C_2H_2		C_3H_6	C_2H_2	C_2H_2	C_2H_2	C_2H_2	C_2H_4	C_2H_4	C_3H_8	C_2H_2	C_2H_2	C_2H_2	C_2H_2
HCHO					NO_x	CO	CO	C_2H_2	NO_x	C_2H_6	NO_2	CO		CO

Table 15 The effect of model resolution on performance: summary statistics for modeled vs. observed values along C-130 flight paths, STEM model run I

	Mean Observed	Mean Modeled (60km)	Mean Modeled (12km)	R (60km)	R (12km)
O_3	58.36	67.38	66.12	0.57	0.58
CO	144.4	184.8	184.65	0.58	0.66
NO_y	2.81	3.89	3.54	0.58	0.68
NO_x	0.76	0.37	0.51	0.50	0.70
ARO_1	0.44	0.41	0.47	0.58	0.76
C_3H_8	1.75	6.95	1.98	0.60	0.75

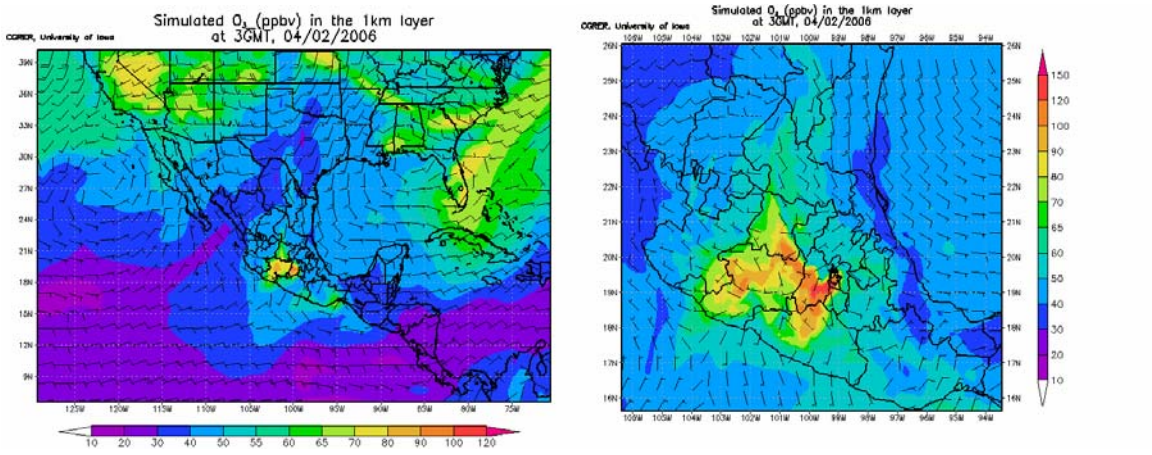

Figure 18 Model domains for MIRAGE campaign. Left: 60km, 100x64x21 domain. Right: 12km, 110x95x21 domain.

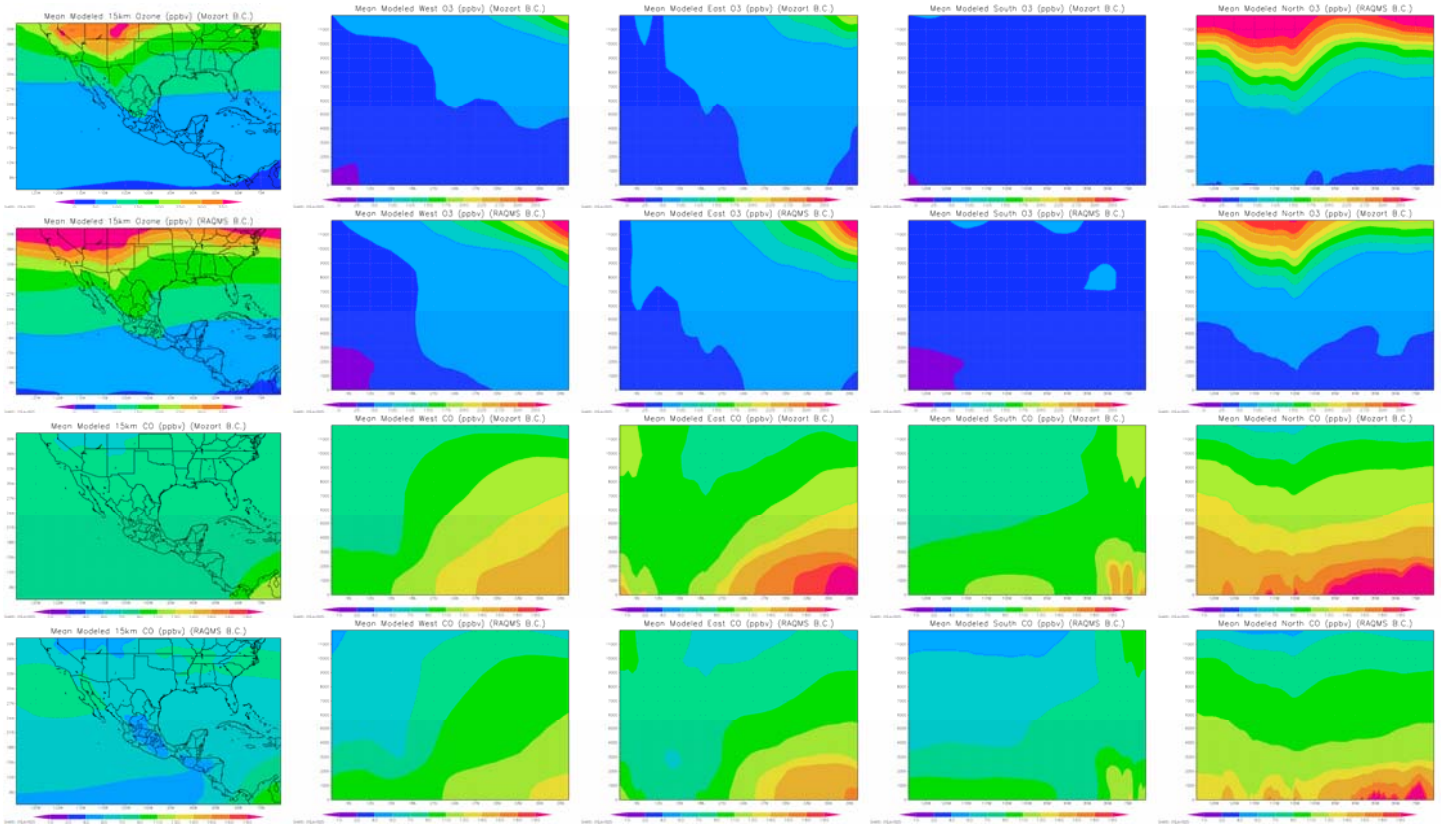

Figure 19 Effect of boundary conditions on mean modeled values from March 1-30, 2006. Top row: Mean ozone concentrations for RAQMS boundary conditions. Second row: Mean ozone concentrations for MOZART boundary conditions. Third row: Mean CO concentrations for RAQMS boundary conditions. Bottom row: Mean CO concentrations for MOZART boundary conditions. Values calculated using 60km model resolution

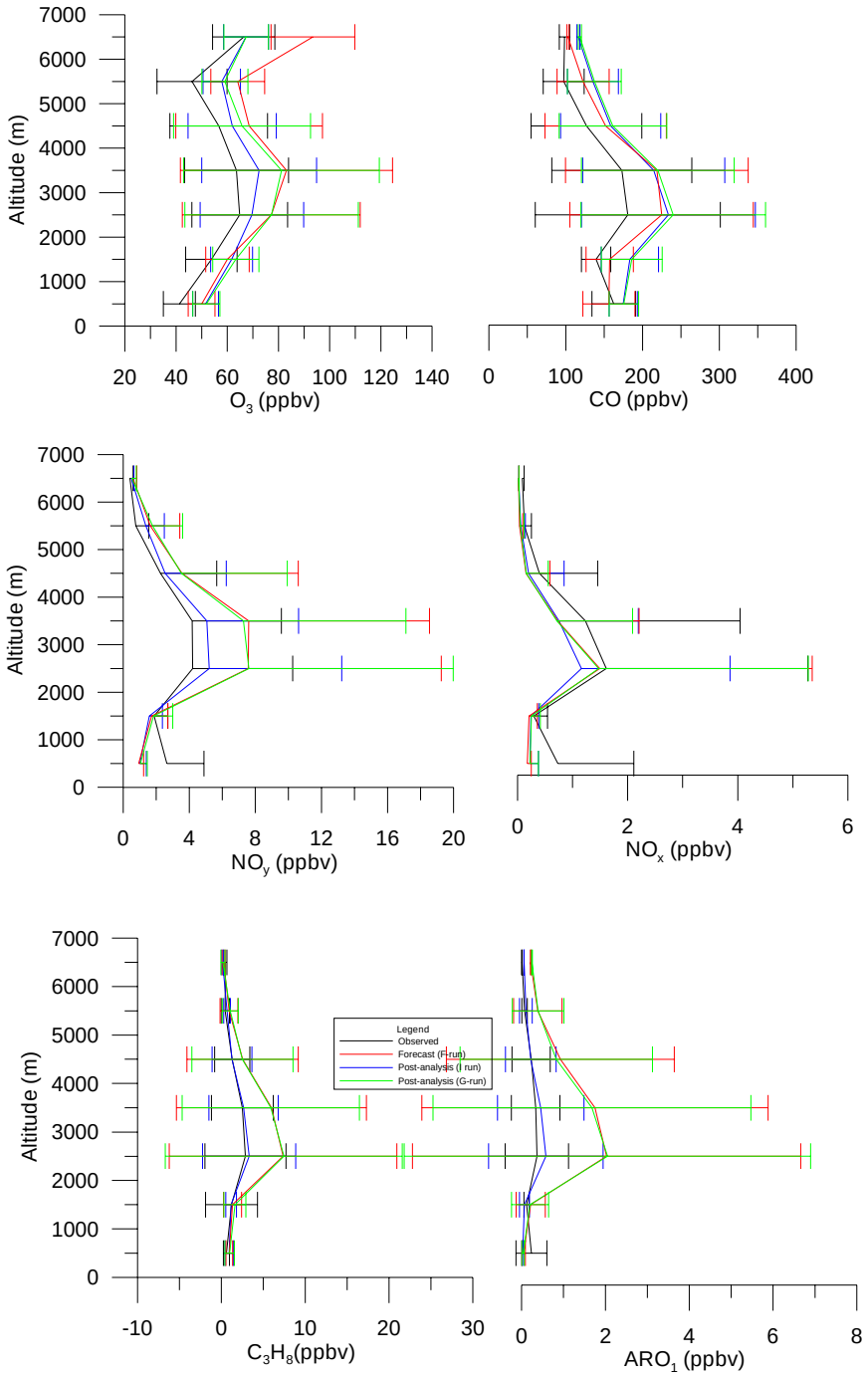

Figure 20 Observed and 12km-simulated O_3, CO, and NO_x, NO_y, C_3H_8, and ARO_1 vertical profiles and standard deviations for all C-130 flights

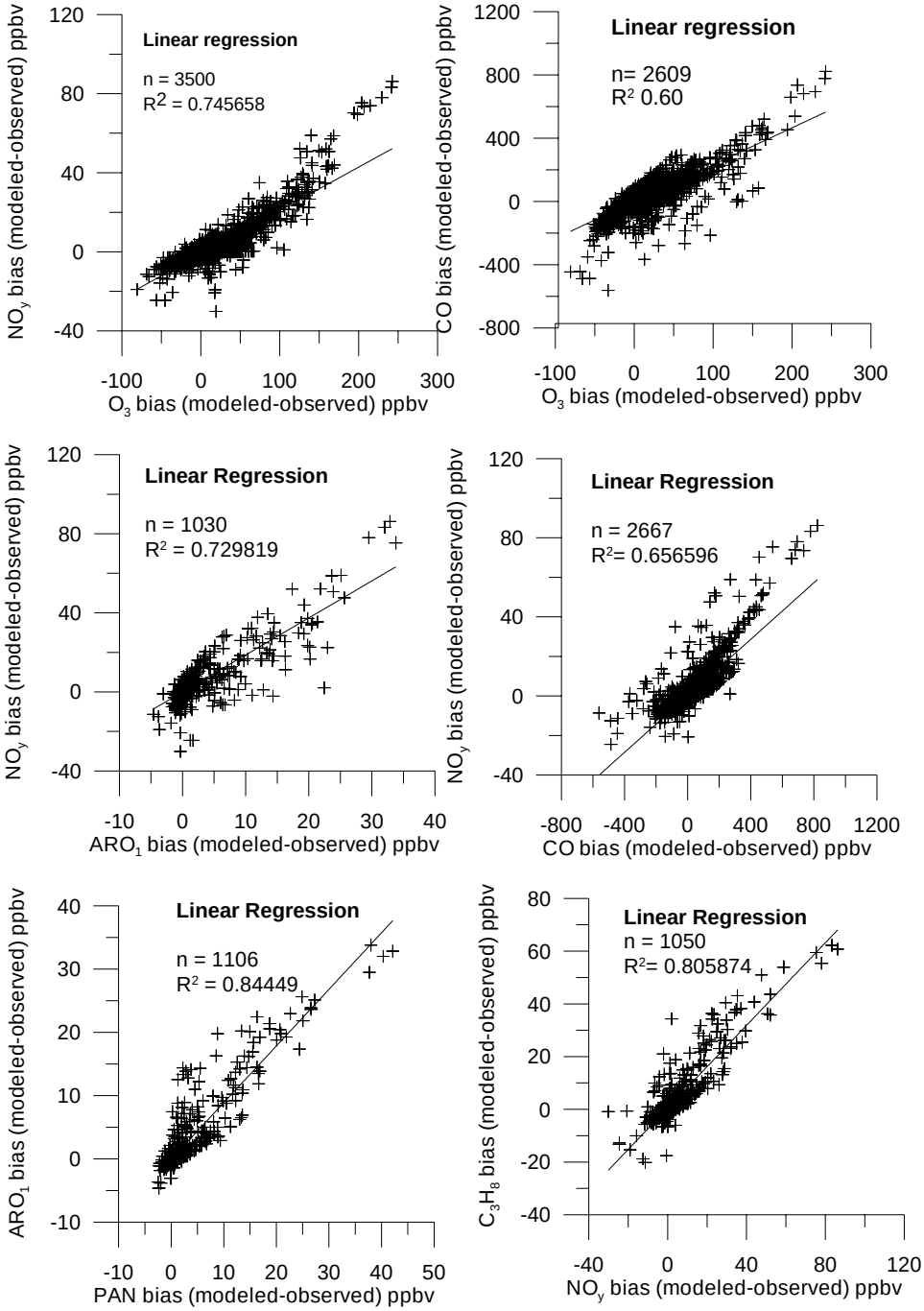

Figure 21 Correlation of bias (modeled-observed) of selected species involved in ozone formation. Modeled values based on forecast run F along C-130 flight tracks during MILAGRO

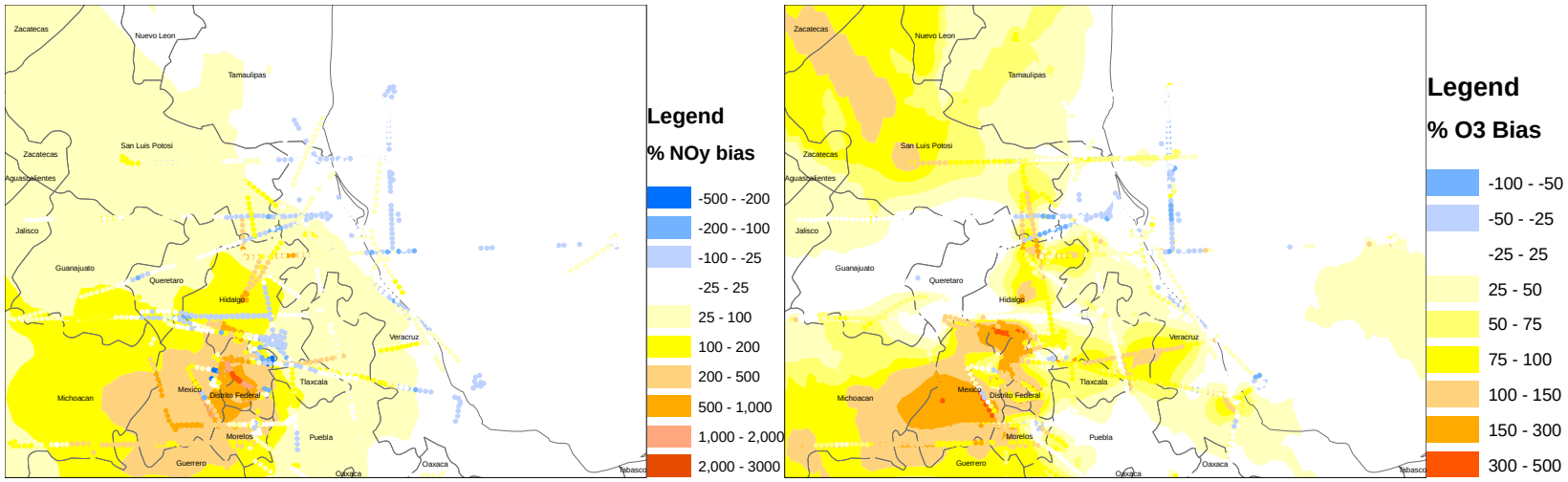

Figure 22 Kriged ozone (n=4061) and NO_y(n=3909) percent bias (modeled-observed) for C-130 platform, Left: NO_y. Right: O_3. Model configuration: Forecast run F: RAQMS boundary conditions, RAQMS biomass burning, base emissions inventory

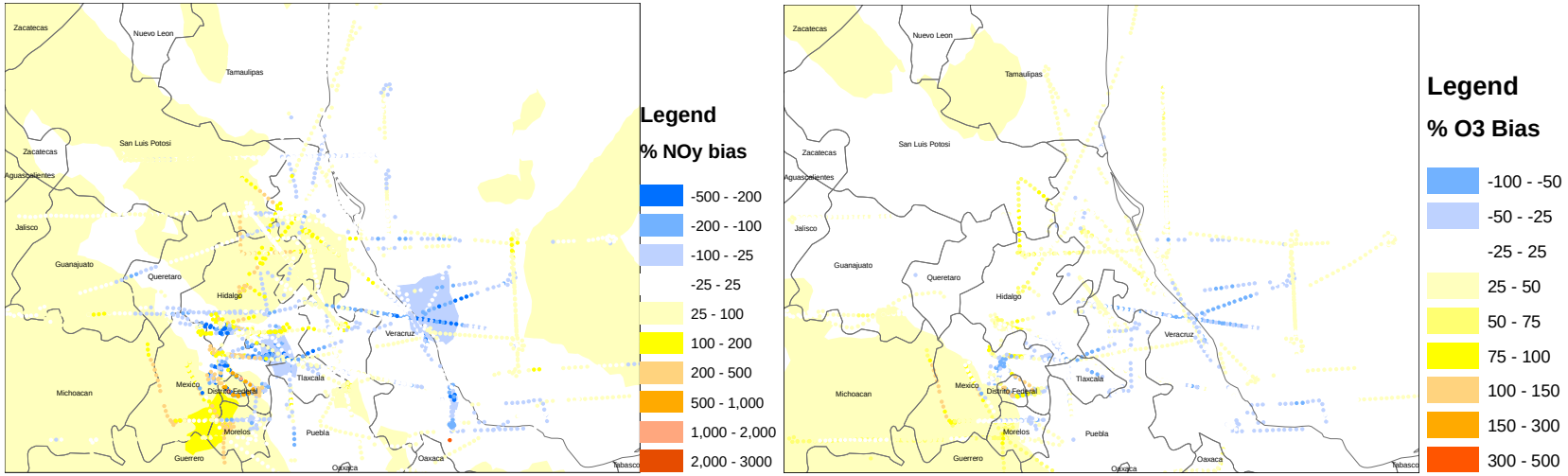

Figure 23 Kriged ozone (n=4061) and NO_y(n=3909) percent bias (modeled-observed) for C-130 platform, Left: NO_y. Right: O_3. Model configuration: Post analysis run I: RAQMS boundary conditions, RAQMS biomass burning, reduced base emissions inventory

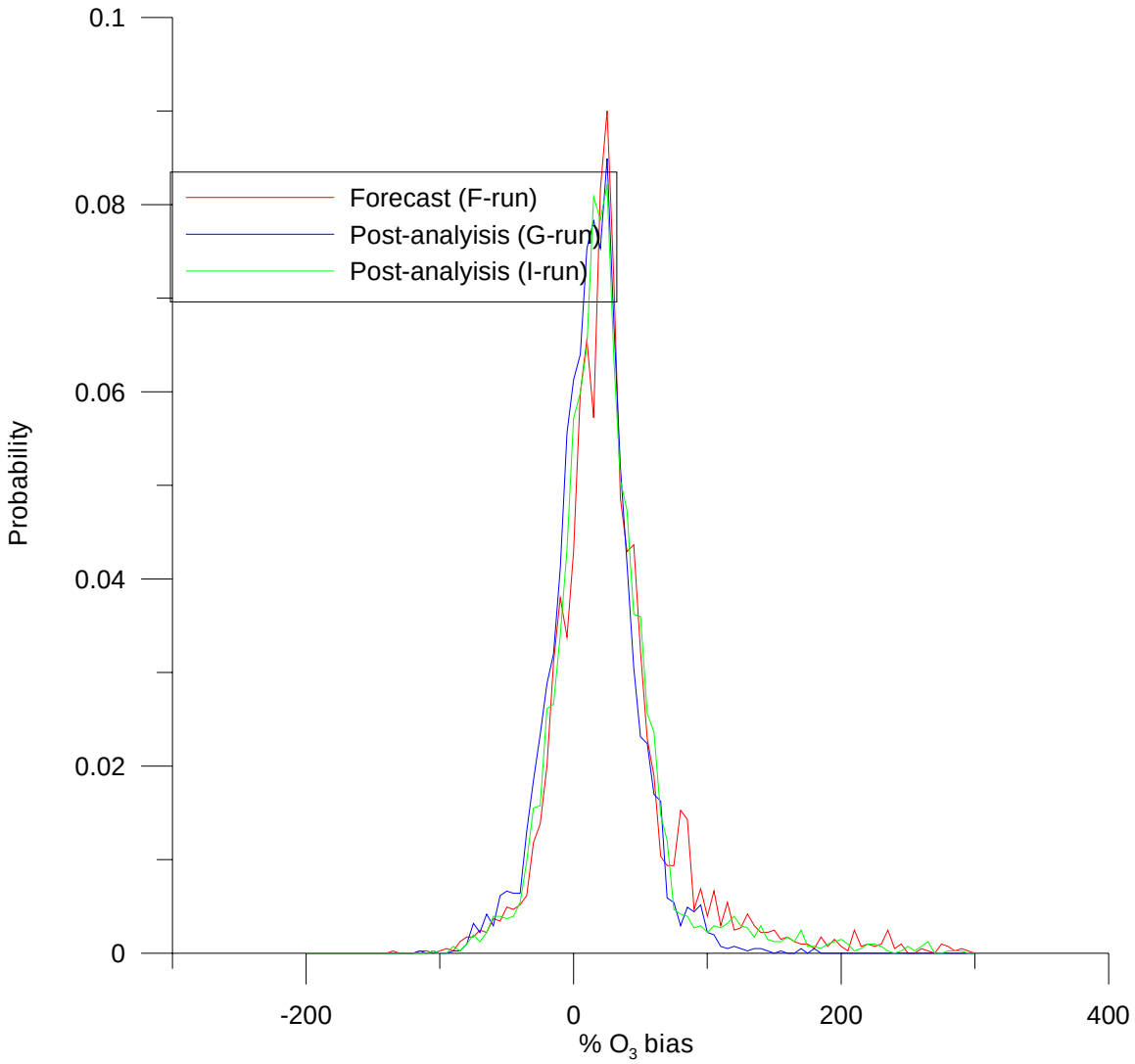

Figure 24 Probability distribution of percent ozone bias for MILAGRO forecast and post analysis runs, based on values extracted along C-130 flight tracks, all altitude ranges

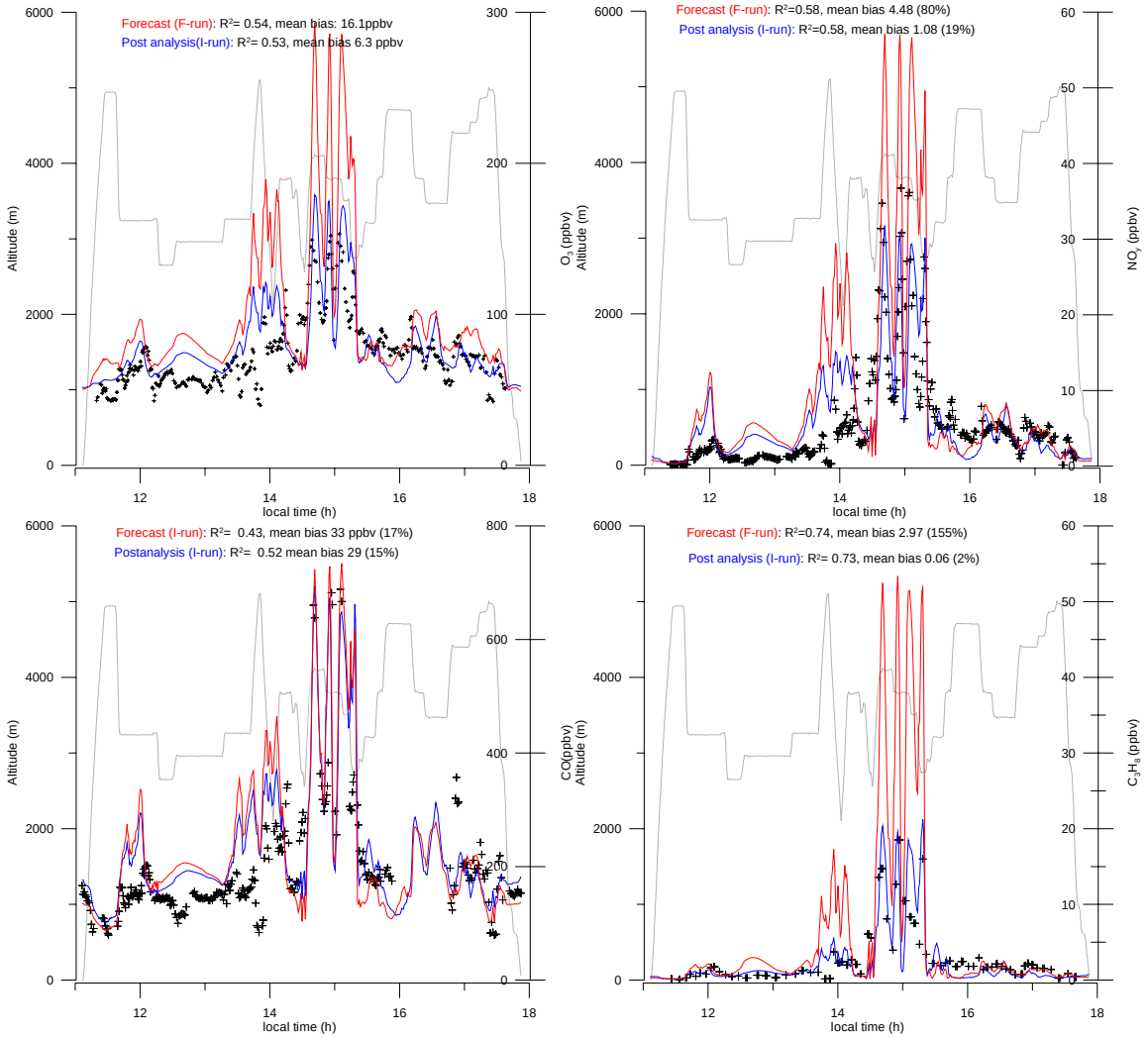

Figure 25 Observed and modeled concentrations along C-130 flight 2 (March 8, 2006) for forecast (Red) and post-analysis with reduced Mexico City emissions (Blue). Gray lines denote flight altitude. Top Left: O_3, Top Right: NO_y, Bottom left: CO, Bottom Right: C_3H_8

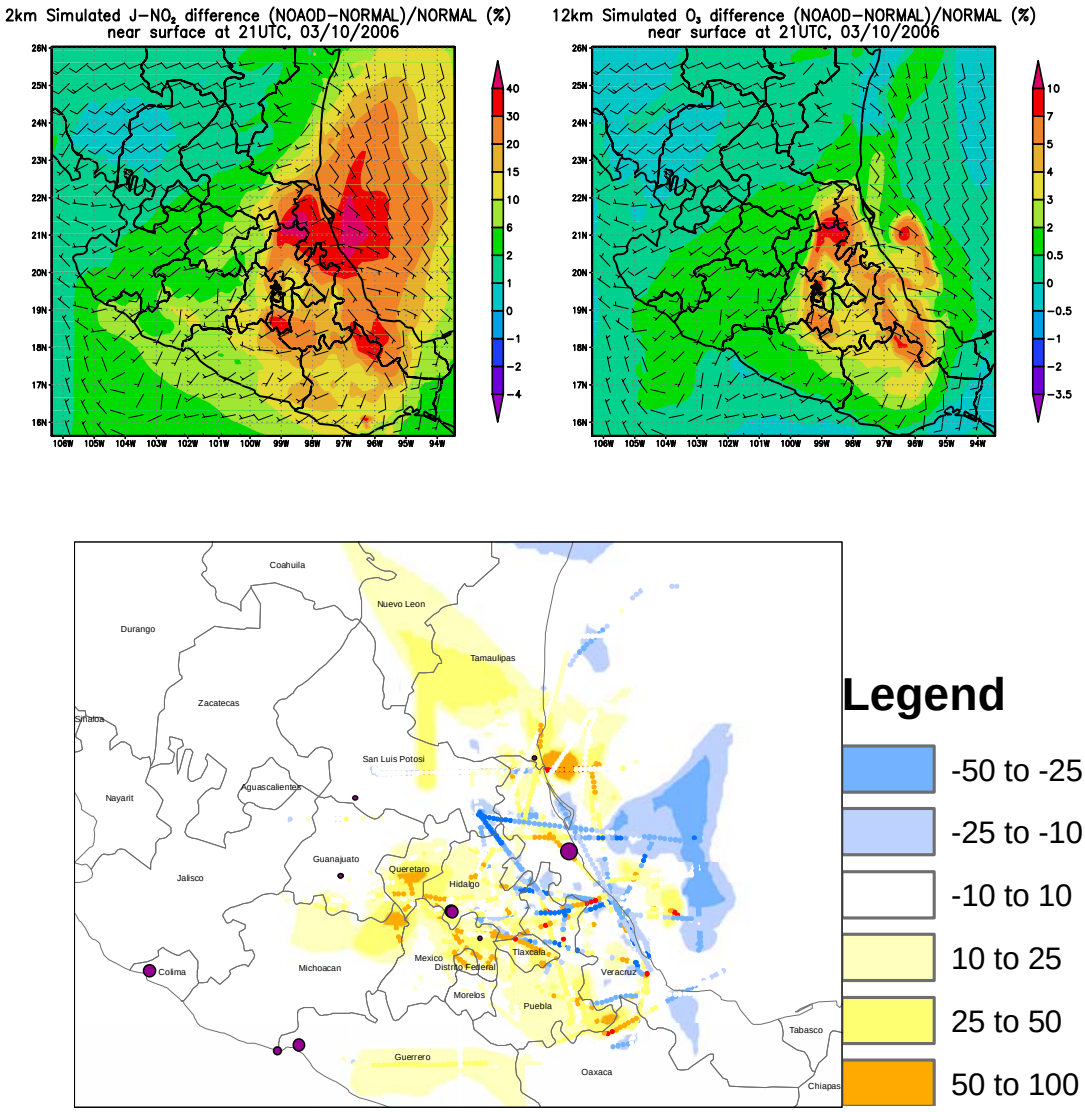

Figure 26 Effect of Mexico City aerosol on regional photochemistry. Top left: Effect of aerosol on simulated photolysis rate calculations for March 10, 2006 (21UTC). Right: Effect of aerosol on O_3 formation for March 10, 2006 (21UTC). Bottom interpolated percent bias of modeled vs. observed J[$NO_2 \rightarrow NO+O$] for values extracted along C-130 flight tracks (all flight tracks)

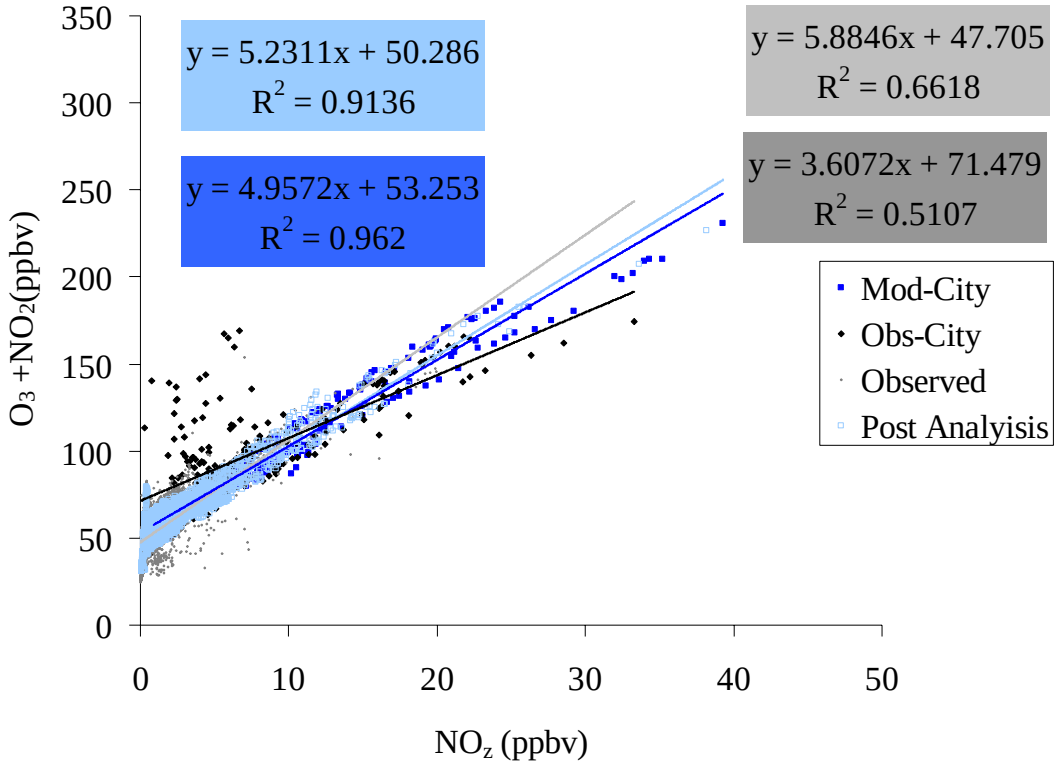

Figure 27 Calculated ozone production efficiency extracted along C-130 flight tracks for modeled (I-run) and observed concentrations, March 1-30, 200. Darker colors denote values in Mexico City (city loop)

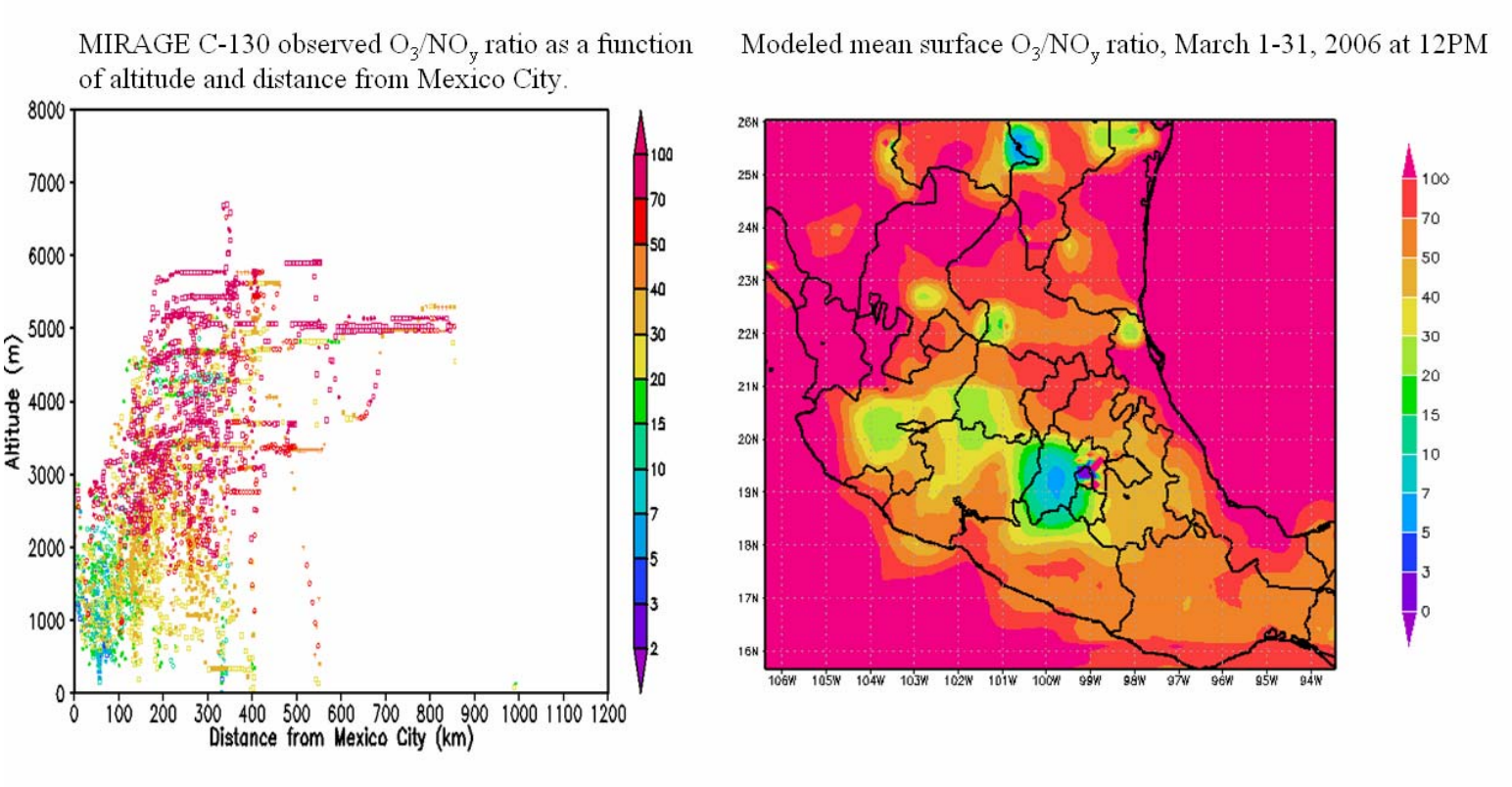

Figure 28 Ozone production regimes in Mexico. Top Left: Observed O_3/NO_y ratios along C-130 flight tracks, as a function of distance from Mexico City and altitude. Right: Mean modeled surface O_3/NO_y ratio, March 1-31, 2006, at 12PM

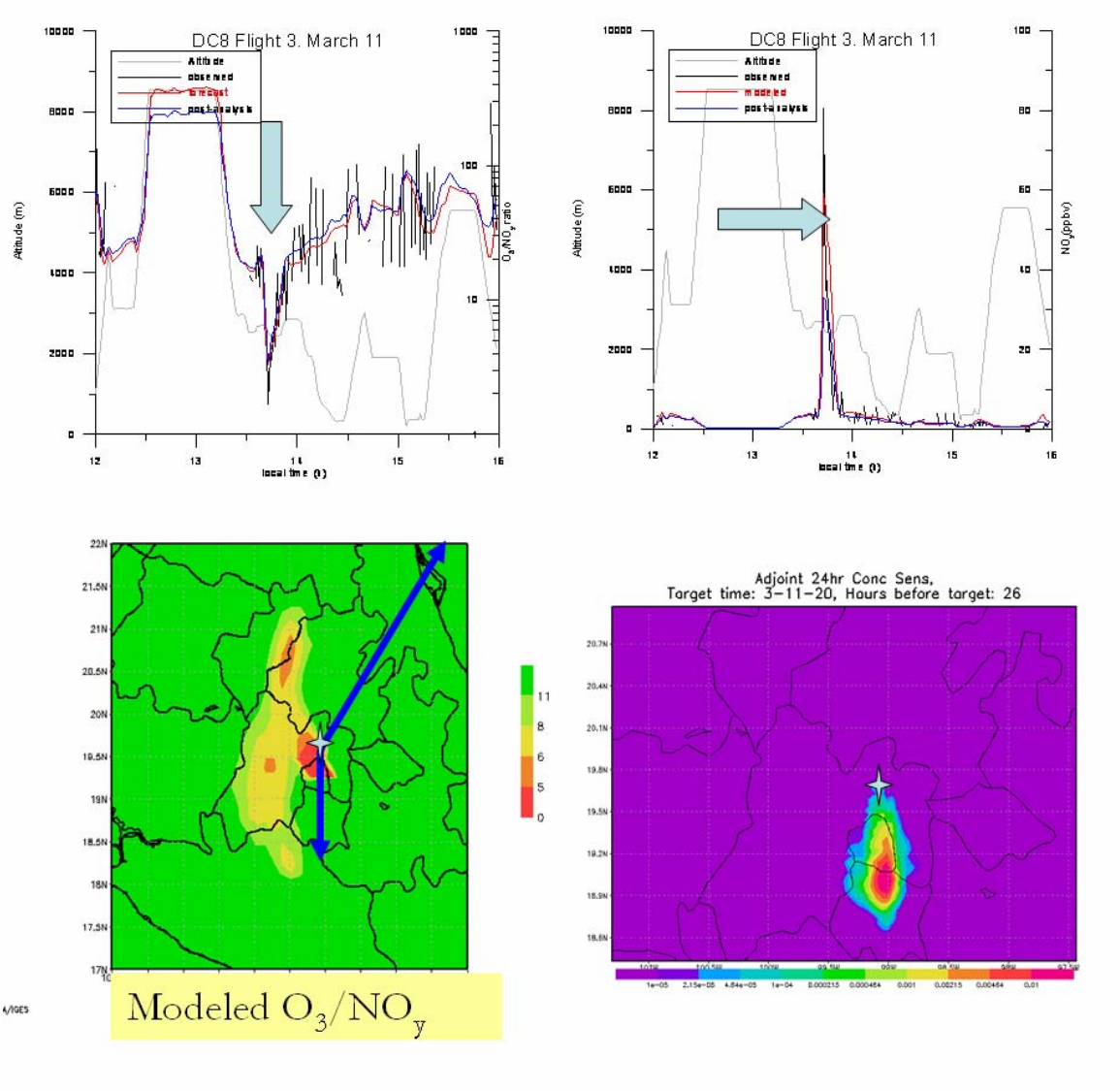

Figure 29 March 11, 2006 DC-8 flight ozone production regime. Top left: Observed and modeled O_3/NO_y (12km meteorology). Top right: Observed and modeled NO_y. Bottom left: Surface modeled (I-run) O_3/NO_y Bottom right: Adjoint sensitivity analysis on point using 4km meteorology

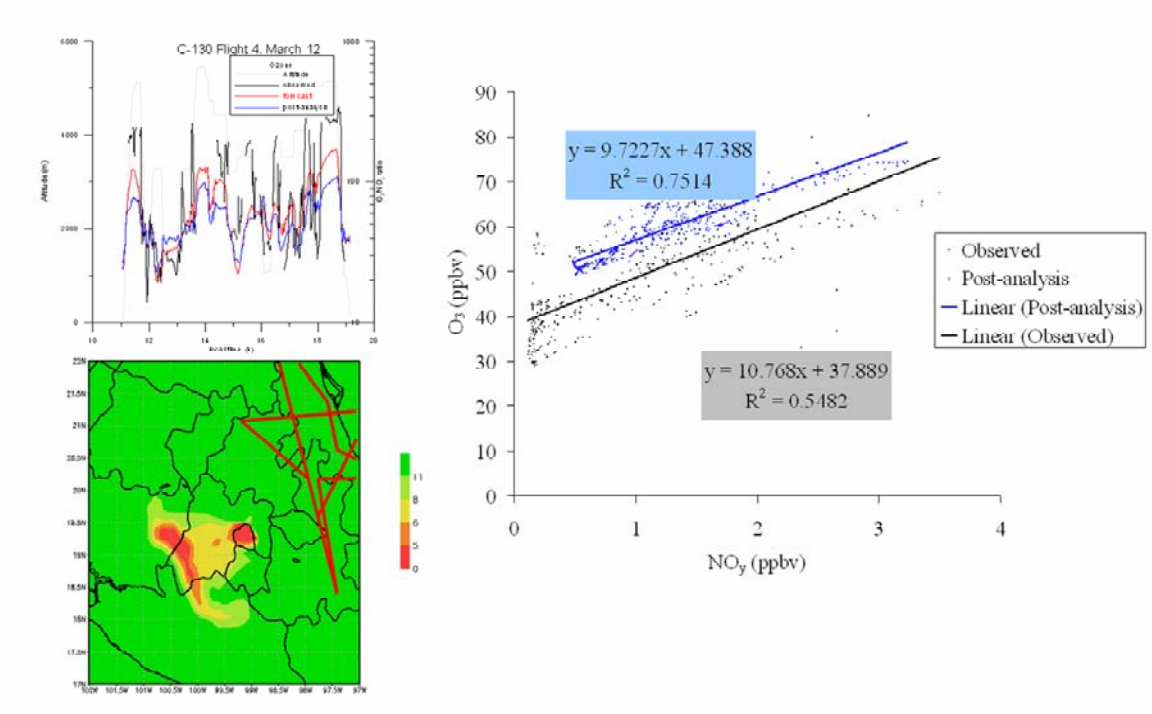

Figure 30 March 12, 2006 C-130 flight ozone production regime. Top left: Observed and modeled O_3/NO_y (12km meteorology). Bottom left: Surface modeled (I-run) O_3/NO_y Right: Ozone vs. NO_y (modeled and observed) along C-130 flight track

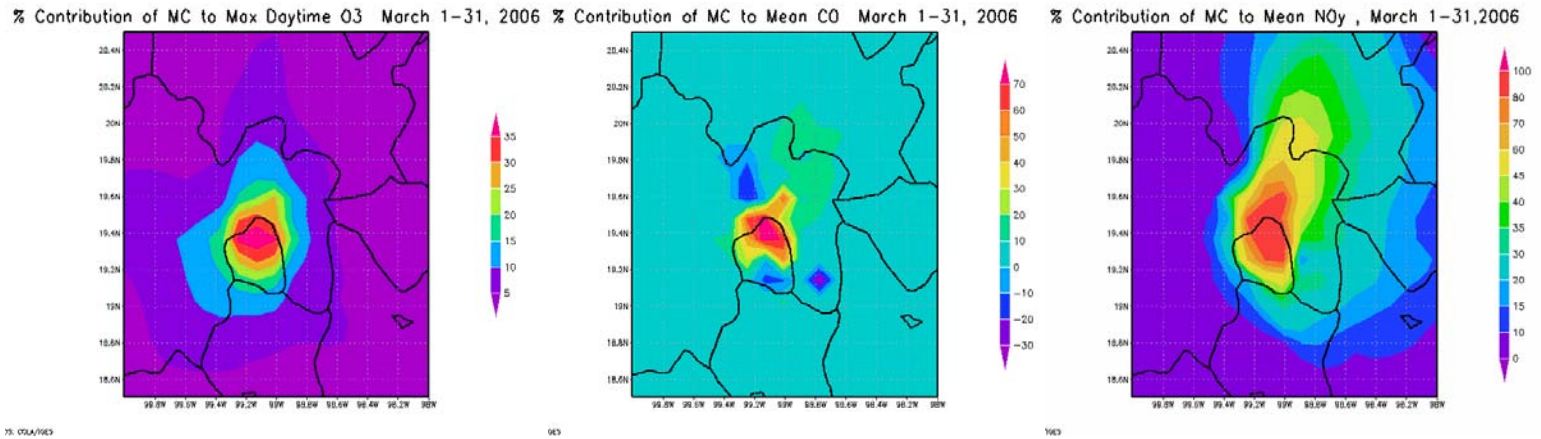

Figure 31 Calculated effect of Mexico City on regional air quality. Left: Simulated percent contribution to maximum daytime surface ozone. Center: Simulated percent contribution to mean CO. Right: Simulated contribution to mean NO_y. Calculated for March 1-31, 2006, as the difference in concentrations with and without Mexico City emissions from I-run

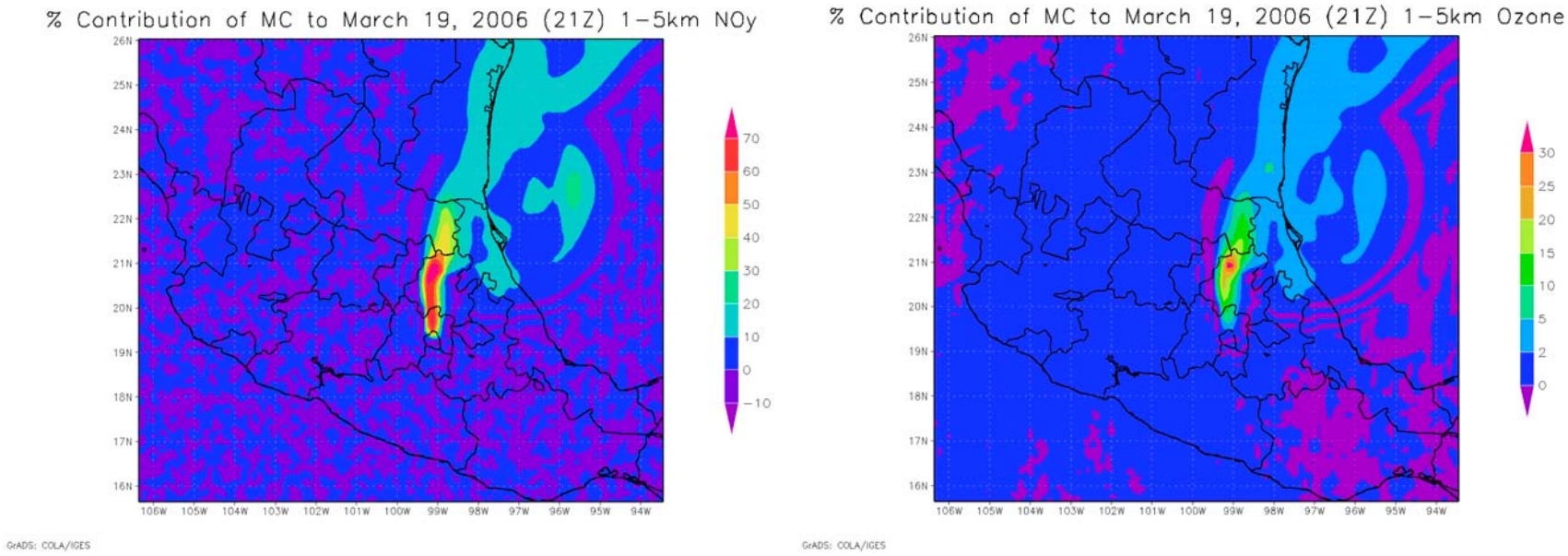

Figure 32 Calculated effect of Mexico City on regional air quality. Left: Simulated contribution to mean 1-5.4 km NO_y. Right: Simulated percent contribution to March 19, 2006 (21Z) 1-5.4km mean ozone. Calculated as the difference in concentrations with and without Mexico City emissions from I-run

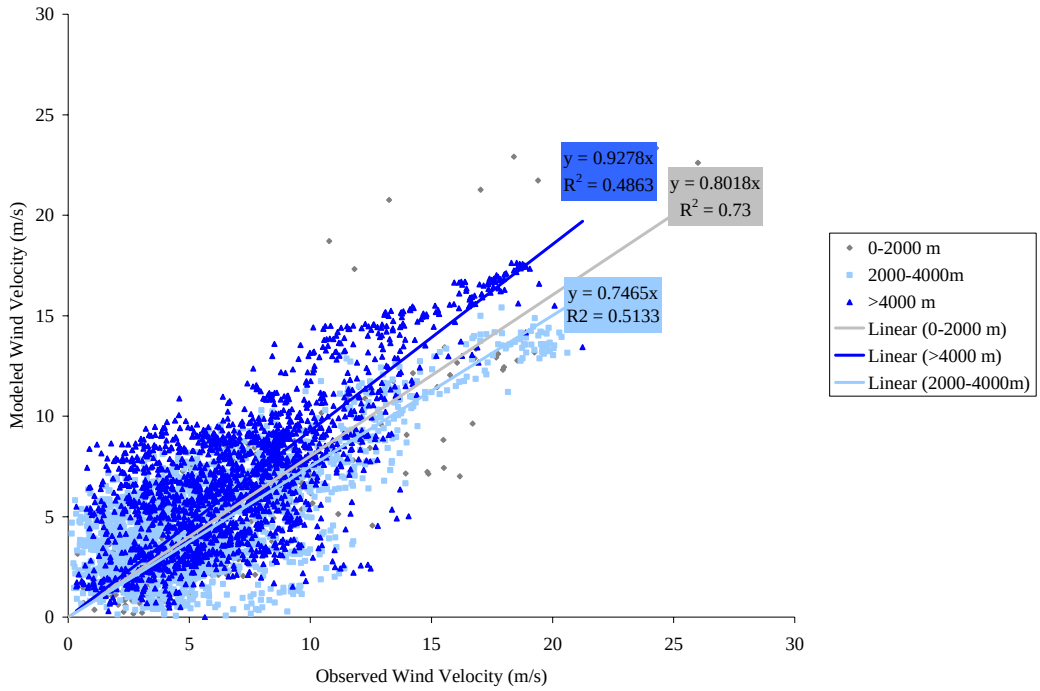

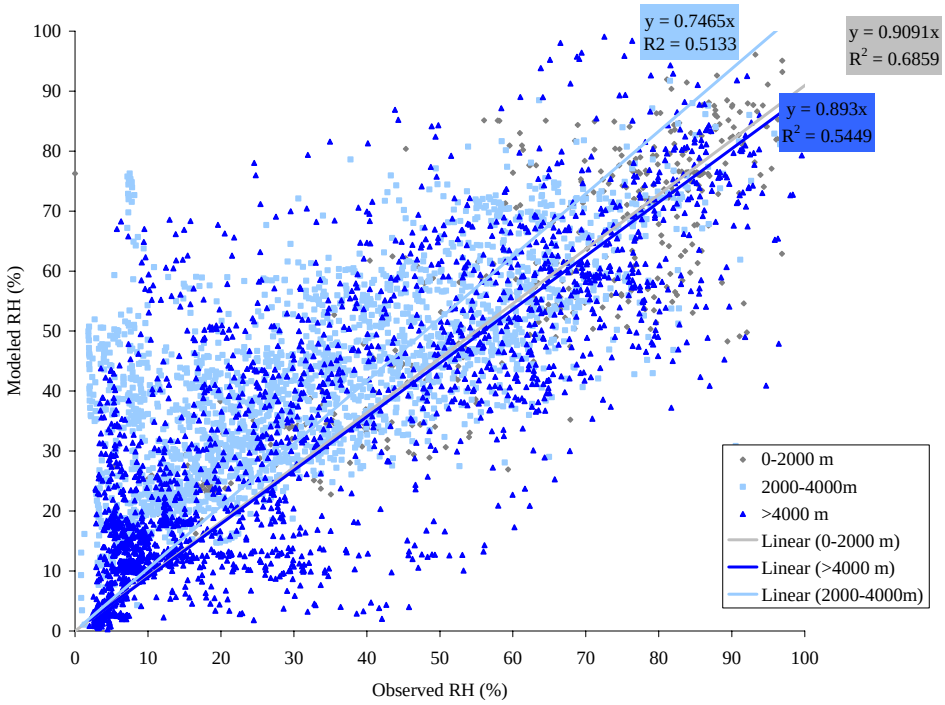

Figure 33 Modeled and observed meteorological parameters separated by altitude. Top: Wind velocity. Bottom: Relative humidity

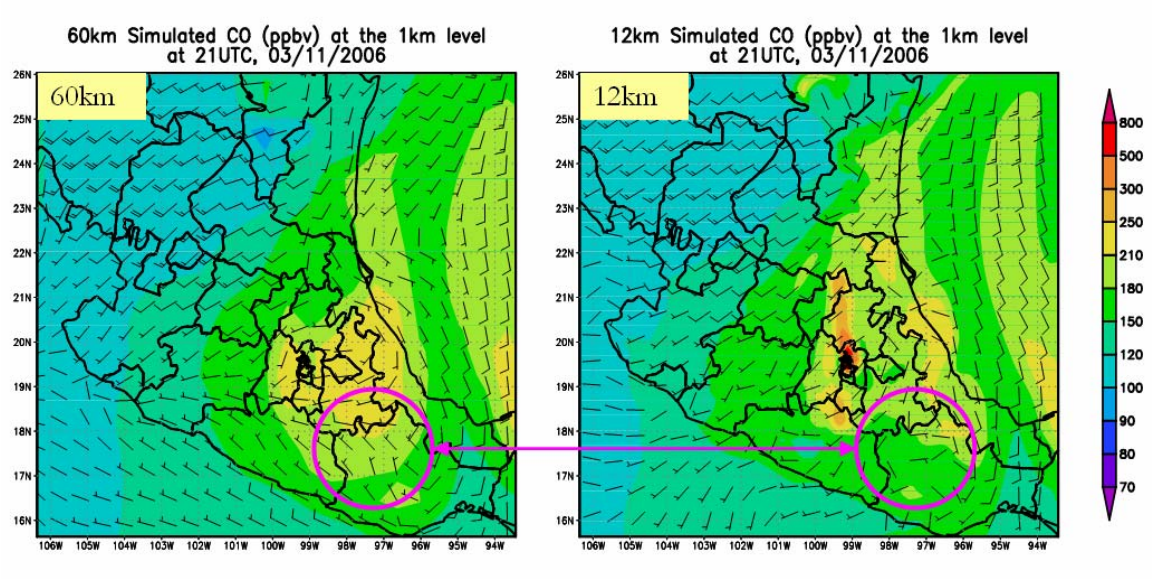

Figure 34 The effect of model resolution on model results. Left: 60km STEM, Right: 12km STEM

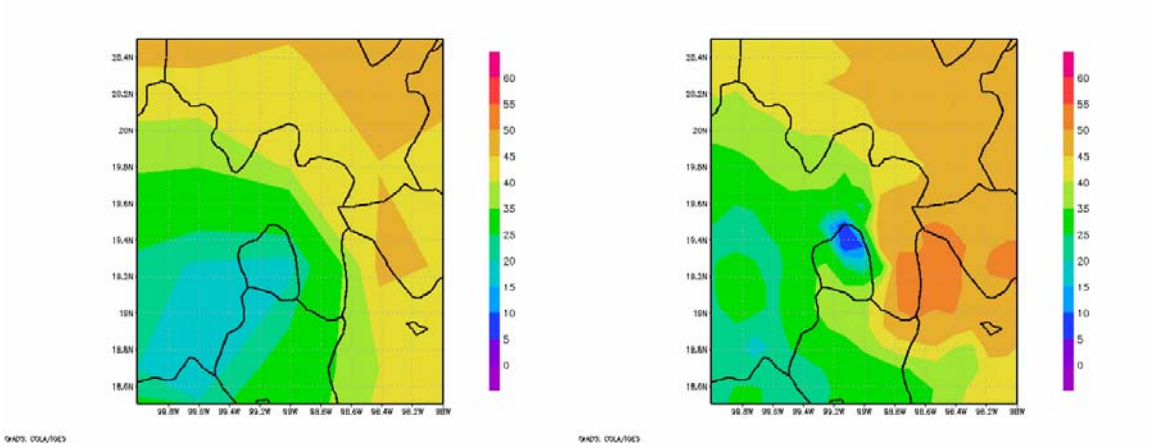

Figure 35 Comparison of mean modeled surface nighttime ozone from March 1-30, 2006 for 60km (left) and 12km (right) model resolutions, I run.

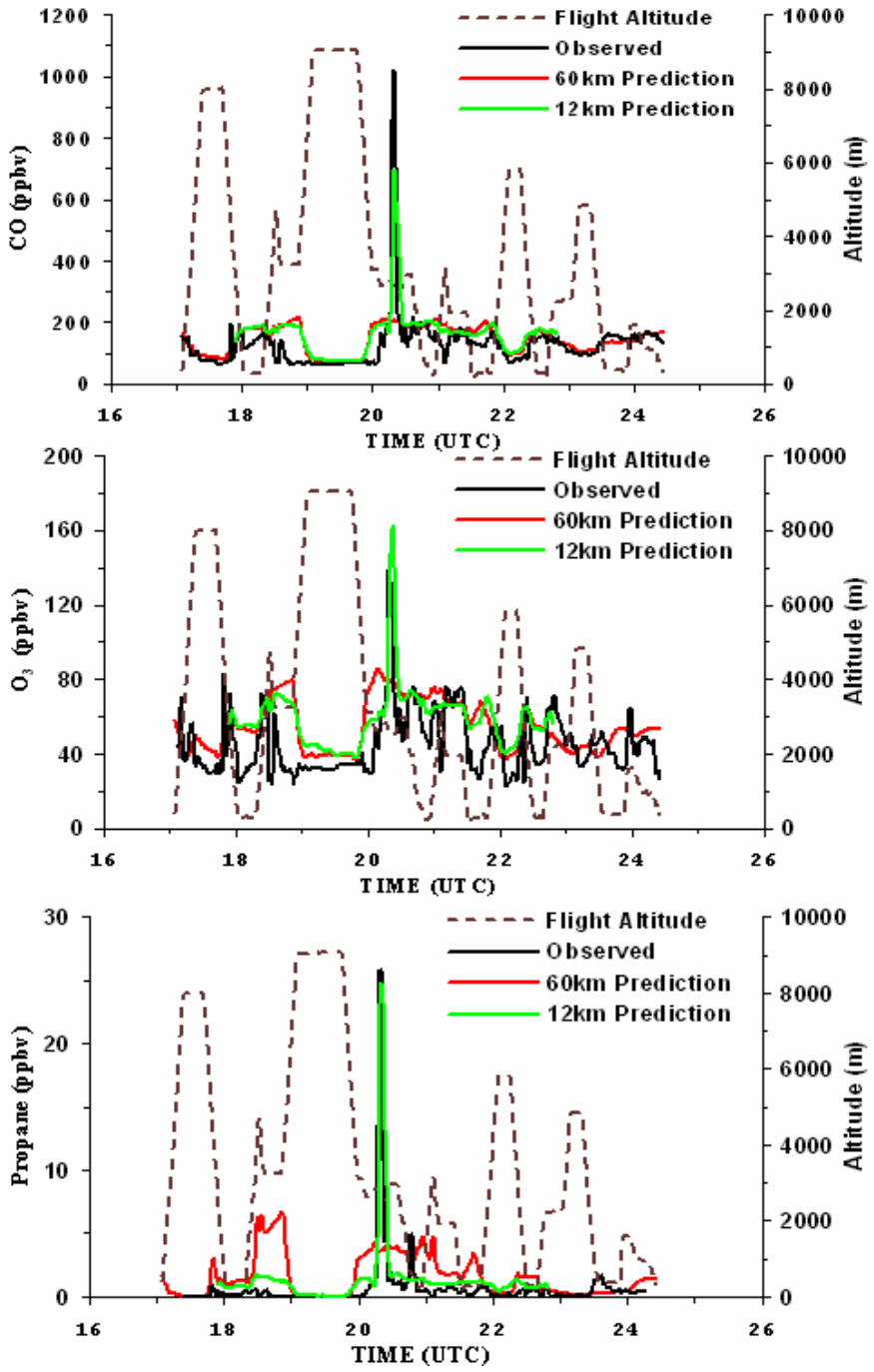

Figure 36 Effect of model resolution on model performance. Values extracted along March 11, 2006 flight for DC-8. Top: CO Center: O_3, Bottom: Propane. In red is 60km I run results, in green, 12km I run results

CHAPTER 4 EMISSIONS INVENTORY

This section summarizes some valuable capacity in emissions inventory development that was gained in the midst of two projects at CGRER: The Bahia project and MILAGRO. The first project was a consulting project for the Petrochemical Pole of Camacari, in Salvador, Bahia. This complex wanted to evaluate its regional impact on ozone formation. During the project a ground up emissions inventory was developed. The second inventory was developed for the MILAGRO campaign, making use of information that became available after the forecast stage of the campaign, to provide an inventory that is readily used by the modeling community.

4.1 Salvador, Bahía

Before this project started, there was no emissions inventory of the Salvador, Bahia domain, so one was developed based on the best available information for the estimation of area and road emissions. Point source emissions used in the inventory had been previously been measured or estimated by the petrochemical complex. Emissions are considered to have a diurnal cycle as is shown in Figure 37. In this figure we observe higher emissions during the morning and evening rush hour, and to a lesser extent during lunch time. The emissions inventory was reported in CO, NO_x, PM_{10}, VOC, and SO_2. NO_x emissions were estimated to be 90% NO and 10% NO_2, since it is estimated that primary combustion sources generate mostly NO and not NO_2[1]. In the case of VOC, which is an operationally defined compound, it is assumed that it is a speciated into 18 lumped chemical compound groups, according to the SPRC 99 chemical mechanism (ftp://ftp.cert.ucr.edu/pub/carter/pubs/s99appa.pdf). This speciation is used to run STEM's 218 chemical reactions, since separating VOCs into more compounds would increase the number of species in the model largely, and making it computationally more intense. The emissions inventory considered a 3km resolution, meaning that all emissions are placed in the center their corresponding grid. Figure 38

shows the emissions inventory of CO, in which we observe that most emissions are mainly located near Salvador, the Petrochemical Complex, and the copper smelter.

4.1.1 Road emissions

The road emissions, or transport emissions, were calculated based on emission factors; vehicular kilometers traveled (VKT) and the number and age of vehicles. The estimation of emissions, calculated in tons per year, is done by multiplying the emission factor (EF) times the quantity (N), times the vehicular kilometers traveled per year (VKT).

$$M_i = \sum M_{ij} = \sum\sum\sum EF_{ijk} * N_{jk} * VKT_j \quad (12)$$

Where:

M_i: emission of species i

M_{ij}, emissions of species i, due to vehicle type j, g/year.

EF_{ijk}, emission factor of species i, due to vehicle type j, of the age group k, g/km/vehicle

N_{jk}, quantity of vehicle type j, of age group k, vehicle

VKT_j, number of vehicular kilometers traveled per year for vehicle type, km/year

The vehicular age distribution was obtained from the Bahia Department of Transport. We estimated the vehicular kilometers traveled (VKT) per vehicle based on information provided by CETREL for cars, and based on typical values taken from a World Bank study.

Table 16 shows the age distribution of the vehicles of Salvador. Table 17 shows the VKT for each vehicle group, and Table 18 shows the emission factors per VKT for every vehicle type. Figure 38 shows our estimated mobile source emissions, considering

that the domain of the model is 39% of the total area of Salvador. Table 20 shows that most of the road emissions are due to the truck and buses of the Salvador area.

Mobile source emissions are distributed in each grid according to the amount of roads and population in each cell. The distribution of roads and population information was manipulated and regrid into the model cells using ArgGis. The following shows how each grid cell's emissions are estimated.

$$E_k = \sum \sum E_{jk} = \sum\sum \sum EF_{ik} * A_{ij} \quad (13)$$

Where :$RE_{i,j,k}$ represents the road emissions of compound k, for cell i,j.

TE_k: total road emissions of compound k

$P_{i,k}$: population in cell i,j

$L_{i,k}$: total km of roads in cell i,j

TP: total population of domain

TL: total km of roads in domain

Figure 38 shows the CO emissions for the domain. In it we observe that most emissions occur in more densely populated areas, and of course in areas in which there are more roads.

4.1.2 Point sources.

Point source emissions were estimated based on the emission inventory submitted by CETREL. These point emissions are grouped in each grid cell, and placed geographically in the center of the grid.

Table 21 shows the summary of the emissions of different sources for the domain we are modeling. Figure 38 shows the point source emissions in our gridded domain. In it we observe that point source emissions are mainly concentrated near the Polo and the refinery complex.

4.1.3 Area sources

Area sources were estimated from the fuel use of the region of Salvador, based on information obtained from a personal communication with Joao Antonio Moreira Patusco, the general coordinator for the Brazil Energy Balance from Mines and Energy Ministry of Brazil. This information includes all fuel sources used in the region, separated by economic sector of use.

Anthropogenic area emissions are defined as those due to combustion of fuels from residential, commercial, public and agricultural sources The fuel sources that were considered in the inventory were natural gas, coal, timber, sugar cane bagasse, diesel, liquid petroleum gas (LPG), naphta and light kerosene. Emission factors were taken from the Clean Air Climate Protection software package, developed by the International Council for Local Environmental Initiatives (www.iclei.org) for all fuel sources. Total area emissions for each species are estimated according to the following equation:

$$E_k = \sum \sum E_{jk} = \sum\sum \sum EF_{ik} * A_{ij} \quad (13)$$

where,

E_i=emission of species k,

E_{jk}=emission of species k, due to economic sector j

EF_{ik}=emission factor of k, due to fuel source j, kg of compound per million ton million m^3

A_{ij}= Use of fuel type i, due to economic sector j, m^3/year or ton/year.

Emissions are then distributed in the model grids, proportional to the population of each grid, similar to the road emissions. The following equation shows how area emissions are estimated, as proportional to the population in each grid cell in comparison to the total population of the domain.

$$E_{i,j,k} = \frac{E_k * P_{i,j}}{TP} \quad (14)$$

Where :$E_{i,j,k}$ represents the area emissions of compound k, for cell i,j.

E_k: total road emissions of compound k

$P_{i,j}$: population in cell i,j

TP: total population of domain

Table 22 shows the emission factors of each fuel source, in which we observe that natural gas and LPG have considerably lower emissions per unit of weight, for all of the primary pollutants, while we can also observe that heavy fuels, such as diesel, fuel oil, jet fuel, naphtha, and kerosene have considerably higher emissions of the majority of the pollutants. Table 23 shows that the majority of emissions come from residential sources, followed by agricultural sources, for all species emitted. Figure 38 shows that most area emissions are located where there is more population. Essentially, we can observe that most emissions are located near Salvador, and the bigger surrounding cities.

4.1.4 Summary of emissions

Table 24 shows the summary of emissions of each primary pollutant, separated by emission type. In Table 25 it is shown that most CO, VOC, and NO_x emissions come from the transport sector, while PM_{10} comes mostly from area sources. Finally, SO_2 emissions are mostly from point sources.

4.2 Mexico National Emissions Inventory

For post analysis a first national emissions inventory for Mexico was published (EPA, 2006) which was the result of work from numerous Mexican and US government and non governmental organizations. The inventory, which used both a top down and bottom up approach to estimate area, mobile, and point sources, considered emissions of primary pollutants CO, volatile organic compounds (VOC), nitrogen oxides (NOx), sulfur dioxide (SO2), NH3, and primary PM10 and PM2.5. Detailed methodology to

estimate these emissions is available in a report by the Eastern Research Group [*ERG*, 2006].

4.2.1 Point sources

Information on point source name, location, category, emissions intensity, was extracted from the Mexico National Emissions Inventory webpage, using a relational database to consolidate multiple sources for each location. Point sources from border states have source category information associated to it, but internal states lack of this information. A total of over 3800 point sources were considered for this work, with the emissions being calculated from a combined methodology of activity based emission factors and smokestack measurements when available. These sources are show in Figure 39.

4.2.2 Area sources

A top down estimation of emissions was used to calculate emissions for the following source categories:

- anthropogenic combustion processes from industrial, domestic, agricultural, and commercial activities.
- Bus and truck stops,
- Commercial and domestic use of solvents
- Painting, degreasing, dry cleaning, graphic arts, asphalt, brick production, construction activities
- Distribution of gasoline and liquid petroleum gas (LPG)
- Street restaurants, bakeries
- trains, airplanes, ships
- applying pesticides, fertilizer, animal feeding operations, agricultural burns
- open burning of waste, wastewater treatment, landfills

- Domestic ammonia emissions
- Forest fires, domestic fires
- Particulate matter from wind erosion, and from paved and unpaved roads.

However a geographical distribution of these emissions was required to use this inventory for the model. For this a simple approach distributing emissions using ambient population from Landscan [*ORNL*, 1999] (0.008333° resolution, regrid to 0.025°) as proxy using the following expression to calculate emissions of each individual cell as is shown in the following equation.

$$E_{ij_k} = \frac{E_{ik} * Pi_j}{P_i} \quad (15)$$

Pi: Total population state i.

Pij: Population of grid cell j of state i.

E_{ik}: Total emissions of species k for state i (Mg/year)

E_{ijk}: Emissions of species k of grid cell j for state i (Mg/year)

The same approach was used to calculate the distribution of non-road mobile sources (such as tractors, construction machinery, etc). Figure 40 shows the gridded emissions for Mexico City at a 0.025° resolution.

4.2.3 Mobile sources

Similarly a geographical distribution to emissions from mobile sources was also required. For this a comparable approach was taken, distributing emissions based on population, but only in grid cells in which roads detected by Landscan exist (for areas outside of Mexico City) and from the INEGI's GIS Database (INEGI, 2007) for Mexico City, in a Boolean approach. This also resulted in an inventory with 0.025° resolution, as is shown in Figure 41.

4.3 Results using Mexico NEI

The Mexico National Emissions Inventory was evaluated by comparing model results extracted along C-130 flight tracks and compared to observations. The model run (NEI-run) was configured using the same parameters as the I-run (MOZART boundary conditions, RAQMS biomass burning emissions, WRF meteorology) but the emission distributions were taken from the new inventory. Diurnal emission profiles were not used for this run. One of the problems with this inventory is that VOCs are reported as tons/year, without a clear definition of VOC. It is for this reason that VOCs were speciated for this run using the total emissions of each compound that were used in the I-run. Unfortunately this was unavoidable as the methodology that was employed to calculate VOC totals blended heterogeneous emission factors (that represent specific species) into a total mass sum that does not provide information on molar totals. Table 26 shows that NOx and SO2 emissions in the Mexico National Emissions Inventory were considerably higher than the inventories used in Chapter 3 (F and I runs). From previous analysis it was known that total NOx emissions in the I run yielded only ~20% mean error in NOy modeling, so total NOx in the Mexico Emissions Inventory needed to be adjusted downward (80% reduction) to avoid overprediction. SO2 and CO were not adjusted. Figure 42 shows that when comparing to observations extracted along C-130 flight tracks this inventory yields mean biases of 15% for ozone , 20% for CO, 47% for NO_y, and -30% for C_3H_8, with correlation coefficients lower than post-analysis run I (shown in Table 12). Also high observed values of NO_y , O_3, and CO are underpredicted (probably near Mexico Cit). Figure 43 shows that regional distribution of model error of O_3, NO_y, CO, and C_3H_8, where NO_y is underpredicted to the NW of Mexico City, while overpredicted E of the city. Ozone in turn presents similar underprediction NE of the city, and overpredictions South and West of the city. Figure 44 shows that for specific flights however, such as March 16, 2006, modeling performance is substantially better using this

emissions inventory. In this flight correlation coefficients for ozone improved from R^2=0.07 to 0.40, and from 0.06 to 0.20 for NO_y and CO.

4.4 Conclusion

Methodology to determine a bottoms up emissions inventory for Bahia and Mexico is presented. This methodology is reproducible and useful in locations where emissions inventories do not exist. The Mexico National Emissions Inventory probably presents overestimation of NO_x emissions (by a factor of 4 compared to run I), while CO totals are similar. SO_2 emissions are higher than the I run, but probably consider a more complete total of large point sources. VOC emissions in the inventory are difficult to use due to the lack of definition of VOC totals, and lack of speciation. A model run using the Mexico City Emissions Inventory (adjusting VOC and NO_x totals to totals in I run) showed promising results in areas surrounding Mexico City. Correlation coefficients were lower than previous work. This may be attributed to lack of a diurnal profile of emissions.

Table 16 Age distribution of vehicles in Salvador, Bahia[a]

Age	Vehicle type				
	Cars	Buses	Trucks	Motorcycles	Pick-ups
0-4	213995	7598	34743	81164	19390
5-9	138800	4534	20014	16178	24817
10-14	85015	3786	21323	19675	15362
15-19	80164	2618	15264	15194	10584
20-24	80400	2156	18715	1178	8588
25-29	25613	603	7184	166	3250
30-34	3502	115	2241	10	364
> 34	1098	30	838	21	142

[a](http://www.detran.ba.gov.br/estatistica/veiculos/veicadmundez2003.pdf)

Table 17 Vehicular Kilometers Traveled for Salvador Vehicles

Vehicle Type	VKT (km/day)	Vehicle Type	VKT (km/day)
Motorcycles	60	Truck	200
Cars	64.4	Buses	270
Pickup Truck	80		

Table 18 Emission Factors for Cars, Pickup Trucks and Motorcycles (g/km/veh)

	Cars and Pickup Trucks				Motorcycles			
Age	CO[a]	VOC[a]	PM_{10}[b]	NO_X[b]	CO[a]	VOC[a]	PM_{10}[b]	NO_X[b]
0-4	0.788	0.144	0.14	0.236	19.1	5.6	0.12	0.1
5-9	5.4	0.56	0.19	0.64	19.1	5.6	0.13	0.1
10-14	16.1	1.6	0.22	1.6	19.1	5.6	0.13	0.1
15-19	28.8	2.56	0.22	1.58	19.1	5.6	0.14	0.1
20-24	33	3	0.22	1.4	19.1	5.6	0.14	0.1
25-29	33	3	0.22	1.4	19.1	5.6	0.14	0.1
30-34	33	3	0.22	1.4	19.1	5.6	0.14	0.1
> 34	33	3	0.22	1.4	19.1	5.6	0.14	0.1
Age	Buses				Trucks			
0-4	55.7	13.6	2.33	72.8	55.7	13.6	2.22	72.8
5-9	60	15	2.40	77.1	60	15	2.40	77
10-14	61.4	15.4	2.40	78.9	61.4	15.4	2.40	78.9
15-19	61.4	15.4	2.40	78.9	61.4	15.4	2.40	78.9
20-24	61.4	15.4	2.40	78.9	61.4	15.4	2.40	78.9
25-29	61.4	15.4	2.40	78.9	61.4	15.4	2.40	78.9
30-34	61.4	15.4	2.40	78.9	61.4	15.4	2.40	78.9
> 34	55.7	13.6	2.33	72.8	61.4	15.4	2.40	78.9

[a]from Instituto Brasileiro do Meio Ambiente e dos Recursos Naturais Renováveis (http://www.ibama.gov.br/proconve/home.htm)

[b] from Clean Air Climate Protection software, www.iclei.org

Table 19 Mobile Source Emissions for Salvador

Vehicle Type	Emissions (ton/year)				
	CO	VOC	PM_{10}	SO_2	NO_x
Motorcycles	21977	6443	144	249	115
Cars	16147	1519	198	422	1032
Pickup Truck	12734	1210	188	386	908
Truck	205605	50873	8113	14761	37885
Buses	49095	12105	1973	2613	9003
TOTAL	305558	72150	10616	18431	48943

Table 20 Mobile Sources, Vehicle Type Contribution, in %.

Vehicle Type	% Emissions				
	CO	VOC	PM_{10}	SO_x	NO_x
Motorcycles	7.19	8.93	1.36	1.35	0.24
Cars	5.28	2.11	1.86	2.29	2.11
Pickup Truck	4.17	1.68	1.77	2.09	1.85
Truck	67.29	70.51	76.42	80.09	77.41
Buses	16.07	16.78	18.59	14.18	18.40

Table 21 Total Point Source emissions for Salvador

CO	HC	PM10	SO2	NOx
25,150	35,914	3,829	19,124	26,406

Table 22 Emission factor for fuel-based area emissions

Fuel Type	Emission factor (kg/ton or kg/m^3)				
	NO_X	CO	SO_2	VOC	PM_{10}
Natural Gas	0.0027	0.00070	0.0001	0.00015	0.000083
Coal Burning	10.61	4.32	56.82	0.27	4.98
Timber	0.29	24.04	0.04	4.43	3.14
Bagasse[b]	0.49	0	0	0	6.13
Diesel Oil	16.39	8.63	77.80	1.39	4.69
Fuel Oil	16.39	8.63	77.80	1.39	4.69
Jet Fuel	16.39	8.63	77.80	1.39	4.69
LPG	3.27	0.44	0.0000036	0.12	0.09
Naphta	16.39	8.63	77.80	1.39	4.69
Illumination Kerosene	2.48	8.55	11.88	1.76	0.19
Aviation Kerosene	16.39	8.63	77.80	1.39	4.69

[b]http://www.epa.gov/ttn/chief/ap42/ch01/final/c01s08.pdf

Table 23 Summary of fuel-based area emissions

Fuel Type	Emission factor (tons/year)				
	NO_X	CO	SO_2	VOC	PM_{10}
Residential	12968.31	371992.44	29467.27	68508.48	49869.94
Commercial	24.32	3.30	0.00	0.87	0.69
Public	190.29	73.11	574.37	12.71	36.62
Agricultural	4112.28	38644.03	17447.37	7076.58	5837.61
Total	17,295	410,713	47,489	75,599	55,745

Table 24 Summary of Emissions Inventory for Salvador (tons/year)

Source type	CO	VOC	PM_{10}	SO_2	NO_x
Point	25,150	35,914	3,829	19,124	26,406
Area	107,607	19,807	14,605	12,442	4,531
Mobile	305,559	72,151	10,616	18,431	48,944

Table 25 Summary of Emissions Inventory, Contribution by source type, in percentage

Source type	CO	VOC	PM_{10}	SO_2	NO_x
Point	5.74	28.09	13.18	38.25	33.06
Road	69.71	56.42	36.54	36.86	61.27
Area	24.55	15.49	50.28	24.89	5.67

Table 26 Summary of total yearly emissions (Tg/year) of inventories used in study

	NO_x (as N)	SO_x (as SO_2)	CO (as C)
F run	0.353	1.273	9.686
I run	0.312	1.085	9.686
NEI99	1.57	3.140	8.286

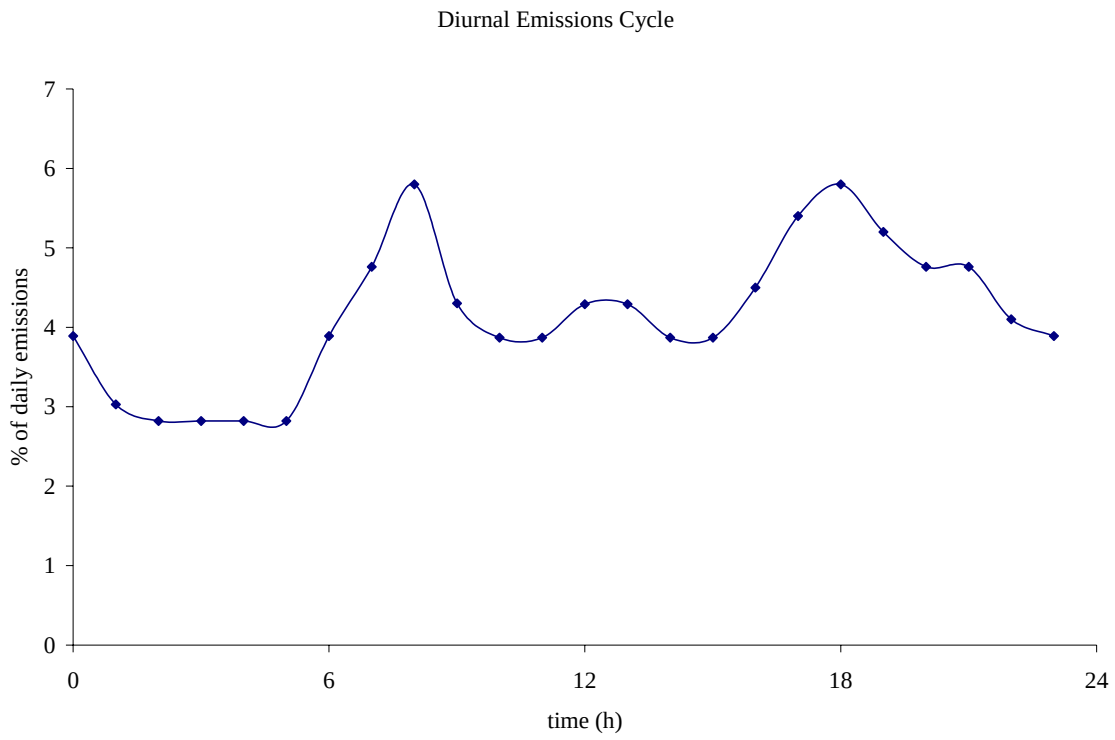

Figure 37 Diurnal emissions cycle used in Salvador Bahia anthropogenic mobile and rea emissions

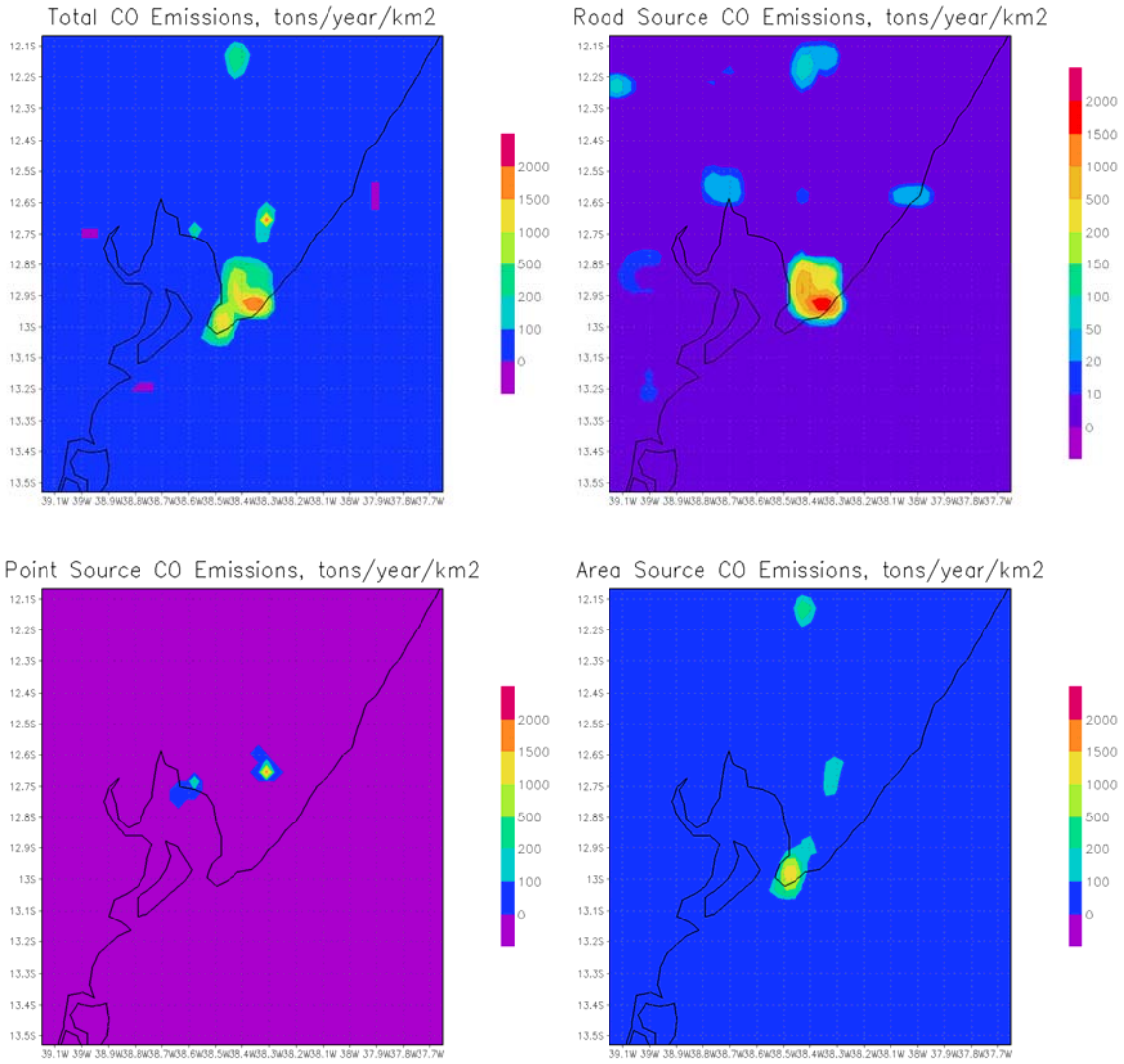

Figure 38 Bahia region emissions inventory for CO. Top Left: Total emissions. Top Right: Road or mobile emissions. Bottom left: Point source emissions. Bottom Right: Anthropogenic area Area source emissions. All emissions in tons/year/km^2

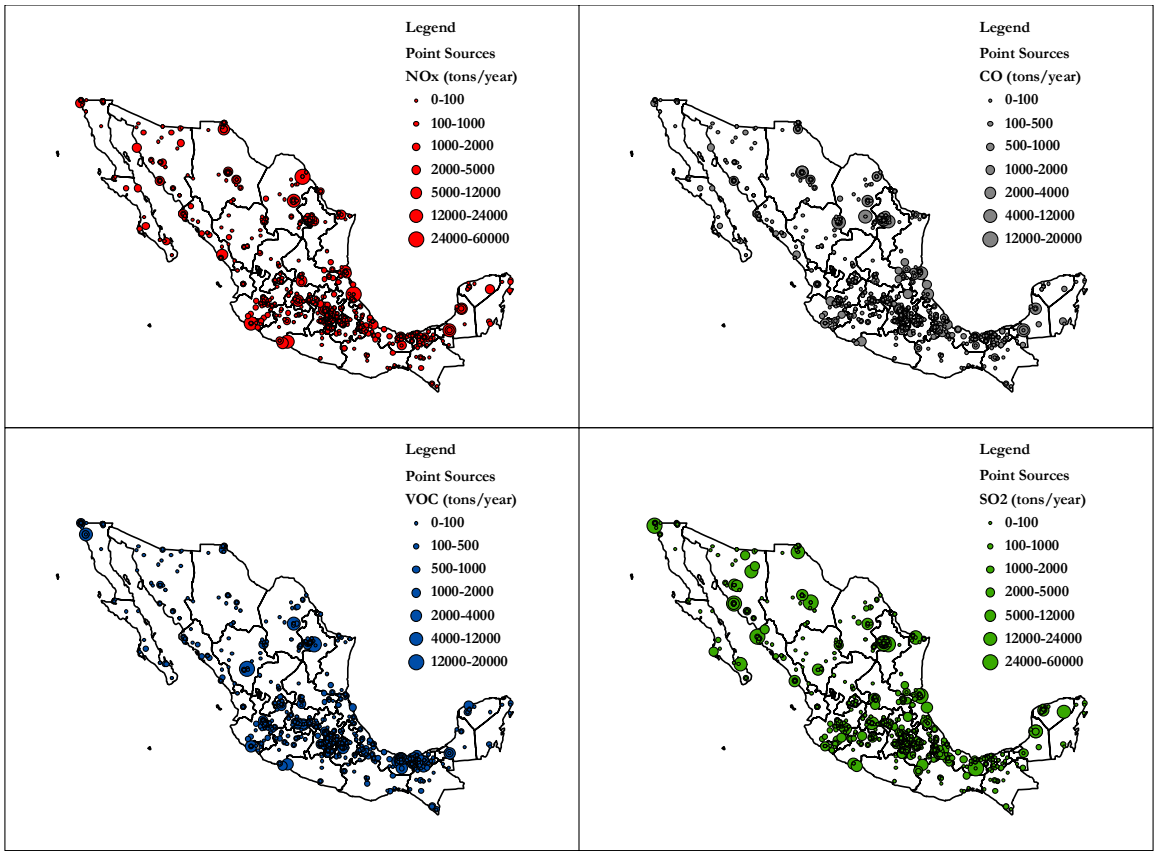

Figure 39 Large point sources for Mexico National Emissions Inventory 1999. Top Left: NO_x, Top right: CO, Bottom Left: VOC, Bottom right: SO_2

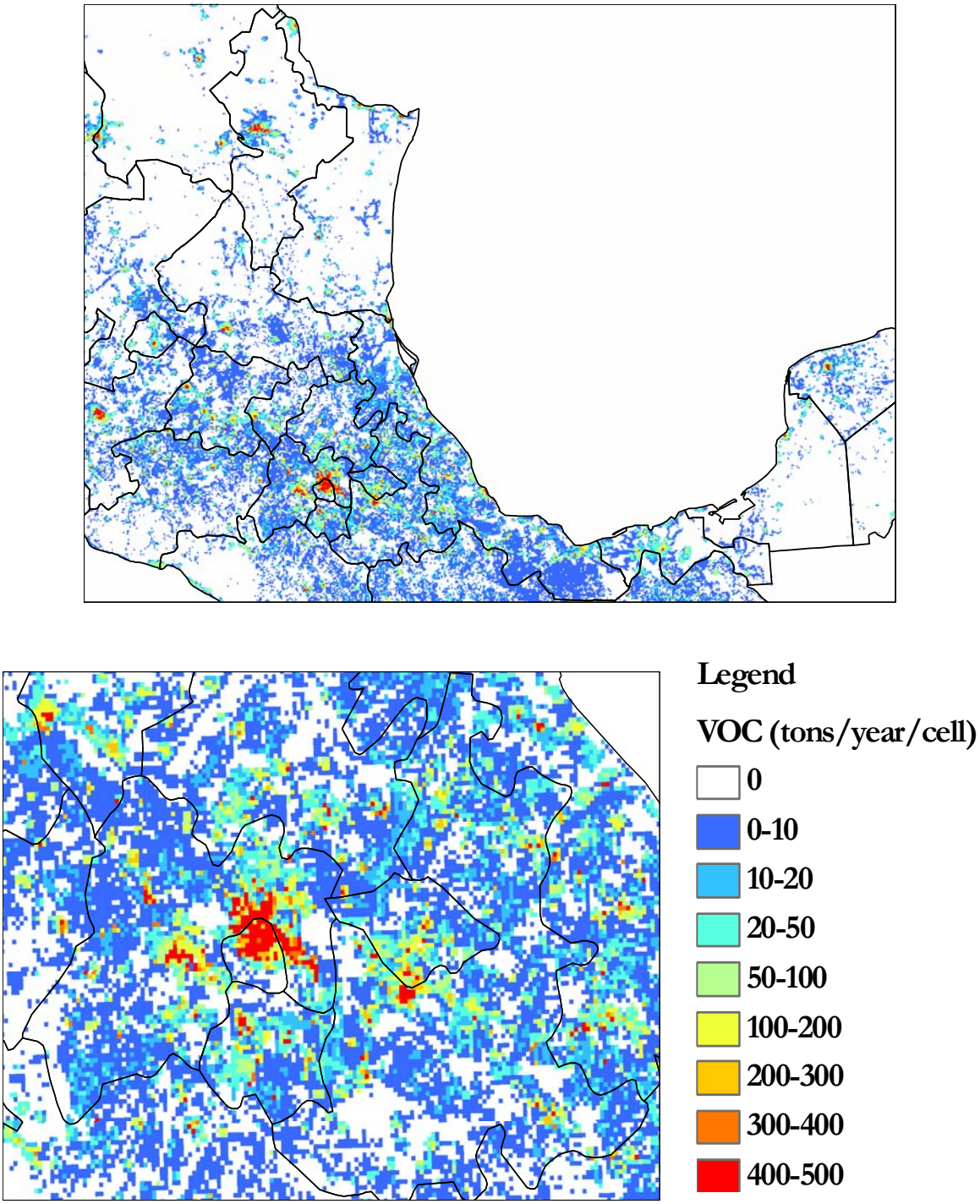

Figure 40 Anthropogenic area sources of VOC (tons/year/cell of 0.025°) for Mexico National Emissions inventory 1999 . Top: National view. Bottom: Close-up to Mexico City area

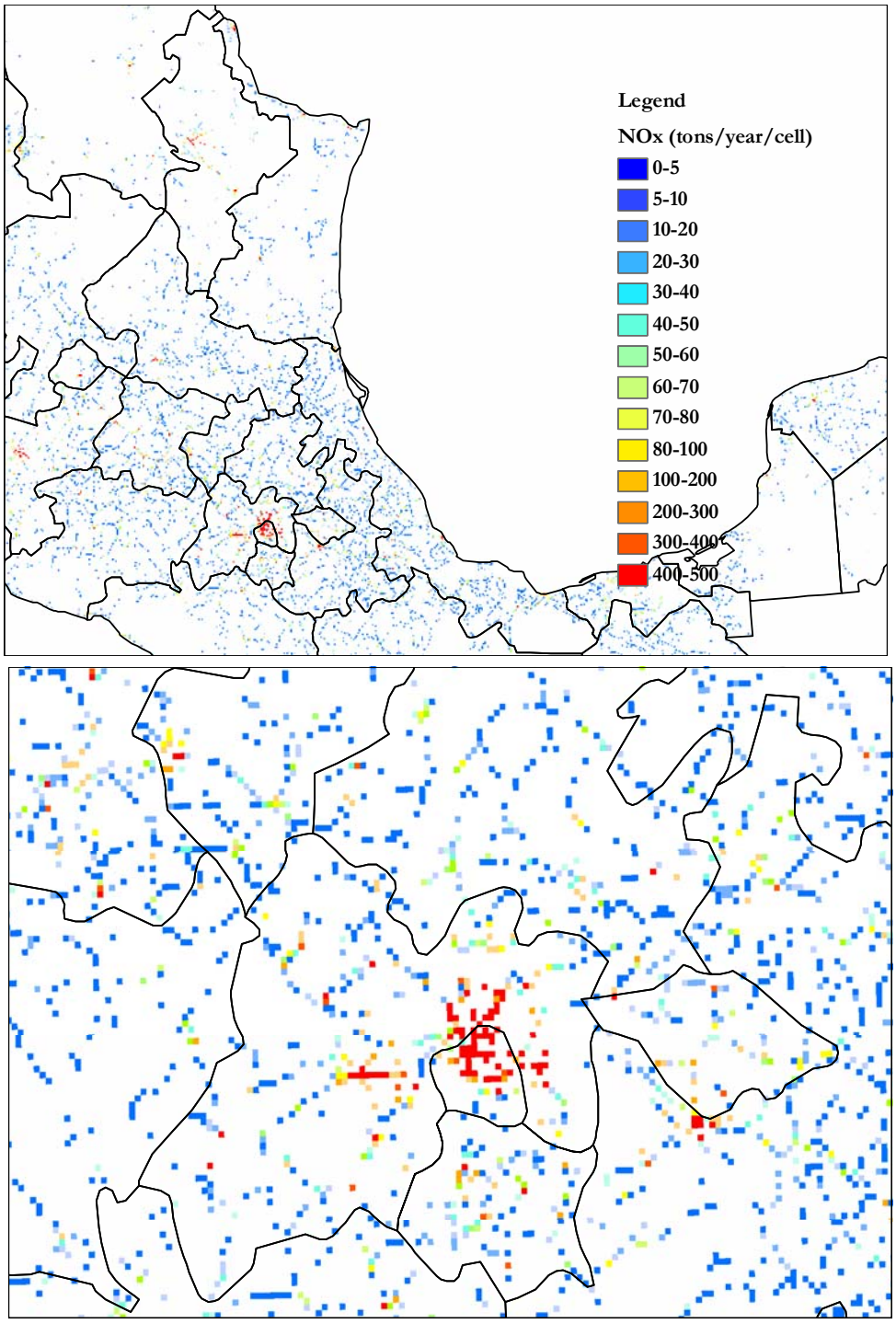

Figure 41 Mobile source emissions for Mexico National Emissions inventory. Top: National view: Bottom: Close-up to Mexico City area

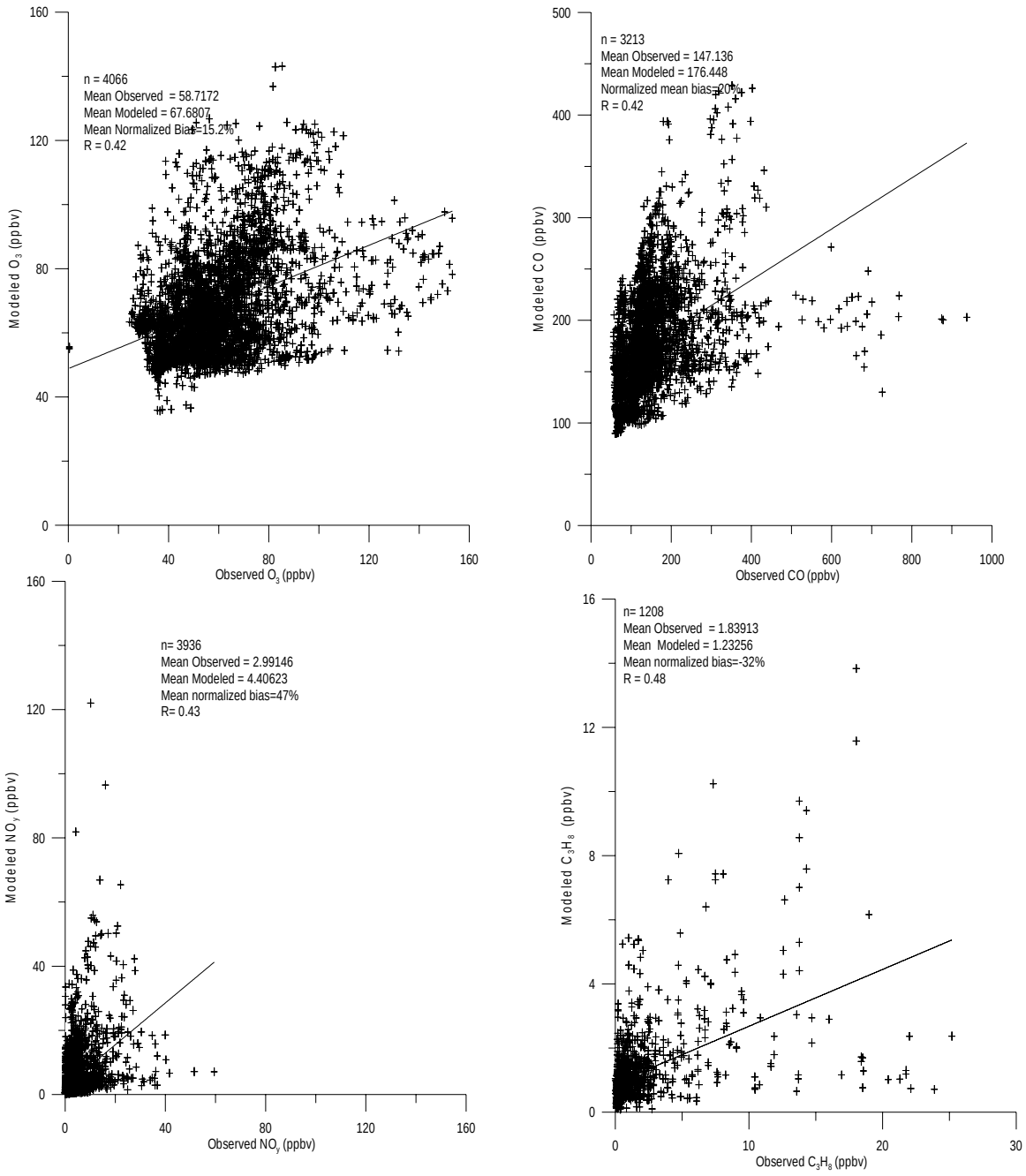

Figure 42 Modeled vs. Observed O_3 (Top Left), CO (Top Right), NO_y (Bottom Left), and C_3H_8 (Bottom Right) extracted along C-130 flight tracks using Mexico National Emissions Inventory 1999 Stem 12km run

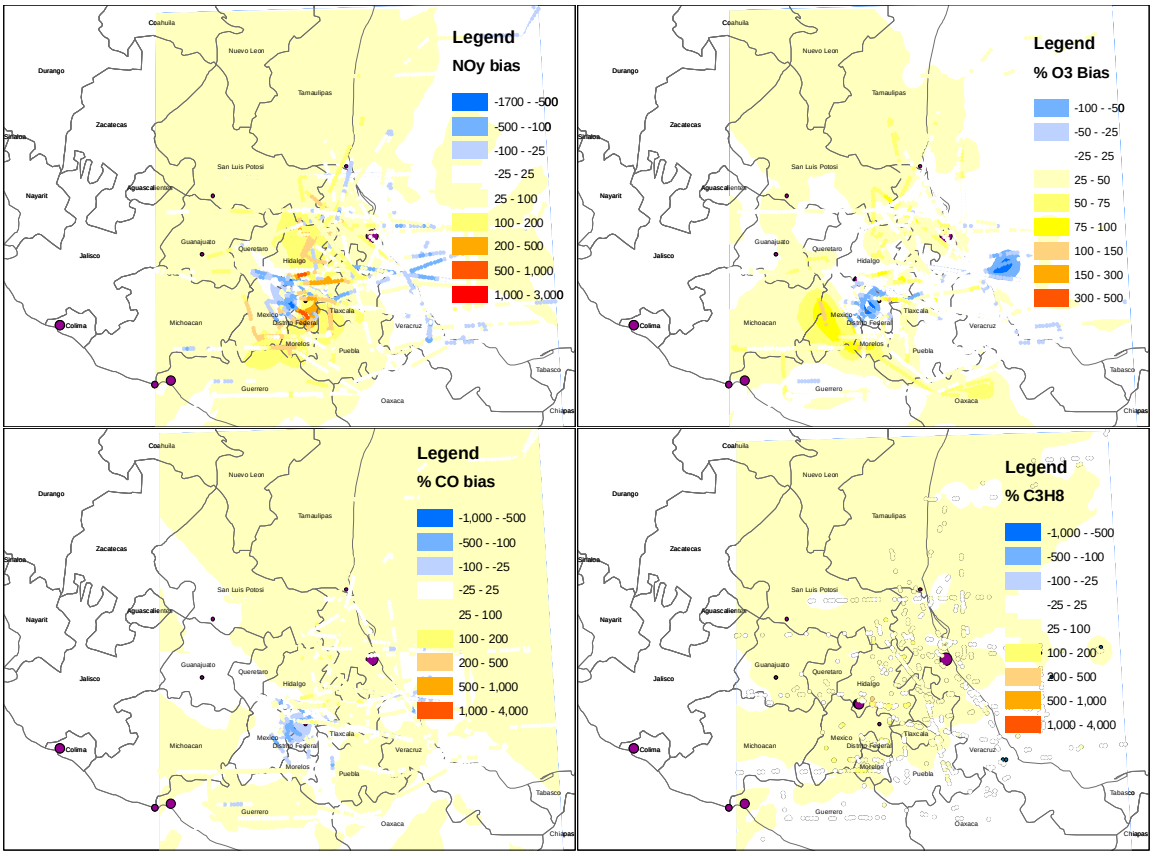

Figure 43 Kriged percent bias (modeled-observed) for Mexico National Emissions Inventory extracted values along C-130 flight tracks (12km resolution, RAQMS biomass burning, NCAR Mozart boundary condition)

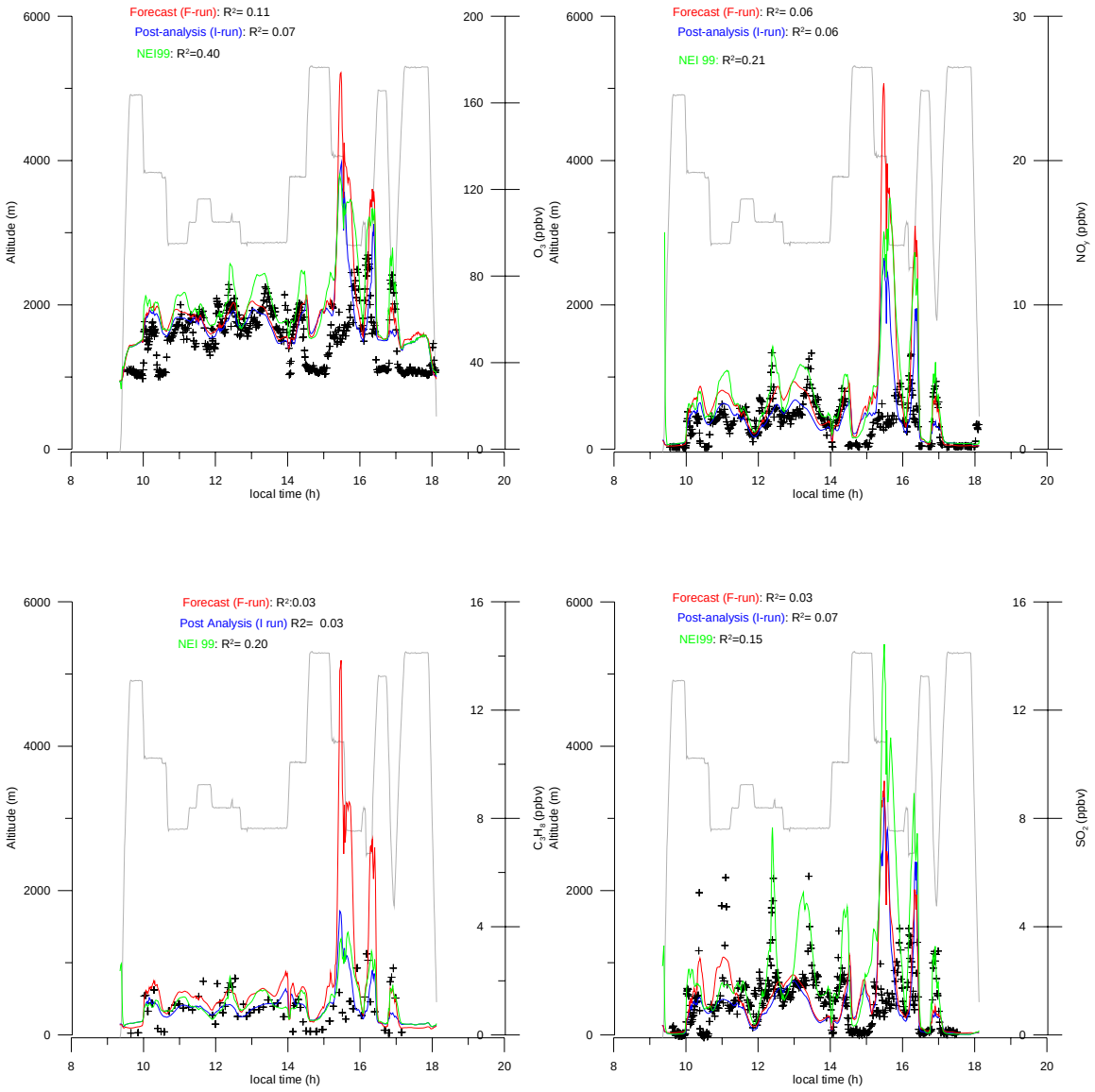

Figure 44 Comparison of modeled and observed concentrations along C-130 flight track for March 16, 2006 (Flight 5). Red: Forecast. Blue: Post-analysis run I, Green: National Emissions Inventory 1999

CHAPTER 5 INTERPOLATING AIRCRAFT OBSERVATIONS DURING MILAGRO USING KRIGING

The present study shows how interpolating measurements along the aircraft flight tracks can provide valuable information on the shape and extension of outflow plumes from Mexico City. Additionally the spatial relationship between secondary pollutants (O_3 and SO_4^{-2}) to their precursors can be elucidated.

5.1 Methods

Merged observations from the C-130 and DC-8 aircraft with a 1 minute temporal resolution was used (NASA, 2007). Direct measurements of O_3, NO_x, NO_y (Heard, 2006, for the C-130), CO [*Takegawa et al.*, 2001], SO_2 and SO_4 were used, while calculated mixing ratios of NOy (as the sum of NO_x, PAN, and HNO_3) were used for the DC-8. Volatile organic compounds (VOC) ethane, propane, benzene, and toluene were measured using whole air sampling [*Colman et al*, 2001] Observations were interpolated using kriging to generate a mixing ratio surface. Kriging is an interpolation technique [*Oliver and Webster*, 1990] that has been used by the mining industry for many years. It has also been used to interpolate surface measurements of particulate matter in the context of pollution exposure studies [*Liao et al.*, 2006], to make air quality maps for the AIRNOW network [*EPA*, 1999], and has been used to interpolate model error along aircraft flight tracks during the INTEX-NA campaign [*Mena-Carrasco et al.*, 2007a]. The technique assumes that mixing ratios are spatially related, and that this relationship has three terms: an average term, a spatially correlated term, and a random error term. This correlation is calculated using a semi variogram, constructed by correlating the semi-variance among observations as a function of distance. In this study the semi-variogram selected correlated mixing ratios with distance. The analysis is limited to altitudes less than 5500m. This assumes that the vertical variability in this range is smaller than the

horizontal variability, and that sampling is done within the mixing layer at the time of the flights [*Fast et al.*, 2007].

Interpolations were performed using ARCGIS 9.1 Geospatial Analyst using a minimum of 50 points. For comparison to the forecasted plumes during the campaign (using F-run described in Table 8 in Chapter 3) results available in the STEM forecast webpage are used (http://nas.cgrer.uiowa.edu/MIRAGE/mirage-2k6.html).

5.2 Results and discussion.

The quality of the interpolated surfaces, which is quantified by uncertainty, is different for each aircraft, largely due to their sampling strategies. The DC-8 had a mean horizontal sampling resolution of 10.4±2 km (95% confidence interval), while the C-130 sampled at resolution of 7.5±1.1 km (95% confidence interval). The DC-8 aircraft, was based in Houston, Texas, and only flow over Mexico City 4 times in very direct routes, while the C-130 sampled near Mexico City roughly 12 times, at more diverse and indirect patterns (zig zags, and multiple altitude measurements along a flight leg). The C-130 also had a city sampling pattern called the "city loop" which was a trapezoidal in shape, and was repeated five times during the campaign. Figure 45 and Figure 46 show the flight tracks for both the DC-8 and C-130 aircraft and their sampling altitudes. Note that Mexico City and its surrounding areas are located above 2200 m, so sampling near in the city loop ranged from 200-2500m.

5.2.1 Outflow from Mexico City

Model studies showing the fate and transport of emissions from Mexico City were used to design pre-campaign sampling strategies for the participant aircraft [Madronich, 2005]. It was anticipated through tracer models (for previous years) that during March emissions from Mexico City would likely be transported to the Northeast, over the Gulf

of Mexico, while also synoptic conditions could also be beneficial to Southwest transport, towards the Pacific Ocean[Fast et al., 2007].

5.2.1.1 March 8, 2006

This research flight was carried out by the C-130 aircraft taking off from Veracruz, with the objective to sample the Mexico City plume to the south as far as Acapulco ~300km from the city) and southwest (as far as Zahuatajeno ~300km from the city). Figure 47 (top left panel) shows that observed ozone can reach values between 70-80 ppbv some 200km southwest of the city, at the same time NO_y concentrations range from . It is also seen that as NO_x is emitted (center left panel) it is transformed into NO_y (top right). Interpolation of observations is also useful to illustrate plume aging. Figure 48 (bottom right) shows that aged plumes were sampled to the south and southwest of Mexico City, and fresh plumes near the city, and to the southeast. The method is also valuable to provide information with respect to source categories. Figure 48 (top panels) shows the enhanced CO values to the southeast of the city are associated to high HCN levels, suggesting the influence of biomass burning. Finally indicator ratios can interpolated along flight tracks (bottom right panel) to show the extent of VOC limited conditions in Mexico City (limited to metropolitan area).

5.2.2 Outflow events over Gulf of Mexico

5.2.2.1 March 10 and 11, 2006

During the campaign southerly and southwesterly flow was predicted to occur for March 10 to 12. A sampling strategy was devised in which the C-130 would sample the plume at the beginning of the event (March 10) followed by the DC-8 (March 11) and both the C-130 and DC-8 (March 12). Figure 49 and Figure 50 show interpolated values of NO_x, NO_y along the C-130 flight tracks for March 10 and 12, respectively. In these figures it is apparent that outflow from Mexico City is sampled, and as the plume ages,

NO_x is transformed into NO_y, at the same time ozone is also being formed. The bottom panels of these figures show that the forecasted model predictions during flight planning correctly placed the outflow plume more than 400km from Mexico City. The DC-8 interpolated values are not shown as the direct sampling pattern did not provide enough information for credible interpolation.

5.2.2.2 March 19, 2006

March 19 represents a day in which emissions from Mexico City were expected be transported deep into the Gulf of Mexico. Figure 51 shows the model prediction for Mexico City outflow (bottom panels). The top left panel shows that NO_y is detected up to 3.5ppb some 900km northeast of Mexico City, while O_3 is measured at 75ppb. The center right panel shows that the air mass is very aged, with NO_x/NO_y values under 0.1. The top right panel shows that methyl ter-butyl ether (MTBE), an oxygenate of gasoline, and a combustion product of mobile sources, is also detectable along the outflow, and in geographical correspondence to NO_y and O_3. This seems to indicate some long range transport of reactive nitrogen originated in Mexico City, of which a large component PAN may thermally decompose to form O_3 as the plume ages.

5.3 Discussion

During this work it was clear that direct sampling patterns intercepting outflow from Mexico City do not provide sufficient information for convincing interpolations (such as the DC-8 sampling). The C-130 sampling strategies were effective to provide information for interpolation, maintaining uncertainty levels acceptably low.

5.4 Conclusion

Interpolation of observations along flight tracks is a valuable tool to provide geographical contextualization to them. Mexico City outflow to the south was mapped through successful interpolation of O_3, CO, NO_x, and NO_y measurements. Modeled

outflow patterns show great agreement with interpolated plume structures. The method provides additional information on source categories and plume aging. For the March 8, 2006 flight high levels of CO to the SE were associated to high values of HCN. Plume aging was illustrated by interpolation of NO_x/NO_y ratios. A multiple day outflow event for March 10 and 12 showed that fresh emissions were sampled near the source regions for March 10, while aged airmasses originated in Mexico City were sampled on March 12. During a March 19 flight enhanced concentrations of O_3 (75ppbv) and NO_y (3.5ppbv) were sampled as far as 900km from Mexico City, over the Gulf of Mexico, off the coast of Texas. Interpolated NO_x/NO_y suggests that airmass is aged.

This method is not only a useful to to infer on the shape of the Mexico City outflow plume, but also valuable to assess the quality of plume placement predictions for flight planning.

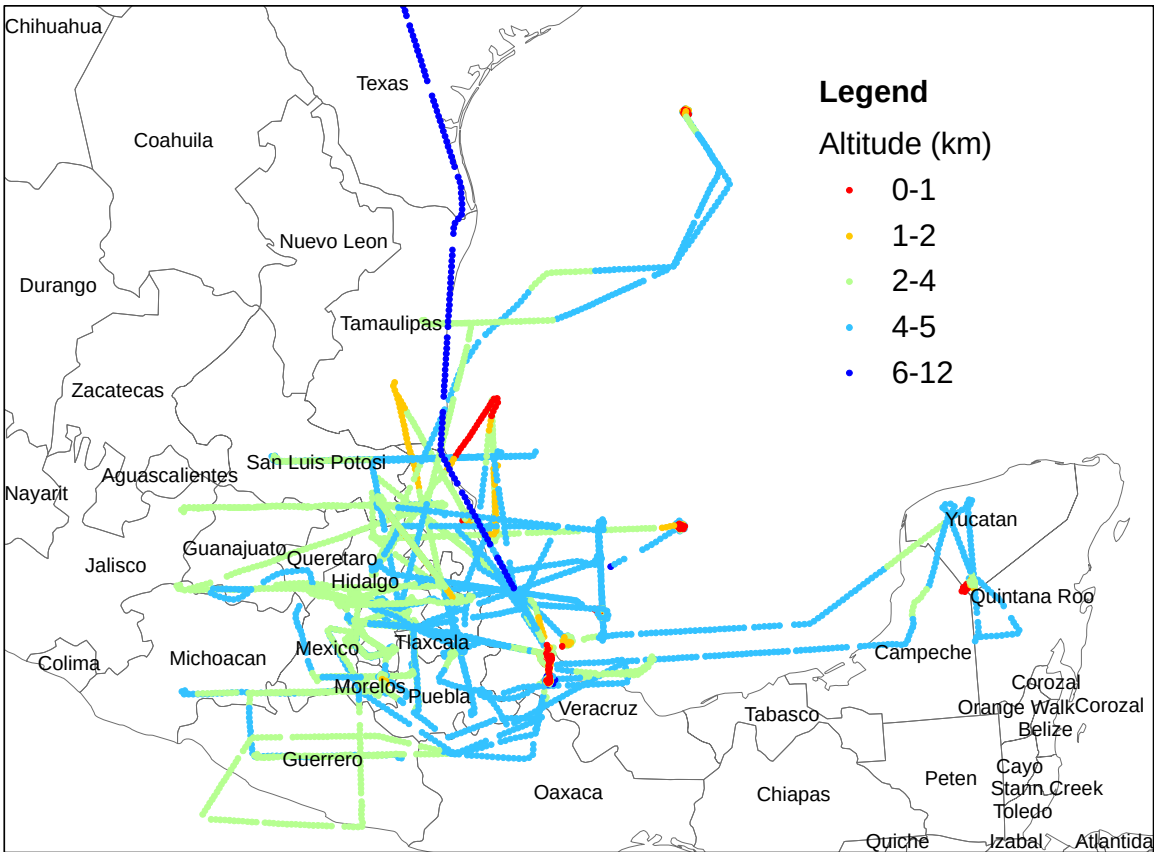

Figure 45 C-130 flight tracks and sampling altitudes

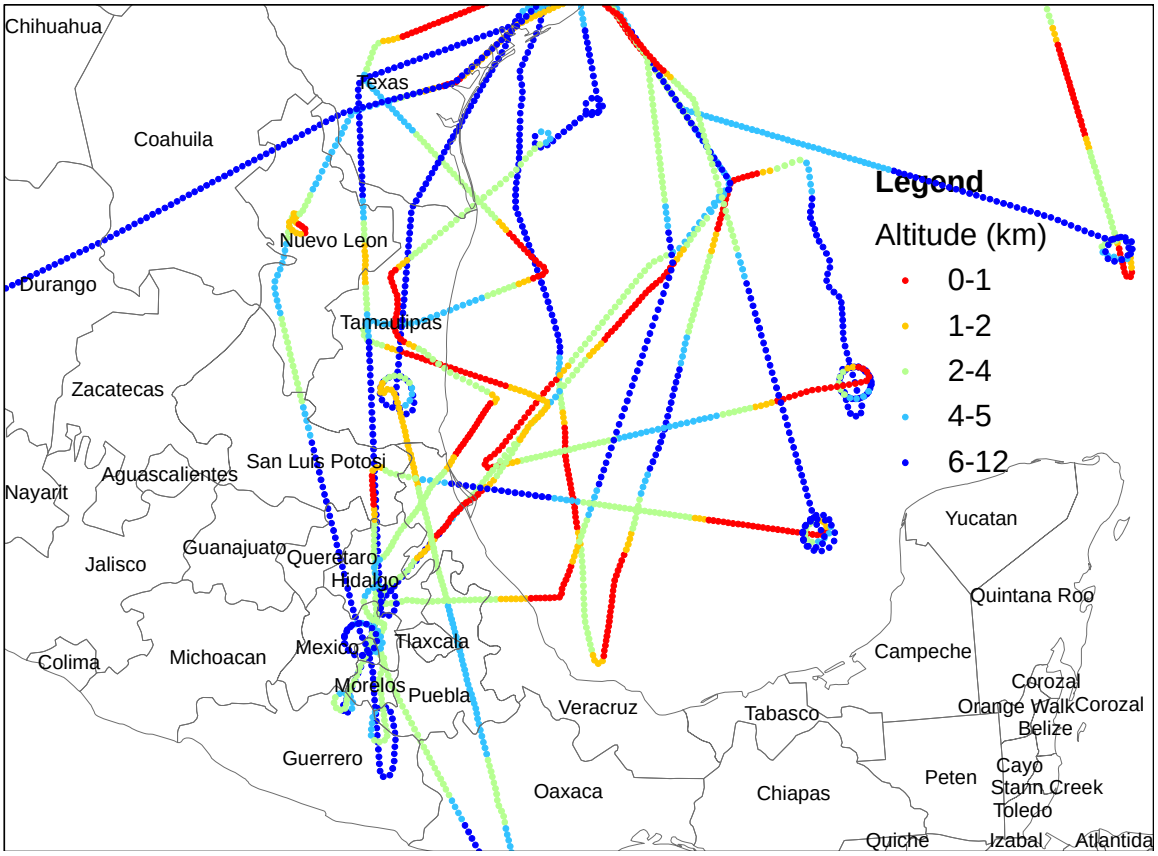

Figure 46 DC-8 flight tracks and sampling altitudes

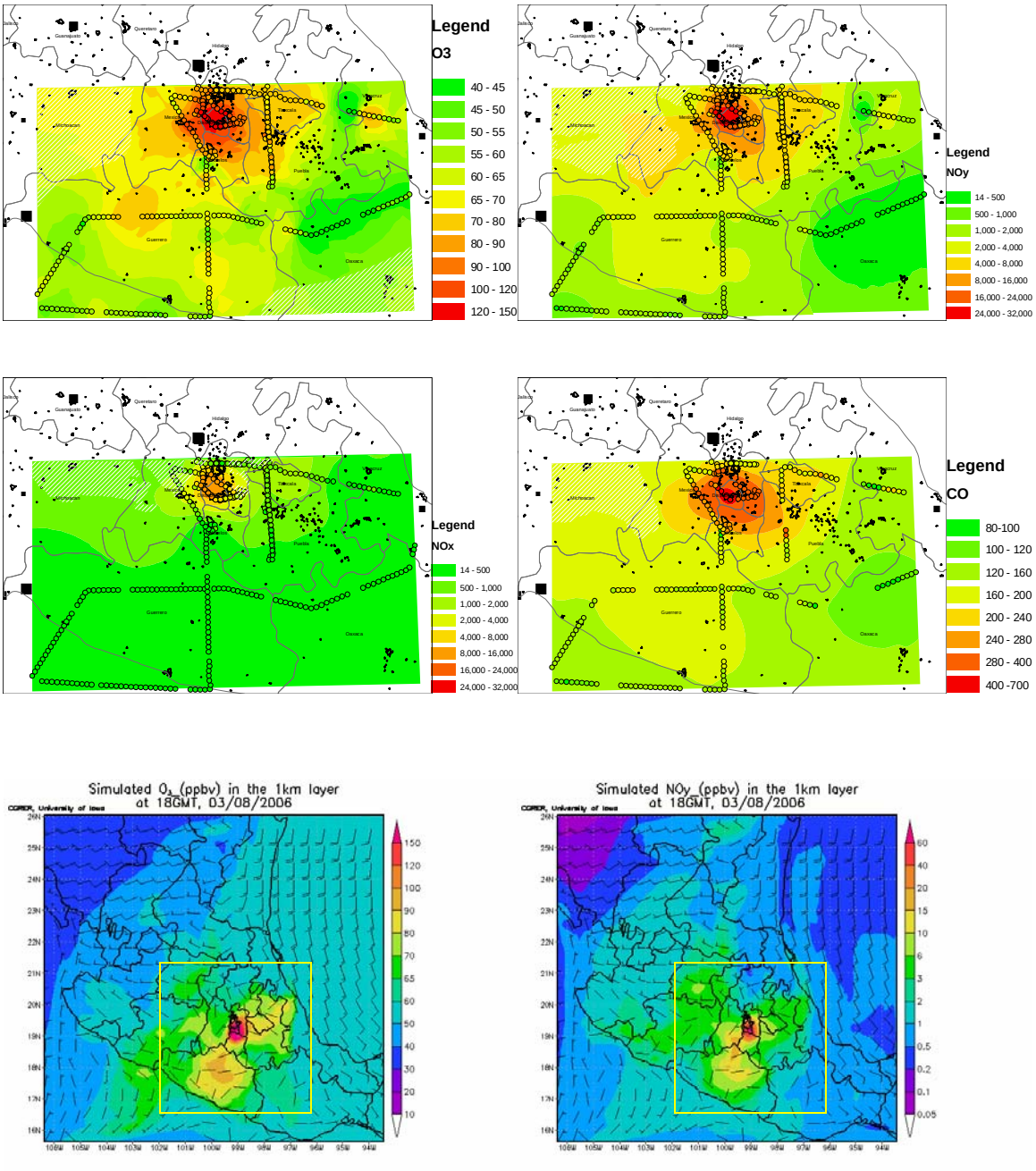

Figure 47 Interpolated observations along C-130 flight track, March 8, 2006 using kriging, Top left: O_3 (n=324),Top right: NO_y (n=324). Center Left: NO_x (n=352) Center Right: CO (n=220). Data under 5.5km above sea level, and using exponential variogram and the 50 nearest neighbors per lag. Shaded areas represent method uncertaintly over threshold of O_3: 25ppbv, NO_y (20ppbv), NO_x (5ppbv), and CO (80ppbv). All concentrations in ppbv. Bottom left: Modeled 1km O_3 during forecast. Bottom Right: Modeled 1km NO_y during forecast. Model configuration: F-run (12km, base emissions, RAQMS boundary conditions)

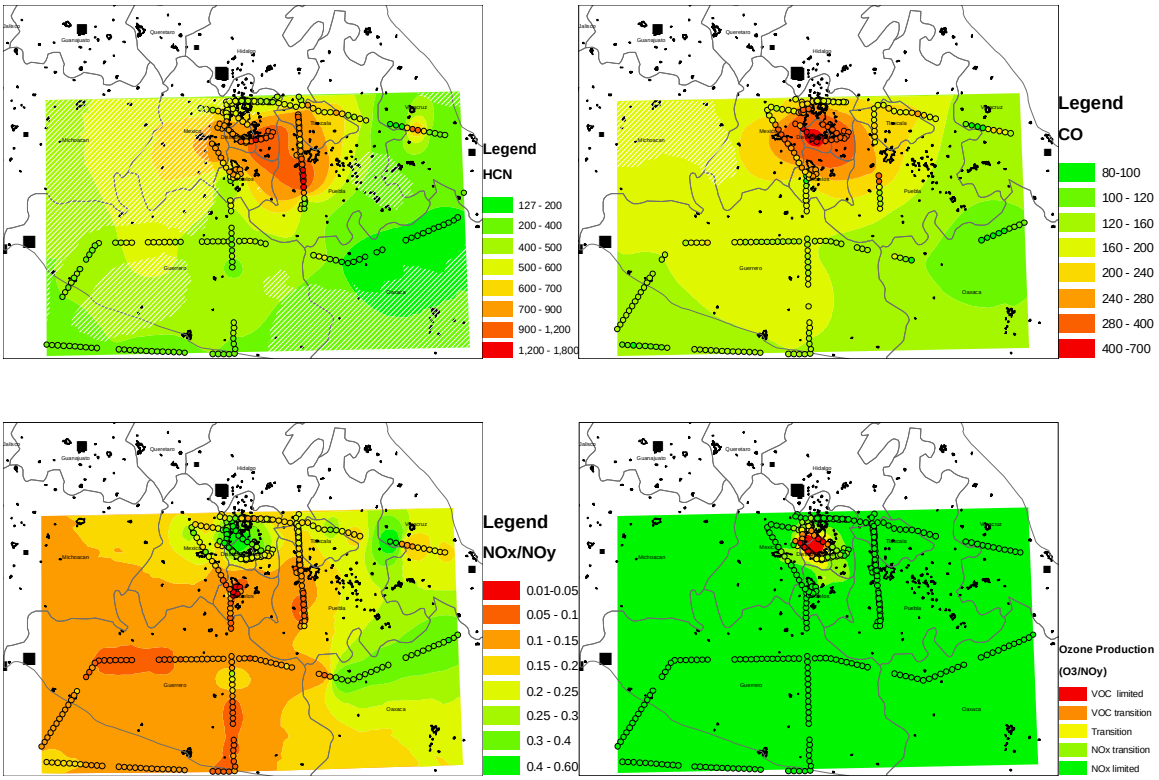

Figure 48 Interpolated observations and indicators along C-130 flight track, March 8, 2006 using kriging, Top left: HCN(n=220),Top right: CO (n=220). Bottom Left: NO_x/NO_y (n=352) Bottom Right: Ozone production regimes (n=220). Data under 5.5km above sea level, and using exponential variogram and the 50 nearest neighbors per lag. Shaded area represents method uncertainly over the threshold of HCN (80pptv), CO (80ppbv)

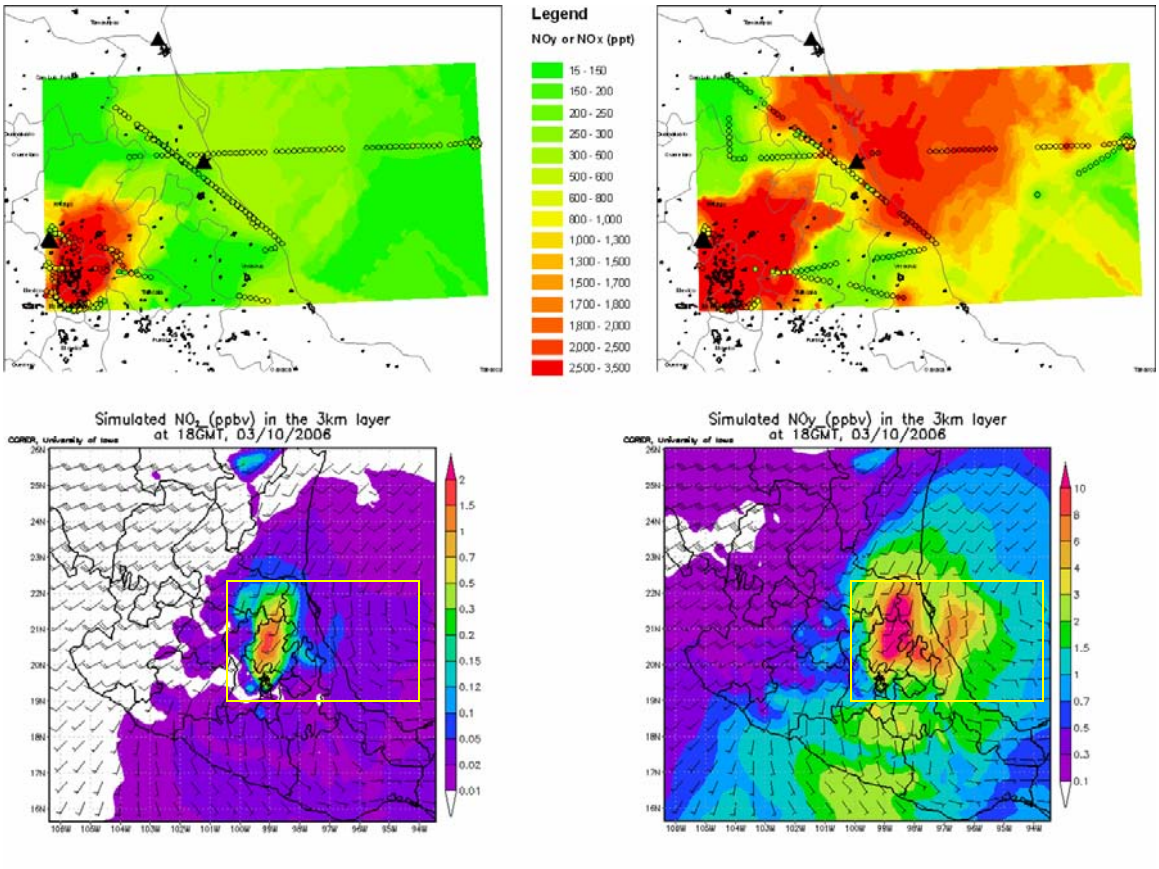

Figure 49 Interpolated observations through kriging for C-130 March 10,2006 flight. Top Left: NO_x (ppt) Right: NO_y. Bottom Left: Modeled 3km NO_2 (Forecast) Bottom Right: Modeld 3km NO_y (Forecast)

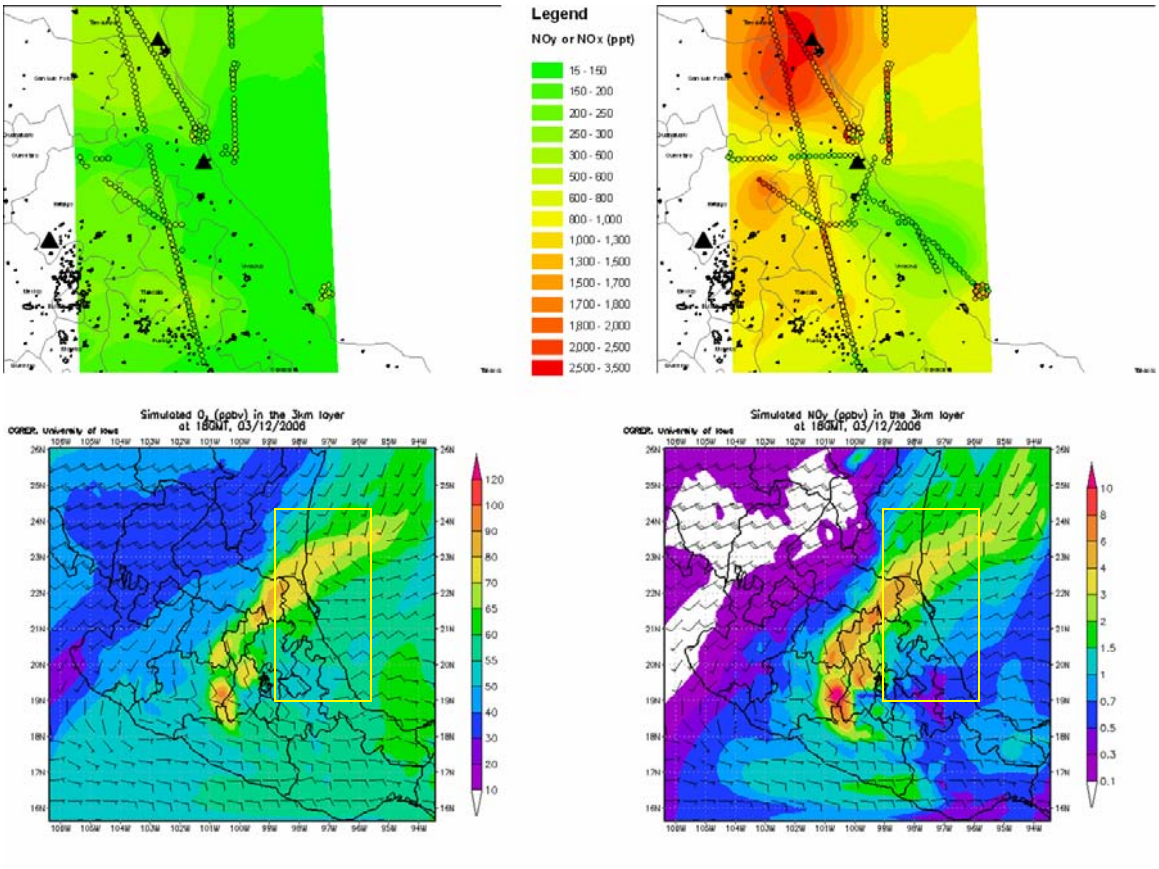

Figure 50 Interpolated observations through kriging for C-130 March 12,2006 flight. Top Left: NO_x (ppt) Right: NO_y. Bottom Left: Modeled 3km NO_2 (Forecast) Bottom Right: Modeld 3km NO_y (Forecast)

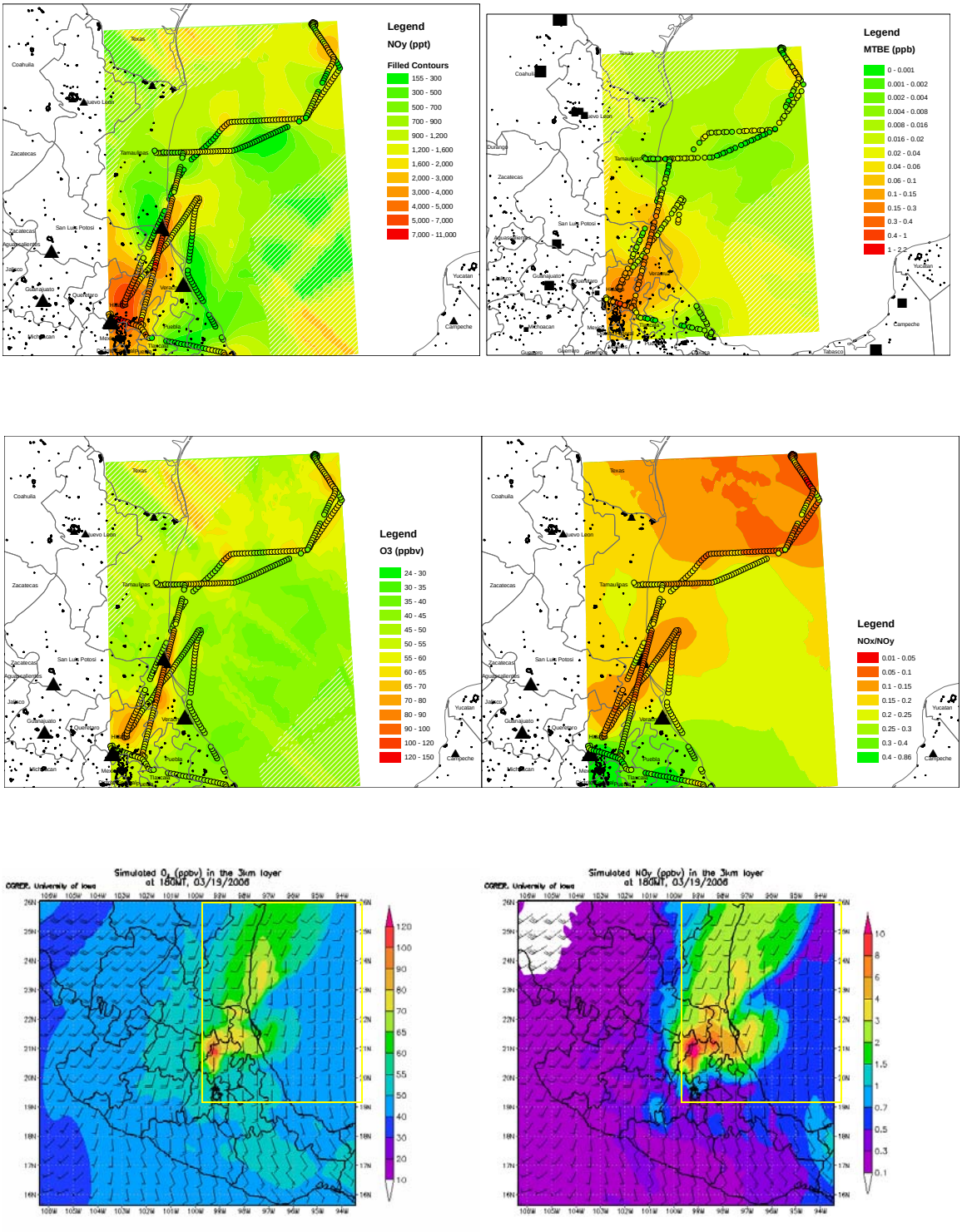

Figure 51 Interpolated observations through kriging for C-130 March 19, 2006 flight. Top Left: MTBE Right: NO_y. Center left: O_3, Center right: NO_x/NO_y, Bottom Left: Modeled 3km O_3 Bottom Right: NO_y (Forecast) Shaded area represents method uncertainly for NO_y (1500 pptv), NO_x (800pptv) and O_3 (17 ppbv)

CHAPTER 6 SUMMARY AND RECOMMENDATIONS

A method was presented to improve modeling of ozone by systematic analysis of model error using conventional statistics, vertical profiles and horizontal interpolation. Model improvements were documented for the ICARTT and MILAGRO campaigns. In general ozone bias was highly correlated to bias of its precursors VOC and NO_x. Sensitivity studies for ICARTT showed that ozone formation in the United States is most sensitive to increased emission in NO_x. Sensitivities studies for MILAGRO showed that Mexico City is mostly VOC limited, and surrounding areas are NO_x limited. When areas are under the influence of Mexico City outflow, NO_x limited conditions may convert to VOC limited. Regionally emissions from Mexico City can increase long range ozone concentrations by up to 10%. Aerosol from Mexico City decreases regional photolysis rates, decreasing ozone formation from its potential by 5-10%. Interpolated observations along flight tracks of C-130 can be used to observe outflow patterns. The location of Mexico City outflow shows good agreement with forecasted outflow patterns. The use of this technique was instrumental in identifying sources of ozone and NO_y in a March 19, 2006 research flight from Veracruz, into Mexico City, and out over the coast of Texas, and tracing it back to Mexico City.

Some sensitivity studies during MILAGRO used brute force methods to evaluate the impact of Mexico City emissions (runs with and without Mexico City emissions). While insightful this type of analysis ignores the change in ozone production regime inherent in large changes in emissions. It is therefore recommended to carry out a sensitivity analysis using infinitesimal changes in emissions to calculate the effect of Mexico City on certain arbitrary policy parameters, similar to the work of Hakami et al.

[2006]. Also the high correlation in recurring ozone bias to CO bias (and CO to other precursors) in post-analysis in MILAGRO suggest that a strategy to recover emissions through inverse analysis should consider four dimensional variational data assimilation framework using CO as a tracer to recover emissions (and scale emissions of other precursors accordingly).

REFERENCES

Ashmore, M. R. Assessing the future global impacts of ozone on vegetation. Plant, Cell and Environment (2005), 28(8), 949-964

Aunan, K. T., Bernsten, T.K. (2000), Surface ozone in China and its possible impact on agricultural crop yields, AMBIO: A journal of the human environment, 29, 294-301.

Avery, R. (2006), Reactivity-based VOC control for solvent products: more efficient ozone reduction strategies, Environmental Science and Technology, 40, 4845-4850.

Bates, T. S., B. J. Huebert, J. L. Gras, F. B. Griffiths, P. A. Durkee (2003), International Global Atmospheric Chemistry (IGAC) Project's First Aerosol Characterization Experiment (ACE 1): Overview, J. Geophys. Res., 103(D13), 16297-16318, 10.1029/97JD03741

Bell, M., Peng, R., Dominici, F. (2006), The exposure response curve for ozone and risk of mortality and the adequacy of current ozone regulations, Environmental Health Perspectives, 114.

Blond, N., L. Bel, and R. Vautard (2003), Three-dimensional ozone data analysis with an air quality model over the Paris area, J. Geophys. Res., 108(D23), 4744, doi:10.1029/2003JD003679

Cardelino, C. A., Chameides, W.L. (1995), An observation-based model for analyzing ozone precursor relationships in the urban atmosphere, Journal of Air Waste Management Association, 45, 161-180.

Carmichael, G. R., Y. Tang ,G. Kurata, I. Uno, D.G. Streets, N. Thongboonchoo, J. Woo, S. Guttikunda, A. White, T. Wang, D.R. Blake, E. Atlas, A. Fried, B. Potter, M.A. Avery, G.W. Sachse , S.T. Sandholm, Y. Kondo, R.W. Talbot, A. Bandy, D. Thorton, A.D. Clarke (2003), Evaluating regional emission estimates using the TRACE-P observations, Journal Of Geophysical Research-Atmospheres, 108, 8810

Carmichael, G.R, L.K. Peters, R.D Saylor. (1991), The STEM-II regional scale acid deposition and photochemical oxidant model--I. An overview of model development and applications, Atmospheric Environment, 25 (10), 2077-2090

Carnevale, Claudio; Pisoni, Enrico; Volta, Marialuisa. Selecting effective ozone exposure control policies solving a two-objective problem. Ecological Modelling (2007), 204(1-2), 93-103

Carter, W. P. L. (1994), Development of ozone reactivity scales for volatile organic compounds, Journal of Air Waste Management Association, 44, 881-899.

Carter, W. P. L. (2000), Documentation of the SAPRC-99 Chemical Mechanism for VOC reactivity assessment, Final Report to California Air Resources Board Contract No. 92-329, University of California, Riverside, May 8, 2000.

Carter, W. P. L., Atkinson, R. (1987), An experimental study of incremental hydrocarbon reactivity, Environmental Science and Technology, 21, 670-679.

Chai, T., Carmichael, G., Sandu, A., Tang, Y., Daescu, D. (2006), Chemical data assimilation of Transport and Chemical Evolution over the Pacific (TRACE-P) aircraft measurements, Journal of Geophysical Research-Atmospheres, 111.

Chai, T., G.R. Carmichael, Y. Tang, A. Sandu, D.G. Streets (2007) Evaluating and improving regional emission estimates using the ICARTT observations , Journal Of Geophysical Research-Atmospheres, 112

Civerolo, K., C. Hogrefe, B. Lynn, J. Rosenthal, J.-Y. Ku, W. Solecki, J. Cox, C. Small, C. Rosenzweig, R. Goldberg, K. Knowlton, and P. Kinney (2007) Estimating the effects of increased urbanization on surface meteorology and ozone concentrations in the New York City metropolitan region. Atmos. Environ., 41, 1803-1818, doi:10.1016/j.atmosenv.2006.10.076.

Colman, J.J., A.L. Swanson, S. Meinardi, B.C. Sive, D.R.Blake, and F.S. Rowland (2001) Description of the analysis of a wide range of volatile organic compounds in whole air samples collected during PEM-Tropics A and B, *Anal. Chem., 73*, 3723-3731

Davison, A. W., Barnes, J.D. (1998), Effects of ozone on wild plants, New Phytologist, 139, 135-151.

De Foy, B., E. Caetano, V. Magaña, A. Zitácuaro, B. Cárdenas, A. Retama, R. Ramos, L. T. Molina, M. J. Molina (2003), Mexico City Basin Wind Circulation during the MCMA-2003 Field Campaign, Atmos. Chem. Phys., 5, 2267-2288

Diem, J. (2003), Potential impact of ozone on coniferous forests of the interior Southwester United States, Annals of the Association of American Geographers, 93, 265-280.

Eastern Research Group (2006). Mexico National Emissions Inventory: 1999, October 2006.

EPA (1999), Report of the December 15, 1999 EPA Satellite Forum on Ozone Monitoring, Mapping, and Public Outreach, http://epa.gov/empact/techtransfer/satellite.htm, 1995 (Accessed June 2006).

EPA (2006), 1999 National Emission Inventory, http://www.epa.gov/ttn/chief/net/1999inventory.html#final3crit (Accessed June 2006).

EPA (2006). North American Emissions Inventories – Mexico. (http://www.epa.gov/ttn/chief/net/mexico.html) Accessed March 2007.

Fast, J.D., B. de Foy, F. Acevedo Rosas, E. Caetano, G. Carmichael, L. Emmons, D. McKenna, M. Mena, W. Skamarock, X. Tie, R. L. Coulter, J. C. Barnard, C. Wiedinmyer, S. Madronich Page(s) 2037-2089. SRef-ID: 1680-7375/acpd/2007-7-2037. Atmospheric Chemistry and Physics Discussion

Frost, G. J., et al. (2006), Effects of changing power plant NOx emissions on ozone in the eastern United States: Proof of concept, J. Geophys. Res., 111, D12306, doi:10.1029/2005JD006354.

Fumagali, I., Gimeno, B.S. (2001), Evidence of ozone-induced adverse effects on crops in the Mediterranean region, Atmospheric Environment, 35, 2583.

Geron, C., A. Guenther, and T. Pierce (1994), An improved model for estimating emissions of volatile organic compounds from forests in the eastern United States, J. Geophys. Res. 99, 12773-12792

Glendening, J (2006). How do meteorological models work? Accuracy and Resolution. (http://www.drjack.info/INFO/model_basics.html). Accessed May 2007.

Gurjar, B. R.; Lelieveld, J. New directions: Megacities and global change. Atmospheric Environment (2005), 39(2), 391-393

Guttikunda, Sarath K.; Tang, Youhua; Carmichael, Gregory R.; Kurata, Gakuji; Pan, Li; Streets, David G.; Woo, Jung-Hun; Thongboonchoo, Narisara; Fried, Alan. Impacts of Asian megacity emissions on regional air quality during spring 2001. Journal of Geophysical Research, [Atmospheres] (2005), 110(D20), D20301/1-D20301/18

Grell, G., J. Dubhia, D.R. Stauffer (1995), Description of the Fifth Generation Penn State/NCAR Mesoscale Model (MM5), http://cng.ateneo.net/cng/wyu/resources/mm5/desc/cover.pdf (Accessed, June 2006).

Hakami, A., Seinfeld, J.H., Chai, T., Tang, Y., Carmichael, G.R., and Sandu, A. (2006). Environ. Sci. Technol., 40, 12, 3855 - 3864, 2006, 10.1021/es052135g

Heard, D. (2006) Analytical techniques for atmospheric measurement. Chapter 7. 528 pages, 148 illustrations.Blackwell

Hong, S.-Y., H-L Pan (1996), Non Local Boundary Layer Vertical Diffusion in a Medium-Range Forecast Model, Monthly Weather Review, 124, 2322-2339

Horowitz L. W., et al. (2003), A global simulation of tropospheric ozone and related tracers: Description and evaluation of MOZART, version 2, J. Geophys. Res., 108 (D24), 4784, doi:10.1029/2002JD002853

Huang, H-M. H., S-Y. Hong, M. Kanamitsu (1997), The NCEP Regional Spectral Model: Update. Bulletin of the American Meteorological Society 78 (10) 2125- 2143

Jacob D. J., J. H. Crawford, M. M. Kleb, V. S. Connors, R. J. Bendura, J. L. Raper, G. W. Sachse, J. C. Gille, L. Emmons, C. L. Heald (2003), Transport and Chemical Evolution over the Pacific (TRACE-P) aircraft mission: Design, execution, and first results, J. Geophys. Res., 108 (D20), 9000, doi:10.1029/2002JD003276

Jaimes-Lopez, J. Luis; Sandoval-Fernandez, Julio; Gonzalez-Ortiz, Emmanuel; Vazquez-Garcia, Marcos; Gonzalez-Macias, Uriel; Zambrano-Garcia, Angel. (2005) Effect of liquefied petroleum gas on ozone formation in Guadalajara and Mexico City. Journal of the Air & Waste Management Association 55(6), 841-846

Kalnay, E. (2002), Atmospheric Modeling, Data Assimilation and Predictability, Cambridge University Press, Chapter 5.

Kiley C. M., et al. (2003), An intercomparison and evaluation of aircraft-derived and simulated CO from seven chemical transport models during the TRACE-P experiment, J. Geophys. Res., 108 (D21), 8819, doi:10.1029/2002JD003089

Kim, S.-W., A. Heckel, S. A. McKeen, G. J. Frost, E.-Y. Hsie, M. K. Trainer, A. Richter, J. P. Burrows, S. E. Peckham, and G. A. Grell (2006), Satellite-observed U.S. power plant NO_x emission reductions and their impact on air quality, Geophys. Res. Lett., 33, L22812, doi:10.1029/2006GL027749.

Kim, Y. P., and J. H. Seinfeld (1995), Atmospheric gas-aerosol equilibrium III: Thermodynamics of crustal elements Ca^{2+}, K^{+}, Mg^{2+}, Aerosol Sci. Technol., 22, 93–110.

Kim, Y. P., J. H. Seinfeld, and P. Saxena (1993a), Atmospheric gas-aerosol equilibrium I: Thermodynamic model, Aerosol Sci. Technol., 19, 151–181.

Kim, Y. P., J. H. Seinfeld, and P. Saxena (1993b), Atmospheric gas-aerosol equilibrium II: Analysis of common approximations and activity coefficient calculation methods, Aerosol Sci. Technol., 19, 182–198.

Kleinman, L., Daum, P.H., Lee, Yin-Nan, Nunnermacker, L. J., Springston, S.R. (2001), Sensitivity of ozone production rate to ozone precursors, Geophysical Research Letters, 28, 2903-2906.

Kleinman, L., D.G. Daum, F. Brechtel, Y. Lee, J. Nunnermacker, S. Springton, J. Weinstein-Lloyd (2002), Efficiency of ozone production in the Houston plume, American Meteorological Society, Proceedings for Fourth Conference on Atmospheric Chemistry.

Kleinman, L. I. (2005), The dependence of tropospheric ozone production rate on ozone precursors, Atmospheric Environment, 39, 575-586

Krige, D.G (1951) A statistical approach to some mine valuations and allied problems at the Witwatersrand, Master's thesis of the University of Witwatersrand

Kuhns H., Knipping EM, Vukovich, JM. (2005). Development of a United States-Mexico Emissions Inventory for the Big Bend Regional Aerosol and Vility Observationsl (BRAVO) Study. Journal of the Air Waste Management Association, 2005, 55, 5, 677

Kulkarni, S. (2004), Surface elemental composition of aerosols at Beijing (China), Gosan (Korea), and Tango (Japan) during ACE-Asia. M.S. Thesis, Chemical and Biochemical Engineering. Iowa City, The University of Iowa: xiv, 183 leaves, bound.

Launay, M., and M. Guerif (2005), Assimilating remote sensing data into a crop model to improve predictive performance for spatial applications, Agriculture, Ecosystems & Environment, 111, 321.

Liang, J., et al. (2006), Evaluation of the ability of indicator species ratios to determine the sensitivity of ozone to reductions in emissions of volatile organic compounds and oxides of nitrogen in northern California, Atmospheric Environment, 40, 5156-5166.

Liao, D., D. Peuquet, Y. Duan, E. Whitsel, J. Dou, R. Smith, H-M. Lin,J-C. Chen, G. Heiss (2006), GIS approaches for the estimation of residential level ambient PM concentrations, Environmental Health Perspectives 114(9):1374-80

Liu, S. C., Trainer, M., Fehsendfeld, F.C., Parrish, D.D., Williams, E.J., Fahey, F.W., Hubler, G., Murphy, P.C. (1987), Ozone production in the rural troposphere and the implications for regional and global ozone distributions, Journal of Geophysical Research-Atmospheres, 92, 4191-4207.

Madronich, S (2005). Megacity impacts on regional and global environments: Mexico City case study (MIRAGE-Mex). First Science Meeting, 24 October, 2005.

Mao, Huiting; Talbot, Robert (2004). O_3 and CO in New England : temporal variations and relationships. Journal of Geophysical Research, [Atmospheres] , 109(D21), D21304/1-D21304/19.

Mayer, H. (1999) Air pollution in cities. Atmospheric Environment 33, 4029-4037.

Mc Keen, S., J. Wilczak, G. Grell, S. Peckham, M. Pagowski (2006), Real-time ozone forecasts over Eastern North America during the summer of 2004: An assessment of several models and their ensemble, Geophysical Research Abstracts, 7, 1-2.

Mena-Carrasco et al (2005), The Ozone Story: Using extensive ICARTT measurements and air quality models to improve ozone budgets in North America., Eos Trans. AGU, 86, Fall Meeting Suppl., Abstract A11B-0882.

Mena-Carrasco, M., et al. (2007a), Improving regional ozone modeling through systematic evaluation of errors using the aircraft observations during the International Consortium for Atmospheric Research on Transport and Transformation, J. Geophys. Res., 112, D12S19, doi:10.1029/2006JD007762.

Mena-Carrasco, M, G.R. Carmichael, J.E. Campbell, Y. Tang, T. Chai (2007b) Improving emissions inventories in Mexico through systematic analysis of model performance along C-130 and DC-8 flight tracks during MILAGRO. Eos Trans. AGU,88(23), Jt. Assem. Suppl., AbstractA31C-04

Mendoza-Dominguez, A., Russel, A. (2000), Iterative Inverse Modeling and Direct Sensitivity Analysis of a Photochemical Air Quality Model, Environmental Science and Technology, 34, 4974-4981.

Mendoza-Dominguez, A., Russel, A. (2001), Estimation of emission adjustments from the application of four-dimensional data assimilation to photochemical air quality modeling, Atmospheric Environment, 35, 2879-2894.

Menut L., R. Vautard, C. Flamant, C. Abonnel, M. Beekmann, P. Chazette, P. H. Flamant, D. Gombert, D. Guedalia, D. Kley, M.P. Lefebvre, B. Lossec, D. Martin, G. Megie, M. Sicard, P. Perros, G. Toupance (2000), Atmospheric pollution over the Paris area: The ESQUIF projec', Annales Geophysicae, 18, 1467-1481

Michalak, A (2006). Geostatistics: Principles of spatial analysis. Workshop on Data Assimilation for the Carbon Cycle, Berkeley, CA, July, 2006.

Miller, P.J., C. Van Atten. (2004), North American Power Plant Emissions. Commision for the Environmental Cooperation of North America. Quebec.

Millet, D. B., A. H. Goldstein, R. Holzinger, B. J. Williams, J. D. Allan, J. L. Jimenez, D. R. Worsnop, J. M. Roberts, A. B. White, R. C. Hudman, I. T. Bertschi and A. Stohl (2006), "Chemical characteristics of North American surface layer outflow: Insights from Chebogue Point, Nova Scotia." Journal of Geophysical Research-Atmospheres 111(D23).

Molina, M. , L. Molina (2004) 2004 Critical Review: Megacities and Atmospheric Pollution. J Air Waste Manag Assoc. 2004 Jun;54(6):644-80.

NHDES, N. H. D. o. E. S. (2006), Ozone Events in New Hampshire (1995-Present), http://www.des.state.nh.us/ARD/ozone/ozone_events.htm (accessed Sept 2006).

Oak Ridge National Laboratory (ORNL) (1999) LandScan Global Population 1998 Database. (http://www.ornl.gov/sci/landscan/landscanCommon/landscan_doc.html#Summary). Accessed March 2007.

Oliver, M.A., R. Webster (1990), Kriging: A method of interpolation for geographical information systems. Int. J. Geogr. Inf. Syst. 4 (3), 313-332

Olivier JGJ, Bouwman AF, Maas CWM van der, Berdowski JJM, Veldt C, Bloos JPJ, Visschedijk AJH, Zandveld PYJ, Haverlag JL (2002). Application of EDGAR. RIVM report 773301001/ NRP Report 410200051.Page(s) 2267-2288

Pan, L., T. Chai, G.R. Carmichael, Y. Tang, D. Streets, J-H. Woo, H. Friedli, L.Radke. (Under Review), Top-down estimate of mercury emissions in China using four dimensional variational data assimilation (4D-Var), Atmospheric Environment.

Parrish, D. D. (2006), Critical evaluation of US on-road vehicle emission inventories, Atmospheric Environment, 40, 2288-2300

Parrish, D. D., et al. (1998), Internal consistency tests for evaluation of measurements of anthropogenic hydrocarbons in the troposphere, Journal of Geophysical Research-Atmospheres, 103, 22,339-322,359.

Pfister, G., P.G. Hess, L.K. Emmons, Lamarque, J-F., Wiedimeyer, C.., Edwards, C.P., Petron, G., Gille, J.C.,Sachse, G.W. (2005), Quantifying CO emissions from the 2004 Alaskan wilfires using MOPITT-CO data, Geophysical Research Letters, 32

Pierce, R. B., et al., Regional Air Quality Modeling System (RAQMS) predictions of the tropospheric ozone budget over east Asia, J. Geophys. Res., 108(D21), 8825, doi:10.1029/2002JD003176, 2003

Pun, Betty K; Wu Shiang-Yuh; Seigneur Christian Contribution of biogenic emissions to the formation of ozone and particulate matter in the eastern United States. Environmental science & technology (2002), 36(16), 3586-96.

Ramana, M. V., V. Ramanathan,I.A. Podgorny,B.B. Pradhan, B. Shrestha (2004), The direct observations of large aerosol radiative forcing in the Himalayan region, Geophysical Research Letters 31

Rao, S. T.; Sistla, G.; Hao, W.; John, K.; Biswas, J. On the assessment of ozone control policies for the northeastern United States. NATO Challenges of Modern Society (1996), 21(Air Pollution Modeling and Its Application XI), 41-51

Rubin, E. (2000), Introduction to engineering and the environment, Chapter 8: Controlling Urban Smog.

Ryerson, T. B., Trainer, M., Holloway, J.S., Parrish, D.D., Huey, L.G., Sueper, D.T., Frost, G.J., Donnelly, S.G., Schauffler, S., Atlas, E.L., Kuster, W.C., Goldan, P.D., Hubler, G., Meagher, J.F., Fehsendfeld, F.C. (2001), Observations of ozone formation in power plant plumes and implications for ozone control strategies., Science, 292, 719-723.

Sandu, A., D. Daescu., G.R. Carmichael, T.Chai (2005), Adjoint sensitivity analysis of regional air quality models, Journal of Computational Physics, 204, 222-252.

SAS Institute. (2004), SAS/STAT 9.1 user's guide. Cary, N.C., SAS Institute.

Seinfeld, J. H. and S. N. Pandis (1998), Atmospheric chemistry and physics : from air pollution to climate change. New York, John Wiley.

Shindell, Drew; Faluvegi, Greg; Lacis, Andrew; Hansen, James; Ruedy, Reto; Aguilar, Elliot. Role of tropospheric ozone increases in 20th-century climate change. Journal of Geophysical Research, [Atmospheres] (2006), 111(D8), D08302/1-D08302/11.

Sillman, S. (1995), The use of NOy, HCHO, H2O2 and HNO3 as indicators for ozone-NOx-hydrocarbon sensitivity in urban locations, *Journal of Geophysical Research-Atmospheres*, *100*, 14175-14188.

Sillman, S. (1999), The relation between ozone, NOx and hydrocarbons in urban and polluted rural environments, Atmospheric Environment, 33, 1821-1845.

Singh, H. B., W. H. Brune, J. H. Crawford, D. J. Jacob, and P. B. Russell (2006), Overview of the summer 2004 Intercontinental Chemical Transport Experiment–North America (INTEX-A), J. Geophys. Res., 111, D24S01, doi:10.1029/2006JD007905

Takegawa, N., K.Kita, Y.Kondo, Y. Matsumi, D.D. Parrish, J.S. Holloway, M.Koike, Y. Miyazaki, N. Toriyama, S. Kawakami, and T. Ogawa (2001). Airborne vacuum ultraviolet resonance fluorescence instrument for in situ measurement of CO. J. Geophys. Res., 106 (D20), 24,327-24,244.

Tang, Y., Carmichael, G.R., Uno, I.Woo, J., Kurata, G., Lefer, B., Shetter, R.E., Huang, H., Anderson, B.E., Avery, M.A., Clarke, A.D., Blake, D.R.(2003a), Impacts of aerosols and clouds on photolysis frequencies and photochemistry during TRACE-P, part II: three-dimensional study using a regional chemical transport model, Journal Of Geophysical Research-Atmospheres. 108 (D21), 8822, doi:10.1029/2002JD003100

Tang, Y., G.R. Carmichael, D. Seinfeld, R.W. Dabdub, B. Huebert, A.D. Clarke, S.A. Guazzotti, D.A. Sodeman, K.A. Prather, I. Uno, J-H. Woo, D.G. Streets, P.K. Quinn (2003b), Three-dimensional simulations of inorganic aerosol distributions in East Asia during spring 2001, Journal Of Geophysical Research-Atmosphere, 109, D19S23, doi:10.1029/2003JD004201

Tang, Y., Gregory Carmichael, Narisara Thongboonchoo, Tianfeng Chai, Larry Horowitz, R. Bradley Pierce, Jassim Al-Saadi, Gabriele Pfister, Jeffrey Vukovich, Melody Avery, Glen Sachse, Thomas Ryerson, John Holloway, Elliot Atlas, Frank Flocke, Rodney Weber, L. Gregory Huey, Jack Dibb, David Streets, William Brune (2007), The Influence of Lateral and Top Boundary Conditions on Regional Air Quality Prediction: a Multi-Scale Study Coupling Regional and Global Chemical Transport Models, Journal of Geophysical Research-Atmospheres.

Tie X., S. Madronich, G. Li, Z. Ying, R. Zhang, A. R. Garcia, J. Lee-Taylor and Y. Liu (2007) Characterizations of chemical oxidants in Mexico City: A regional chemical dynamical model (WRF-Chem) study, Atmospheric Environment, 41(9),1989-2008.

Trainer, M., D. D. Parrish, M. P. Buhr, R. B. Norton, F. C. Fehsenfeld, K. G. Anlauf, J. W. Bottenheim, Y. Z. Tang, H. A. Wiebe, J. M. Roberts, R. L. Tanner, L. Newman, V. C. Bowersox, J. F. Meagher, K. J. Olszyna, M. O. Rodgers, T. Wang, H. Berresheim, K. L. Demerjian, U. K. Roychowdhury (2003), Correlation of ozone within NOy in photochemically aged air, J. Geophys. Res., 98(D2), 291-2925, 10.1029/92JD01910

United States Department of Transportation (2006), Transportation Air Quality: Selected Facts and Figures. Federal Highway Administration Office of Natural and Human Environment Publication No. FHWA-HEP-05-045 HEP/12-05(8M)E

Vautard, R., et al. (2003), A synthesis of the Air Pollution Over the Paris Region (ESQUIF) field campaign, J. Geophys. Res., 108(D17), 8558, doi:10.1029/2003JD003380.Volume 31, Issue 1 , January 2007, Pages 33-51

Wang, Y. D., Jacob, D.J. (1998), Anthropogenic forcing on tropospheric ozone and OH since preindustrial times, Journal of Geophysical Research-Atmospheres, 103, 31123-31136.

West, J. J., M. A. Zavala, L. T. Molina, M. J. Molina, F. San Martini, G. J. McRae, G. Sosa-Iglesias, and J. L. Arriaga-Colina (2004), Modeling ozone photochemistry and evaluation of hydrocarbon emissions in the Mexico City metropolitan area, J. Geophys. Res., 109, D19312, doi:10.1029/2004JD00461

West, J. Jason; Fiore, Arlene M.; Horowitz, Larry W.; Mauzerall, Denise L. Global health benefits of mitigating ozone pollution with methane emission controls. Proceedings of the National Academy of Sciences of the United States of America (2006), 103(11), 3988-3993

Wilczak J., S. M., I. Djalalova, G. Grell, S. Peckham, W. Gong, V. Bouchet, R. Moffet, J. McHenry, J. McQueen, P. Lee, Y. Tang, G. R. Carmichael (Under review), Bias-corrected ensemble and probabilistic forecasts of surface ozone over eastern North America during the summer of 2004, Journal of Geophysical Research-Atmospheres.

Zmirou, D., Schaetz, J, Saez, M, et al. (1998), Time series analysis of air pollution and cause specific mortality, Epidemiology, 9, 495